AN ABSTRACT OF THE THESIS OF

Catherine A. Hess for the degree of Master of Science in Radiation Health Physics presented on March 7, 2014.

Title: Monte Carlo Derived Absorbed Fractions in a Voxelized Model of a Rainbow Trout

Abstract approved:

_____

Camille J. Palmer

The International Commission on Radiological Protection (ICRP) has modeled twelve reference animals and plants (RAPs) with simple geometric shapes to be used when estimating radiation dose to non-human biota (NHB). In recent years, there has been interest in creating more realistic models in order to better understand the radiation interactions that take place in NHB. The work presented here details the creation of a voxelized model of a rainbow trout (*Oncorhynchus mykiss*) and presents absorbed fractions (AFs) of energy in each identified organ derived via Monte Carlo methods. AFs were calculated at several discrete energies: 0.01, 0.015, 0.02, 0.03, 0.05, 0.1, 0.2, 0.5, 1.0, 1.5, 2.0 and 4.0 MeV for photons and 0.1, 0.2, 0.4, 0.5, 0.7, 1.0, 1.5, 2.0 and 4.0 MeV for electrons. The AFs were shown to be dependent on incident radiation energy, as well as the source and target's mass and geometry. This data is consistent with voxelized models of other small organisms.

Monte Carlo Derived Absorbed Fractions in a Voxelized Model of a Rainbow Trout

by
Catherine A. Hess

A THESIS

submitted to

Oregon State University

in partial fulfillment of
the requirements for the
degree of

Master of Science

Presented March 7, 2014
Commencement June 2014

Master of Science thesis of Catherine A. Hess presented on March 7, 2014.

APPROVED:

Major Professor, representing Radiation Health Physics

Head of the Department of Nuclear Engineering & Radiation Health Physics

---

Dean of the Graduate School

I understand that my thesis will become part of the permanent collection of Oregon State University libraries. My signature below authorizes release of my thesis to any reader upon request.

Catherine A. Hess, Author

ACKNOWLEDGEMENTS

I would like to express my gratitude to Dr. Camille Palmer, an amazing advisor and mentor, for making me feel welcome at Oregon State University. She has continually provided encouragement, support and patience throughout this process.

At Oregon State University, I would like to thank Dr. Kathryn Higley for introducing me to the fields of radioecology and radiobiology and for serving as a member on my committee. I owe special thanks to Emily Caffrey, whose assistance with MCNP was invaluable. I would also like to express my appreciation to the other members of my committee: Dr. Laurel Kincl and Dr. Leah Minc.

Last but not least, I am grateful to have had the support and encouragement of my mother, who taught me the importance of getting an education. I also owe special thanks to my sister, Lisa, who has continually helped me become a better writer.

TABLE OF CONTENTS

Page

LIST OF FIGURES

LIST OF FIGURES (Continued)

Figure Page

LIST OF FIGURES (Continued)

Figure Page

LIST OF TABLES

LIST OF APPENDIX FIGURES

Figure Page

LIST OF APPENDIX TABLES

LIST OF APPENDIX TABLES (Continued)

Table Page

1 Introduction

Historically, the stance of regulatory and advisory bodies on the protection of the environment from ionizing radiation has been that if humans are adequately protected then non-human biota (NHB) are in turn afforded the same protection (IAEA, 1992; ICRP, 1977, 1991). In recent years, however, this line of reasoning has been questioned and interest in protecting the natural habitats and ecosystems that make up the environment has increased.

These concerns are reasonable considering there are many situations where humans are absent (e.g. the aquatic environment) or have been removed for their own protection (e.g. near a waste storage facility, clean-up site, or in the event of widespread radiological dispersal). And, even when people are present, the dose rates received by NHB can vary greatly from those received by humans. The International Commission on Radiological Protection (ICRP) now recommends that wildlife populations be considered as a separate protection endpoint (ICRP, 2003, 2007, 2008).

This new protection paradigm has presented numerous challenges to scientists as they seek to understand the relationship between exposure and dose, and dose and effect, with respect to different types of animals and plants. The myriad of biota, diversity of habitats, and different exposure scenarios make determining risk a monumental task.

The ICRP approach for estimating radiation dose to humans has been the use of reference methods, models, and databases (ICRP, 1975, 1994, 2006, 2009). Thus a key component in assessing doses to NHB has been to develop a set of reference models for select organisms, termed reference animals and plants (RAPs). The ICRP

has developed models of the RAPs out of simple geometric shapes and calculated dose conversion factors (DCFs) for 75 radionuclides. These models and DCFs can then be used as a starting point when evaluating dose to individual NHB.

The first attempt at defining a "standard man" was in the ICRP's 1954 recommendations (ICRP, 1959). The major focus at the time was to protect radiation workers and to a lesser extent, the general public. The first comprehensive report on Reference Man was made in 1975 (ICRP, 1975). The human model has evolved from simple shapes to more stylized mathematical models to highly realistic voxel models that are similar to the human body in shape and composition. These voxel models allow accurate simulation of radiation transport and energy deposition using Monte Carlo methods (Zaidi & Xu, 2007).

Realistic voxel models can be developed from images of an organism acquired by a medical imaging modality (usually computed tomography (CT) or magnetic resonance imaging (MRI)). These medical images consist of pixels, each representing a tissue in a 2-D plane. The 3-D volume of the tissue is termed a voxel (volume element), and it is determined by multiplying the pixel size by the thickness of an image slice. The information from these images allows models to be produced that are ever closer to the actual organism in question.

Accurate anatomical modelling is fundamental for performing dosimetry calculations accurately. True estimations of dose to wild populations has extreme importance, as regulations and standards are developed based upon current knowledge about the biological effects of radiation. Biological effects that are associated with an estimated dose that is inaccurately low could lead to costly remediation and financial burden for

certain sites. Conversely, when biological effects are associated with a dose that is erroneously high, sites may conclude that the environment and wild populations that reside therein are adequately protected when, in fact, damage could be occurring.

The goal of this research was to develop a voxelized model of a rainbow trout (*Oncorhynchus mykiss*) and present absorbed fractions (AFs) of energy in each segmented organ with each segment as a radioactive source and also as a target. The voxel model presented herein was created by obtaining a CT scan of a rainbow trout. Several software packages were utilized to create the computerized voxel model from the CT images. Monte Carlo radiation transport simulations were performed with MCNPX. Energy deposition was collected in each segmented organ at several discrete energies for both photons and electrons. The AFs derived in this research can be used to calculate dose conversion factors (DCFs); factors that are far more accurate than those calculated with simplistic geometries and homogenous mediums. These DCFs can be applied to other similar organisms, aiding risk-management decision makers as they decide what environmental protection, if any, is necessary for a given ecosystem.

2 Literature Review

2.1 ICRP Framework for Environmental Protection

The ICRP first addressed environmental protection in its 1977 recommendations with the assumption, "that if man is adequately protected then other living things are also likely to be sufficiently protected (ICRP, 1977)." In 1991, new recommendations were published with their stance on the environment essentially unchanged, stating (ICRP, 1991):

> *The Commission believes that the standard of environmental control needed to protect man to the degree currently thought desirable will ensure that other species are not put at risk. Occasionally, individual members of non-human species might be harmed, but not to the extent of endangering whole species or creating imbalance between species.*

This is a seemingly logical assumption, as man is one of the more radiosensitive species (Sparrow, Underbrink, & Sparrow, 1967); thus establishing safe limits for humans would surely offer adequate protection for the environment. However, situations can arise where humans are absent from a contaminated environment while NHB remain to receive possibly dangerous levels of radiation exposure.

The need to demonstrate explicitly that the environment is protected, along with society's escalating concern about environmental risks, led the ICRP to address the concept of environmental protection anew. In 2000, the ICRP set up a Task Group to develop a policy for the protection of the environment. This group's report (ICRP, 2003), as well as the ICRP's 2007 recommendations (ICRP, 2007), proposed an

approach analogous to human protection by developing a set of reference fauna and flora that could be used as a point of reference for assessing risk to organisms. Their new aim being to "prevent or reduce the frequency of deleterious radiation effects in the environment to a level where they would have a negligible impact on the maintenance of biological diversity, the conservation of species, or the health and status of natural habitats, communities, and ecosystems (ICRP, 2008)." The intent being that these reference fauna or flora could form the basis of a more structured approach to understanding the relationships between exposure and dose, dose and effect, and the potential consequences of such effects (ICRP, 2007).

2.1.1 Reference Animals and Plants

The concept of using a reference organism to relate exposure to dose is not a new idea. Human radioprotection has long been centred around the concept of a reference individual (ICRP 1975, 2002, 2009). The ICRP chose to use a similar system of clearly defined reference animals and plants (RAPs) to assess radiation effects in NHB. ICRP Publication 108 was the ICRP's first attempt at defining and creating a set of reference animals and plants (RAPs). This concept was first introduced by Pentreath, who has written extensively on the subject (Pentreath & Woodhead, 2001; Pentreath, 1998, 1999, 2002, 2004, 2009). The ICRP defines a RAP as follows (ICRP, 2008):

> *A hypothetical entity, with the assumed basic biological characteristics of a particular type of animal or plant, as described to the generality of the taxonomic level of family, with defined anatomical, physiological, and life history properties, that can be*

> *used for the purposes of relating exposure to dose, and dose to effects, for that type of living organism.*

Clearly, it would not be feasible to create a model of every living species. The variability of plants and animals with respect to their dimensions and different habitats is vast, making the task of assessing radiation exposure in these environments challenging. Therefore, a small set of fauna and flora were chosen to use as reference organisms.

The RAPs were chosen based upon several factors which are summarized here from ICRP 108: (1) the amount of radiobiological information that is available on them; (2) their amenability to future research; (3) that they are considered to be typical representative fauna or flora of particular ecosystems; (4) that they are likely to be exposed to radiation from a range of radionuclides in a given situation; (5) that their life cycles are likely to be of some relevance for evaluating total dose or dose rate; (6) that their exposure to radiation can be modelled using relatively simple geometries; (7) that there is a reasonable chance of being able to identify any effects at the level of the individual organism; and (8) that they have some form of public or political resonance (ICRP, 2008). With these criteria in mind, twelve organisms were chosen as RAPs to represent typical organisms in the marine, freshwater, and terrestrial environment. A deer, rat, bee, earthworm, pine tree and a wild grass were chosen to be representative terrestrial organisms. A duck and frog were chosen as reference organisms that inhabit both aquatic and terrestrial environments. A trout was the organism chosen to represent fish in a freshwater ecosystem. A flatfish, crab, and brown seaweed were the reference saltwater marine organisms chosen. Different life stages were also considered for many of the organisms.

2.1.2 Dose Estimation Approaches

Over the years, the ICRP has developed a comprehensive system for human dosimetry. This system allows for the distribution of radionuclides to specific organs and for the clearance of the nuclide over a period of time. Beyond the broad dosimetry principles presented therein, the human models are of little use when evaluating dose to NHB since both the dimensions of the organism and the metabolism vary from that of humans. Moreover, there are innumerable organisms, habitats and exposure situations that could be considered when estimating dose to NHB.

There have been many approaches developed to estimate radiation dose to NHB (Amiro, 1997; Copplestone et al., 2001; DOE, 2002; Golikov & Brown, 2003; Higley, Domotor, Antonio, & Kocher, 2003; NCRP, 1991; Taranenko, Pröhl, & Gómez-Ros, 2004; Ulanovsky & Pröhl, 2006; Vives i Battle, Jones, & Gómez-Ros, 2004). A common difficulty that all approaches face is finding the right balance between the complexity of the modelling that is desired and the amount of data and time that is available. Several of these methods use a tiered assessment structure whose first tier is designed to be highly conservative and simple to use. The aim of this initial tier is to identify sites of negligible concern and to remove them from further consideration with a high degree of confidence (Beresford et al., 2010).

The ICRP dose assessment method for the environment has strong links with the methodology and data developed in two projects supported the European Union (EU): FASSET (C-M Larsson, 2004) and ERICA (Carl-Magnus Larsson, 2008).

The FASSET (Framework for Assessment of Environmental Impact of Ionizing Radiation) project, which began in 2000, made an attempt at bringing a structured framework for protecting the environment from ionizing radiation (C-M Larsson, 2004). A key component of the framework has also been to provide a method for assessing radiation dose factors to aquatic organisms per unit radionuclide concentration in the surrounding media and in the organism itself (J. Brown et al., 2003). The project organized and compiled the available information on radiation effects into FRED (FASSET Radiation Effects Database). Over 1,000 references that covered biological effects to a range of NHB following exposure to ionizing radiation published between 1945-2001 were reviewed and entered in the database (Copplestone, Hingston, & Real, 2008).

ERICA (Environmental Risk from Ionizing Contaminants) provided an integrated approach to scientific, managerial and societal issues concerned with the environmental effects of ionizing radiation. Considerable effort was put into compiling a more complete and quality controlled set of literature. This was an improvement upon the FRED database and also incorporated data from the EPIC (Environmental Protection from Ionizing Contaminants in the Arctic) project. EPIC closely resembled the FASSET project, but strictly focused on Arctic biota (Sazykina, Kryshev, Katkova, & Kryshev, 2002). The upgraded database was termed FREDERICA and added references for the years 2002-2006. The database includes more than 30,000 entries that were obtained from scientific literature on radiation effect experiments. The data is grouped according to wildlife group and the endpoint of effect: morbidity, mortality, reproduction, and mutation (Copplestone et al., 2008). This database is continually updated as new information becomes available. Not only

does this database provide comprehensive information on radiation effects in NHB, it also demonstrates where data gaps exist.

The ERICA tool is freely available software that aids the user in assessing radiological risk to biota. The tool guides the user through the assessment process, keeps records and performs the necessary calculations to estimate dose rates to selected biota (J. E. Brown et al., 2008). The ERICA tool uses a tiered approach allowing the input of site-specific data at higher tiers (Carl-Magnus Larsson, 2008).

2.1.3 ICRP Dose Calculation Methodology

The ICRP has presented absorbed fractions (AFs) of energy for the reference animals and plants utilizing simple three-dimensional ellipsoidal bodies. No internal structures or organs were accounted for, except in the case of the reference deer. For the aquatic organisms, a "uniform isotropic model" was utilized. This model was first introduced by Loevinger and Berman. In this model, the assumption that the radionuclides are homogenously distributed throughout the organism and the surrounding environment is made. The densities of the surrounding medium and the organism's body are also assumed to be equal (Loevinger & Berman, 1976). Since aquatic organisms are surrounded by water and the densities of much of their bodies are very close to water, this model was deemed appropriate. Using these AFs, dose conversion factors for 75 radionuclides were derived. This method mirrors that presented by Ulanovsky and Pröhl.

In 2006, Ulanovsky and Pröhl presented AFs of photon and electron energy that were systematically calculated by Monte Carlo methods for spherical and ellipsoidal shapes

in a water medium. AFs were found to be smooth functions of particle energy and mass of the organism's body; thus allowing interpolation of AFs for non-explicitly calculated masses and energies. AFs can be calculated for body masses ranging from 10^{-6} kg to 10^{3} kg using this method. A rescaling factor was also developed to account for differences in ellipsoidal shapes (Ulanovsky & Pröhl, 2006).

In a study presented by Gómez-Ros et al., a model for calculating the uncertainty associated with the possible nonhomogenous distributions within the body, as an indication of the applicability for the DCFs obtained for homogeneous distributions was presented. Their research showed that for photons, the uncertainty due to a possible non-homogenous radionuclide distribution is less than 30% in the cases considered. For electrons, the uncertainty was negligible depending on the size of the organism (Gómez-Ros, Pröhl, Ulanovsky, & Lis, 2008). While many of the assumptions used in a uniform isotropic model are plausible, there may be situations when nonuniformity of activity distribution in the body becomes an essential parameter for dose calculation (Ulanovsky & Pröhl, 2012).

The benefit of using simplistic models is their ease of use, minimal time involved and their applicability to a wide range of species. The simplified approach used by the ICRP for dose calculation in NHB varies from human dosimetry methodology where realistic voxel models are used that contain various internal organs. Monte Carlo methods have been used to solve radiation transport equations for these models. There are many advantages to using this method: namely, materials differing in composition and density can be used and complex geometries for sources and targets can be utilized.

In a study done by Kramer et al., the dosimetric consequence of replacing an analytical human MIRD (Medical Internal Radiation Dose) model with a voxel model was investigated. This change, along with updating the tissue compositions and radiation transport code, showed a decrease in the effective male dose by up to 25% for external exposures to photons (R. Kramer, Vieira, Khoury, & Lima, 2004). In another study performed by Ruedig, a comparison between a voxelized and a simplistic model of a snail was performed. The AFs calculated with the voxelized model were consistently lower than the AFs calculated with the simple model (Ruedig, 2013). These results indicate that while simplistic models allow for some level of conservatism, which is often desirable in radioprotection, the association of effects of radiation to doses that are erroneously low may often lead to expensive and unnecessary remediation measures. In this case, improving simplistic dosimetry models is warranted.

2.1.4 Absorbed Fraction

Absorbed dose is the basic quantity used when measuring the amount of radiation that is deposited in a material. The radiation absorbed dose (rad) is the amount of energy (from any type of ionizing radiation) deposited in any medium (e.g., water, tissue, air). An absorbed dose of 1 rad means that 1 gram of material absorbed 100 ergs of energy as a result of exposure to radiation. The international unit used to express absorbed dose is the gray (Gy); 100 rad = 1 Gy. A key quantity for estimating internal dose is the absorbed fraction (AF).

The AF is a dimensionless quantity that accounts for the fraction of the energy emitted by a source organ that is absorbed in a target organ, which may be the source organ

itself. The value of the absorbed fraction depends on the type and energy of the radiation; the size, shape, and composition of the source and the target; and the composition of the intervening tissue (Loevinger, Budinger, & Watson, 1991).

Another commonly seen term is the *specific* absorbed fraction (SAF). This value is obtained by dividing the AF of the target organ by the mass of the target organ and has units of g^{-1}. The specific absorbed fraction is useful when the source and target organs are in a homogenous absorbing material sufficiently large so that edge effects are negligible. SAFs are relatively insensitive to small changes in the size and shape of the source and target when the target is distant from the source (Snyder, Ford, & Warner, 1978). This is not the case for small organism dosimetry, in which case, AFs were chosen to be calculated for this model, as opposed to SAFs.

2.1.5 Dose Conversion Factors (DCFs)

Dose conversion factors (DCFs), sometimes referred to as dose conversion coefficients (DCCs), are radionuclide-specific conversion factors that can relate activity concentration values of a radionuclide, either in an organism or in its surrounding medium, to an absorbed dose rate (Ulanovsky & Pröhl, 2006). The units for this factor are μGy h^{-1} per Bq kg^{-1}. DCFs can be expressed in terms of AF as follows:

$$DCF_{int} = \sum_{v}\left(\sum_{i} Y_i E_i \phi_v(E_i) + \int N_v(E) E \phi_v(E) dE\right), \text{ and} \quad (1)$$

$$DCF_{ext} = \sum_{v}\left(\sum_{i} Y_i E_i (1 - \phi_v(E_i)) + \int N_v(E) E \big(1 - \phi_v(E)\big) dE\right); \quad (2)$$

where v indicates radiation type; E_i (MeV) and Y_i (per decay) are energy and yield of discrete energy radiations per decay of the radionuclide, respectively; and $N_v(E)$ (per decay per MeV) is the spectrum of continuous energy radiations of type v (here, for beta particles alone); and $\phi_v(E)$ is the absorbed fraction.

2.1.6 Derived Consideration Reference Levels

The key to any protection paradigm is having numeric guidance upon which to compare current dose rate levels and the effects those radiation levels might have on populations in a given ecosystem. In order to translate knowledge about the effects of radiation on different types of animals and plants into useful information for decision makers, the ICRP recommends an approach considering the effects in terms of bands of dose within which certain effects have been noted (ICRP, 2008). From ICRP 108, a derived consideration reference level (DCRL) is defined as (ICRP, 2008):

> *A band of dose rate within which there is likely to be some chance of deleterious effects of ionizing radiation occurring to individuals of that type of Reference Animal or Plant, derived from a knowledge of defined expected biological effects for that type of organism that, when considered together with other relevant information, can be used as a point of reference to optimize the level of effort expended on environmental protection, dependent upon the overall management objectives and the exposure situation.*

DRCLs are not dose limits, but rather bands of dose rates at which further evaluation might be warranted. These bands are multiples of the natural background dose rates typically seen where the organism resides. Typical background dose rates for the freshwater environment were considered to be approximately 0.5-18 μGy day^{-1} (ICRP, 2008). These bands can be put into perspective by noting the effects at very high levels of dose and by noting what might be expected at natural background radiation levels. These consideration levels are meant to help optimise the level of effort that might be expended on protection of the considered organism or those of similar type.

2.2 Complications of Framework

2.2.1 Relative Biological Effectiveness

Effects of radiation on living tissues are known to depend on the type of radiation, or more precisely, on the density of ionization produced by the radiation in the tissue. This is known as linear energy transfer (LET). The relative biological effectiveness (RBE) of a certain type of radiation is accounted for in human dosimetry by using the equivalent dose and radiation quality factors. The LET at which RBE reaches a peak is much the same for a wide range of mammalian cells due to their similarity in DNA structure (Hall & Giaccia, 2006).

Assigning RBE values for NHB proves to be difficult due to limited research in the area and various endpoints of effect studied. Chamber et al. attempted to compile and summarize the literature on experimentally determined RBEs for internally deposited alpha-emitting radionuclides. In doing so, they recommend a factor of 5 for the purposes of environmental risk assessments. For a conservative based screening, they

recommend that factors of 10 and 20 should be considered for deterministic and stochastic endpoints, respectively (Chambers, Osborne, & Garva, 2006). In their 1992 report, the IAEA discussed this issue and advised the inclusion of a weighting factor in environmental assessments that would account for variations in RBE (IAEA, 1992).

2.2.2 Radionuclide Bioaccumulation and Distribution

Radionuclides can be taken up by fish through ingestion, absorbed through the skin, and adsorbed into the blood through the gills. The rate and amount of uptake is complicated to predict due to the many variables that come into play. The nuclides physiological importance to the organism, the physical and chemical state of the element, the concentration in the environment, the presence of other nuclides which can inhibit or enhance uptake, the age of the organism, the water temperature, the organism's diet and the rate of uptake of those organisms are just a few of the things that should be considered when evaluating bioaccumulation of radionuclides.

There have been many studies done investigating the bioaccumulation and elimination of radionuclides in rainbow trout (Boroughs, Townsley, & Hiatt, 1956a, 1956b; Clulow, Dave, Lim, & Avadhanula, 1998; Hogstrand, Grosell, Wood, & Hansen, 2003; Kimura, Honda, & Nishiwaki, 1978; Olson, Bergman, & Fromm, 1973; Vangenechten, Van Puymbroeck, & Vanderborght, 1989). In a study done by Vangenechten et al., biological uptake of ^{244}Cm and ^{241}Am was determined for rainbow trout. Half of the trout were placed in synthetically prepared water without any organic material with the other half placed in water that contained dissolved natural organic matter. The water was then contaminated with either ^{244}Cm or ^{241}Am. Bioaccumulation of americium and curium from freshwater in rainbow trout was low

as evidenced by concentration factors lower than unity for total animals. However, the nuclides that were taken up were mainly concentrated in the liver and gills for both types of water. The uptake, however, was greater in the water without dissolved organic material (Vangenechten et al., 1989).

Another study investigated the distribution of ^{110m}Ag in juvenile rainbow trout exposed to the radionuclide either as $AgCl_{aq}$ or Ag^{+}. The trout were exposed to ^{110m}Ag contaminated water for 24 hours. They were then placed in depuriation tanks and sampled at various times up to 67 days post exposure. The liver was found to be the major accumulatory organ. The silver speciation did make a difference in the amount of uptake (Hogstrand et al., 2003).

Examining radionuclide uptake into eggs or juvenile fry can be difficult. Complications can arise due to the difficulties of dissection and the ease of cross-contamination. One group of researchers attempt at this showed that the majority of radionuclides accumulated in the egg capsule, followed by the yolk and perivitelline fluid. The embryo showed very little uptake of ^{60}Co, ^{131}I, ^{137}Cs, ^{144}Ce, or ^{106}Ru (Kimura et al., 1978).

These studies all demonstrate that bioaccumulation of radionuclides does not disperse among tissues and organs homogenously. This suggests that simple homogenous models may not be ideal for every situation and dosimetry modelling and dose calculations may benefit from more complicated and realistic models of the organisms. Applying trout specific organ concentration data with the AFs provided in this work could be utilized to accurately determine doses in trout or other similar fish.

2.2.3 Extrapolating the Data

While human protection is focused on minimizing stochastic effects in individuals, within the ICRP's proposed framework, the focus for environmental protection is on protecting *populations* of biota. The endpoint effects considered to be of relevance being: morbidity, mortality, reduced reproductive success, and some observable form of chromosomal damage (ICRP, 2008). Extrapolating radiation effects in an individual organism to possible impacts at a population or community level is problematic. Dose-effect relationships may lose their predictive ability at the system level due to other stressors in the environment and the interaction of the organism in question with other components in the ecosystem. Brechignac in particular advocates for a "top down" approach as opposed to "bottom up" when investigating the effects of radiation on populations or ecosystems (Brèchignac & Doi, 2009; F. Bréchignac, 2005; François Bréchignac, 2003). He argues that the assessment of the effects of radiation at the scale of communities and ecosystems may not be derived only from the effects observed at the scale of individuals. Indeed, there is a knowledge gap between biological effects at the individual level and their consequences at the population and community levels in wild populations. Most studies on the effects of radiation in NHB have been performed in laboratory settings where other stressors in the environment have not been taken into account (Ruedig, 2013).

In an effort to decrease this knowledge gap, Doi and Kawaguchi presented an individual-based computational model to simulate the population dynamics of microorganisms in an aquatic model ecosystem. Their research suggested that there is a synergistic relationship between algae and protozoa, and that "umbrella effects on

the individual level appear to initiate ecological consequences that could indicate potential impacts on community, population, and ecosystem" (Doi & Kawaguchi, 2007).

Woodhead, on the other hand, argues that it is difficult, if not impossible, to identify any population-specific effects directly attributable to radiation exposure without first identifying known effects in individual organisms (Woodhead, 2003b). In an effort to relate the known effects of radiation in individuals to the possible consequences at the population level, Woodhead presented a simple Leslie matrix population model to be used as a tool when investigating how the effects of radiation in individuals may propagate to produce a response at the population level. The results from the model appear to confirm the sensitivities of the plaice (*Pleuronectes platessa*) and the thornback ray (*Raja clavata*) to the possible effects of radiation on individual fertility, fecundity, and mortality (Woodhead, 2003a). However, these results are only as accurate as the data entered to describe populations.

Succinctly, it can be argued that the effects of radioactive contaminants on a population develop from processes that take place in individual organisms. Most of the data on the effects of radiation have been acquired from studies of small groups of individuals (Pentreath, 2009). Thus, in order to fully understand how populations are affected by radiation, understanding the relationship between dose and effect on the individual first is crucial. In this sense, developing models of individual organisms for dosimetry purposes is justified.

The above issues, along with the many differences in biology and exposure situations encountered in the environment, make deciding on an appropriate method to evaluate

the effects of dose rates from activity in the environment perplexing. The enormous biodiversity and complex interconnectivity makes connecting the effects of radiation dose rates on populations of species or the whole ecosystem in general challenging. The symbiotic relationships that exist are not entirely understood and the effects of other stressors in the environment (e.g. drought, predation, etc.) are often not considered when evaluating the effects of radiation on populations. Further research is clearly needed before a defendable and transparent system for protecting the environment is established.

2.3 Other Small Organism Voxel Models

Several researchers have generated voxel models of small animals. This is partly due to the need for realistic models of mice and rats that are used for preclinical pharmokinetic studies (Mohammadi & Kinase, 2011) and partly due to the ICRP's recommendations that models be produced for their list of reference animals and plants (ICRP, 2008).

2.3.1 Rat and Mouse Models

In 2006, Stabin et al. developed voxel-based mouse and rat models. Both animals were imaged with a dedicated small-animal CT scanner. Organs were identified on the images and segmented using in-house software. Radiation transport calculations were performed using MCNP. AFs for all identified organs were calculated at discrete initial energies: 0.1, 0.2, 0.4, 0.7, 1.0, 2.0, and 4.0 MeV for electrons and 0.01, 0.015, 0.02, 0.03, 0.05, 0.1, 0.2, 0.5, 1.0, 1.5, 2.0 and 4.0 MeV for photons. It was found that for electron energies greater than 0.5 MeV, self-irradiation AFs were significantly less

than one (Stabin, Peterson, Holburn, & Emmons, 2006). Essentially, the full amount of energy was not absorbed in the source organ due to the small organ sizes and the range of electrons at these energies.

2.3.2 Frog Model

In 2008, Kinase developed a voxel model of a frog. Segmented images were obtained from cryosection data available from Lawrence Livermore National Laboratory (LLNL). Fifteen organs and tissues were identified. Elemental compositions and densities of the tissues and organs were taken to be the same as humans. Internal organ dose estimates were calculated using the Monte Carlo code EGS4 in the spleen, liver and kidneys. Self-AFs of energy for photons and electrons with energies ranging from 0.01-4.0 MeV were calculated in the segmented organs (Kinase, 2008). This study showed that AFs are largely dependent on organ mass and that electrons with energies above 0.1 MeV should be treated as penetrating radiation.

2.3.3 Flatfish Model

A voxel model of a marine flatfish was developed in 2012 (E. A. Caffrey, 2012). CT and MRI images of the fish were obtained. The MRI images were chosen to be used in creating the model due to the superior contrast. These images were then segmented using 3D-Doctor. Voxelizer read the exportable boundary file from 3D-Doctor to create the MCNP lattice structure. MCNPX was used to run radiation transport simulations. AFs for all identified organs were calculated at several discrete energies ranging from 0.01-4.0 MeV for photons and 0.1-4.0 MeV for electrons. Similar to the previous models, this research showed that electrons above approximately 0.5 MeV

should be treated as penetrating radiation. This research also confirmed that organ mass and geometry are important factors in how energy is distributed among internal organs (E. A. Caffrey, 2012).

These studies show that organ mass and their position in the body are important factors in determining energy deposition. The models all demonstrate that electrons with sufficient energy should be treated as penetrating radiation as seen by the sharp decrease in the source organ energy deposition with increasing energy. This concept is different from the logic used in human dosimetry. In human dosimetry it is assumed that the total electron energy is absorbed in the source organ. These findings suggest that methods used for human dosimetry are not always applicable to small organism dosimetry and that more complex models may prove useful as organ mass and geometry have been shown to be important.

2.4 Rainbow Trout (*Oncorhynchus mykiss*)

Trout belong to the kingdom Animalia in taxonomic structure. All animals are members of this Kingdom. Trout are vertebrates, whose members also include reptiles, amphibians, birds, and mammals. Vertebrates include the overwhelming majority of the phylum Chordata. Trout are further classified as Osteichthyes, meaning they possess a bony as opposed to a cartilaginous skeleton. This classification is further divided into ray-finned (Actinopterygii) or lobe-finned (Sarcopterygii) fish, with trout being the latter. Trout are members of the Salmoniforme Order which has only one family, Salmonidae (NOAA Fisheries: Office of Protected Resources, 2013).

Both salmon and trout belong to the Family Salmonidae. All salmonids spawn in fresh water, but in many cases, the fish spend most of their lives at sea, returning to its natal stream only to reproduce (NOAA Fisheries: Office of Protected Resources, 2013). In order to avoid complications that arise from migration, the trout who lives solely in freshwater was chosen as the reference organism as opposed to the salmon (ICRP, 2008). *Oncorhynchus mykiss*, commonly known as the rainbow trout, was the species of trout used in this study.

The freshwater form of trout are native to North America, however they have been introduced to rivers and streams all across the world and are widely farmed. Both salmon and trout are regarded as biological indicators of good water quality and are the subject of much environmental and fisheries legislation (ICRP, 2008). There have also been many studies performed on trout to evaluate the biological effects of radiation (Edmundson Jr., 1976; Foster, 1949; Knowles, 1992; McGregor & Newcombe, 1972a, 1972b; Niiyama, 1957; J.A. Strand, Fujihara, Burdett, & Poston, 1977; John A Strand, Fujihara, Poston, & Abernethy, 1982; Welander, Wadley, & Dysart, 1971) as well as radionuclide uptake and metabolism (Clulow et al., 1998; Garnier & Baudin, 1990; Hogstrand et al., 2003; Kimura et al., 1978; Olson et al., 1973; Vangenechten et al., 1989). For all of these reasons, the trout was considered an appropriate candidate for the reference freshwater fish (ICRP, 2008).

Trout reside in fresh and brackish waters; thriving in cool rivers and lakes with a high oxygen content. They are found at depths from 0-200 meters and will eat insects, leeches, and small crustaceans (Frost & Brown, 1967).

Oncorhynchus mykiss are iteroparous with an equal gender ratio and high fecundity resulting in distinct cohorts. They spawn twice a year with each female releasing approximately 1,500 eggs per year (ICRP, 2008). The female trout lays her eggs in redds or gravel. Eggs are typically laid in autumn and take approximately 100 days to hatch. The juvenile fish will remain in their natal stream for 1-4 years before migrating to a lake. A trout matures at an age of 4 years and on average dies at age 6 (ICRP, 2008).

Trout are fusiform in shape with four unpaired fins and two sets of paired fins. They have fully scaled bodies with a scaleless head. Three-fifths of a trout's body volume is made up of muscle. Oxygen is absorbed and carbon dioxide is released through the gills. Most of the tissues in the trout are heavier than water; flotation is maintained by the presence of an air bladder which resides below the vertebral column and kidney and above the body cavity. Food is taken in through the mouth and then travels through the esophagus, stomach, pyloric caeca and intestine before being excreted from the body. The gonads vary in size according to the maturity of the fish and the season (both males and females). The gonads are small in spring and, in females, will fill the entire body cavity in the fall (Frost & Brown, 1967).

3 Materials and Methods

The creation of a voxel model involves four general steps: (1) Acquire a set of medical images, (2) classify and segment the organs or tissues of interest (3) specify tissue type and composition of organs, and (4) implement the geometric data into a Monte Carlo code to calculate radiation transport and tally quantities of interest (Zaidi

& Xu, 2007). For this project, images were acquired using computed tomography (CT). Several software packages utilized the CT data to establish the physical parameters to be input into MCNP. Energy absorption was tabulated for each segmented organ via Monte Carlo methods.

3.1 Background on Methods and Software

3.1.1 Computed Tomography (CT)

A CT scanner is capable of producing cross-sectional images of the object it is imaging. The images are in the transverse or axial plane, which divide the body into upper and lower portions. After scanning, the data can be reconstructed to view images in the coronal and sagittal planes. The coronal plane divides the body into anterior and posterior portions. The sagittal plane divides the body into left and right portions.

Inside a CT scanner, an x-ray tube travels in a circle around the patient. A bank of detectors travel around the circle opposite the x-ray tube. Assuming a monoenergetic beam and a homogenous medium being scanned, the transmission of x-rays through the object occurs according to the following equation:

$$I = I_0 e^{-\mu x} \tag{3}$$

where I_0 is the initial intensity of x-rays, I is the final intensity, μ is the linear attenuation coefficient of the material being imaged and x is the thickness of the

material. However, most organisms are not made of a single homogenous material. In most organisms, the x-ray beam would have to travel through many regions with different linear attenuation coefficients along the path. The equation then becomes:

$$I = I_0 e^{-\sum_{i=1}^{n} \mu_i x_i}. \quad (4)$$

With a single transmission measurement through an object, the attenuation coefficients cannot be determined because of so many unknown values. By taking measurements of x-ray transmission through an object at several different positions across the subject and at a sufficient number of angles, it is possible to determine attenuation differences of 0.5%. This allows the small differences in soft tissues and organs to be visualized (Goldman, 2007).

Once all of this data is obtained for each slice, the image must be reconstructed. The objective of reconstruction is to determine the degree of attenuation that occurs in each voxel of the reconstruction matrix. The two voxel dimensions lying in the xy plane of the slice are often referred to as pixels. Adding in the slice thickness in the z direction constitutes a voxel – in essence a volumetric pixel. Computer algorithms are applied to the data and numbers corresponding to the attenuation coefficients that are assigned to each voxel. A grey level is assigned to each number and a two-dimensional image is produced.

These CT numbers are often called Hounsfield units – named after the inventor of the first CT machine. In a CT image, higher CT numbers are brighter and lower CT numbers are darker. The numbers range from -1000 for air to +1000 for bone, with

the CT number for water set at 0. CT number is related to the attenuation coefficient according to the following equation:

$$CT\ Number = 1000\frac{(\mu - \mu_w)}{\mu_w} \quad (5)$$

where μ is the calculated voxel attenuation coefficient and μ_w is the linear attenuation coefficient of water (Hendee & Ritenour, 2002). Scanners determine μ_w from periodic calibration scans of water or water-equivalent phantoms. Proper calibration of the x-ray generator is also necessary since attenuation coefficients are energy dependent.

3.1.2 3D-Doctor

The images obtained from a CT scan are in the Digital Imaging and Communications in Medicine (DICOM) format. Software is required to convert the DICOM image stacks into virtual models through the establishment of boundaries that define internal structures. 3D-Doctor[1] was the software chosen to perform this based on its ease of use and multiple capabilities. By outlining or segmenting regions of interest on the images, the software is able to create a three-dimensional model (Able Software Corporaton, 2008).

---

[1] Able Software Corp. 5 Appletree Lane, Lexington MA 04240. http://www.ablesw.com/3d-doctor/index.html

Segmentation is an automated image processing function to generate object boundaries. This is done by using the image's greyscale range to differentiate between tissues. Due to the similarity in density of many of the internal organs, most boundaries had to be created manually. Using the boundary edit functions within 3D-Doctor, the objects can be modified at will. 3D-Doctor builds the three-dimensional structure based upon these boundaries. After the segmentation process is complete, 3D-Doctor can quickly calculate parameters such as volume, surface area and length. Three dimensional renderings can be generated to aid the user throughout the segmentation process.

3D-Doctor has a "reslice" function which allows the user to view image slices cut at another axis (i.e. sagittal, coronal or axial). This feature aids the user in identifying and contouring organs by allowing the user to see the subject in another plane (Figure 1 and Figure 2).

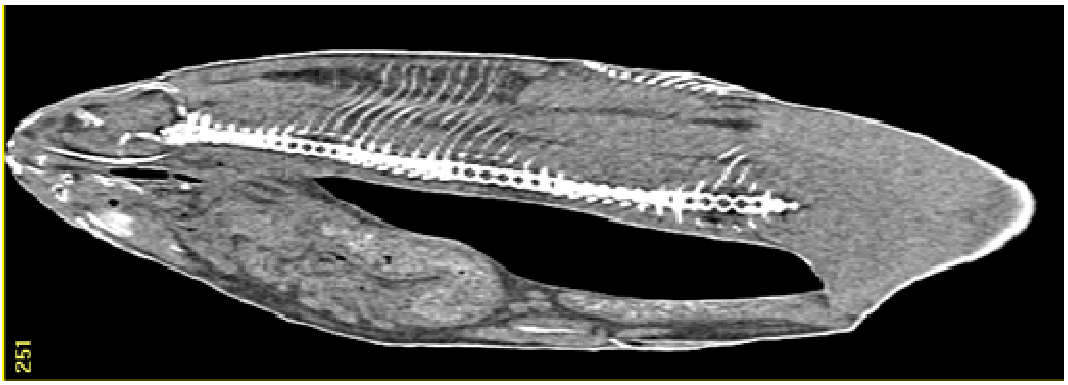

Figure 1: Sagittal image of the trout obtained by using the reslice function in 3D-Doctor.

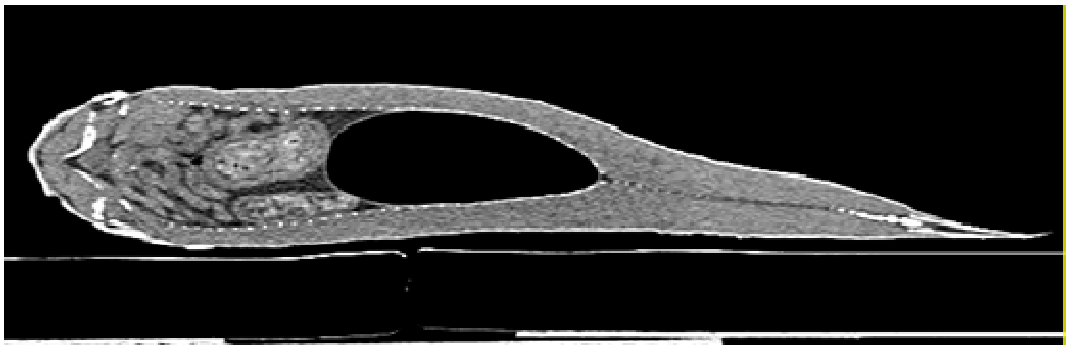

Figure 2: Axial image of the trout obtained by using the reslice function in 3D-Doctor.

The segmented boundaries are saved in a boundary file (*.bnd) format which can then be opened by Voxelizer to generate a lattice structure that can be utilized in a Monte Carlo input file. The boundary file format is a simple ASCII text file. In this file, each contour starts with an integer slice number (for example, Z1, in the range of 0 to the total number of slices). The following lines are the points (X and Y within the slice) along the contour. The last point is always the same as the first point to indicate a closed polygon (Able Software Corporaton, 2008).

3.1.3 Voxelizer

Voxelizer[2] is a publicly available software program that was created in-house at the Human Monitoring Laboratory in Canada. 3D-Doctor boundary files must be converted into a lattice structure readable by MCNP. This in-house code makes it

[2] Human Monitoring Laboratory, National Internal Radiation Assessment Section, Radiation Protection Bureau, 775 Brookfield Road PL6302D, Ottawa, Ontario, K1A 1C1, Canada

possible to convert boundary lines and objects obtained from 3D-Doctor into a repeated structure that can be utilized in Monte Carlo simulations. In order to make this conversion, Voxelizer reads the data from 3D-Doctor's exportable boundary file. From this file, Voxelizer counts and reads the names of each object identified in the boundary file, each of which will correspond to a universe in the lattice structure that forms a portion of the Monte Carlo input file. Voxelizer does this for each image plane. Voxelizer places the corresponding nodes of that plane on a matrix grid, draws the lines between these nodes to obtain the closed boundaries, and then fills the space between each boundary with the appropriate material. The material can be manually changed when working with the MCNP input file (G. H. Kramer, Capello, Chiang, Cardenas-Mendez, & Sabourin, 2010).

3.1.4 MCNPX

The MCNP[3] code was developed and is maintained by Los Alamos National Laboratory. It is a robust code used for analysing the transport of neutrons, electrons and gamma rays by the Monte Carlo method. The user must specify all parameters of the problem. The geometry of the problem is expressed in terms of regions or volumes bounded by surfaces. The geometry necessary for this research proved to be more complicated than the creation of simple shapes and surfaces to describe the fish. MCNP allows a lattice structure to be generated for such geometries. Lattice creation establishes a regular grid within the problem geometry. Each grid location is referred to as an individual voxel. All voxels are assigned to a universe, which correspond to a

[3]Los Alamos National Laboratory, Los Alamos, NM https://mcnpx.lanl.gov/

certain organ or tissue in the problem. The lattice for this work was made of hexahedra shaped voxels. Each voxel is then filled with a material which is specified on the data card. The data specification section of the input file defines the type of particles, problem materials, radiation sources, how results are to be tallied, and cross-section libraries among other things (Shultis & Faw, 2004; X-5 Monte Carlo Team, 2008).

The Monte Carlo method relies on repeated random sampling to obtain estimated averages of tallies of interest (X-5 Monte Carlo Team, 2008). For photons, the code accounts for incoherent and coherent scattering, the possibility of fluorescent emission after photoelectric absorption, and absorption in electron-positron pair production. Electron transport processes account for angular deflection through multiple Coulomb scattering, collisional energy loss with optional straggling, and the production of secondary particles, including K x-rays, knock-on Auger electrons, bremsstrahlung, and annihilation gamma rays from positron annihilation at rest (X-5 Monte Carlo Team, 2008). The simulations track particle or photon histories many times over, modelling each subatomic interaction. The code tracks each particle or photon until it interacts with a material, is absorbed, or escapes the defined problem boundary. As the number of simulated particles increases, the results converge upon a normal distribution. This statistical process can be likened to playing and recording your results in a real casino situation; hence the name.

The statistical sampling process is based on the selection of pseudo-random numbers. Probability distributions are randomly sampled using transport data to determine the outcome at each step of the particle or photon's life (X-5 Monte Carlo Team, 2008).

MCNP generates an output file that tallies the quantities of interest, along with estimates of the statistical precision of the results.

Precision is the uncertainty in the tally mean $\bar{x}$ caused by the statistical fluctuations in the individual scores x_i of the simulated histories. Important to note is that the accuracy of the result is not known (Shultis & Faw, 2004). Accuracy is a measure of how close the tally mean $\bar{x}$ is to the true physical quantity being estimated. The difference between accuracy and precision is the systematic error; a quantity that is seldom known. It is possible to have a highly precise result that is not accurate.

MCNP produces a plethora of information about the simulation including the relative error, figure of merit, and the variance of the variance. This information allows the user to determine the precision of the results. The true average of a result, x, can be defined as

$$E(x) = \int xf(x)dx. \tag{6}$$

The true mean however is not known and is estimated by the Monte Carlo process where the sample mean $\bar{x}$ is defined as

$$\bar{x} = \frac{1}{N}\sum_{i=1}^{N} x_i. \tag{7}$$

Variance is a measure of how far a set of numbers is spread out. The true variance of all x values obtained is given by

$$\sigma^2 = \int (s - E(x))^2 f(x) dx = E(x^2) - E(x))^2. \quad (8)$$

The square root of the variance, σ, is the standard deviation. The estimated standard deviation, *S*, is given as

$$S^2 = \frac{\sum_{i=1}^{N} (x_i - \bar{x})^2}{N - 1}. \quad (9)$$

And finally, the estimated variance of $\bar{x}$ is given by

$$S_{\bar{x}}^2 = \frac{S^2}{N} \quad (10)$$

(X-5 Monte Carlo Team, 2008).

3.2 Trout Specimen

The trout specimen used for the model was physically caught at the Rainbow Trout Farm[4] in Sandy, OR. Figure 3 shows a photograph of a rainbow trout. The trout used in this research measured 35.5 cm from the tip of the head to the end of the tail fin. It measured approximately 40 mm at the thickest point and 80 mm from the bottom of the belly to the dorsal fin. The trout weighed approximately 658 g. The trout was immediately frozen after catch and slightly thawed for the CT scan that took place 3 days later.

Figure 3: Photo of a Rainbow Trout. Image courtesy of Paul at www.freedigitalphotos.net.

[4] Rainbow Trout Farm. 52560 East Sylvan Drive, Sandy OR 97055. http://www.rainbowtroutfarm.com/

3.3 Imaging

Both CT and MRI scans were obtained on the fish and were performed at the Oregon State University School of Veterinary Medicine. There are pros and cons for each type of imaging. MRI is typically superior in showing details of soft tissue and has excellent contrast resolution. CT is the exam of choice when imaging bone and has superior spatial resolution. Trout have a plethora of very tiny bones. The tiny rib bones were unable to be visualized on the MRI images (Figure 4). The CT images demonstrated the bone very well and the soft tissue detail was adequate for defining organ boundaries (Figure 5). For these reasons, the CT images were chosen to be used in the model creation.

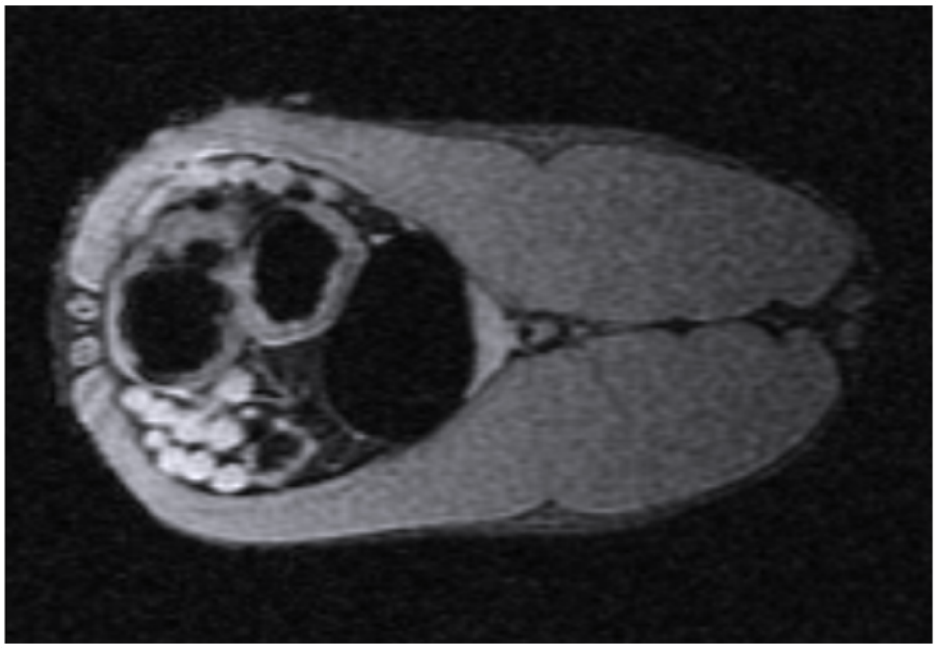

Figure 4: Coronal image slice of a trout obtained with MRI.

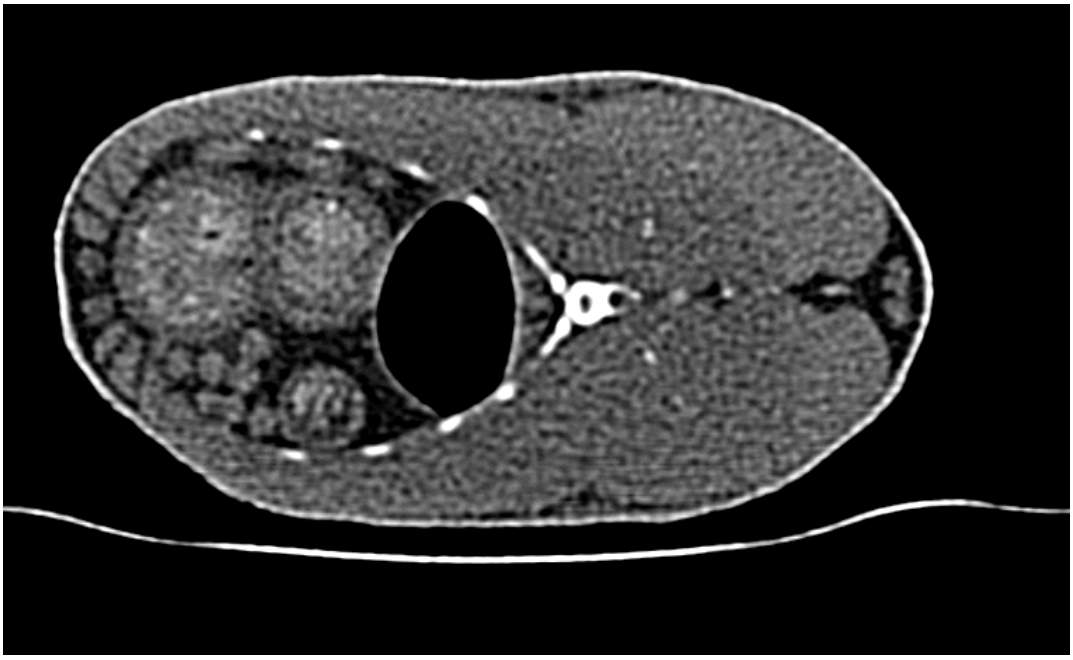

Figure 5: Coronal image slice of a trout obtaining with computed tomography.

The CT scanner utilized was a Toshiba Aquillion 64 slice. A helical scan was performed at 120 kVp, 50 mA and a pitch of 0.5. The slice thickness was 1 mm, resulting in a total of 362 slices. The slice matrix was 512 rows x 512 columns with a DFOV of 112.50 mm.

3.4 Segmentation

The DICOM images from the CT scan were loaded into 3D-Doctor and the relevant internal structures were contoured and segmented. The following segments were identified and contoured: swim bladder, skeleton, eyes, heart, liver, brain, stomach and esophagus, rectum/intestine, spleen, testes, and pyloric caeca. Due to difficulty in

deciphering the boundaries between some organs, multiple organs were included in some of the segments (Table 1). The kidneys were indistinguishable from surrounding tissue, so the area where the kidneys would reside was manually contoured. Figure 6 shows a coronal image of the trout with the boundaries that were drawn within 3D-Doctor. One of the benefits of 3D-Doctor is the ability to create complex surface renderings. These were created often throughout the contouring process to help visualize each organ (Figure 7 and Figure 8). The muscle segment in these figures was turned off in order to better visualize the remaining segments.

Table 1: Organs included in each contoured segment of the trout.

Segment	**Organs Included in Segment**
Brain	Brain
Esophagus	Esohpagus and Stomach
Eyes	Eyes
Heart	Heart
Kidneys	Kidney
Liver	Liver and Gallbladder
Muscle & Soft Tissue	Skin, Scales, Fins, Gills, Pharynx, Thyroid, Spinal Cord, Nerves, Vasculature, Muscle, and Miscellaneous Soft Tissue
Pyloric Caeca	Pyloric Caeca and Pancreas
Rectum	Intestine
Skeleton	Bone and Teeth
Spleen	Spleen
Swim Bladder	Swim Bladder
Testes	Testes

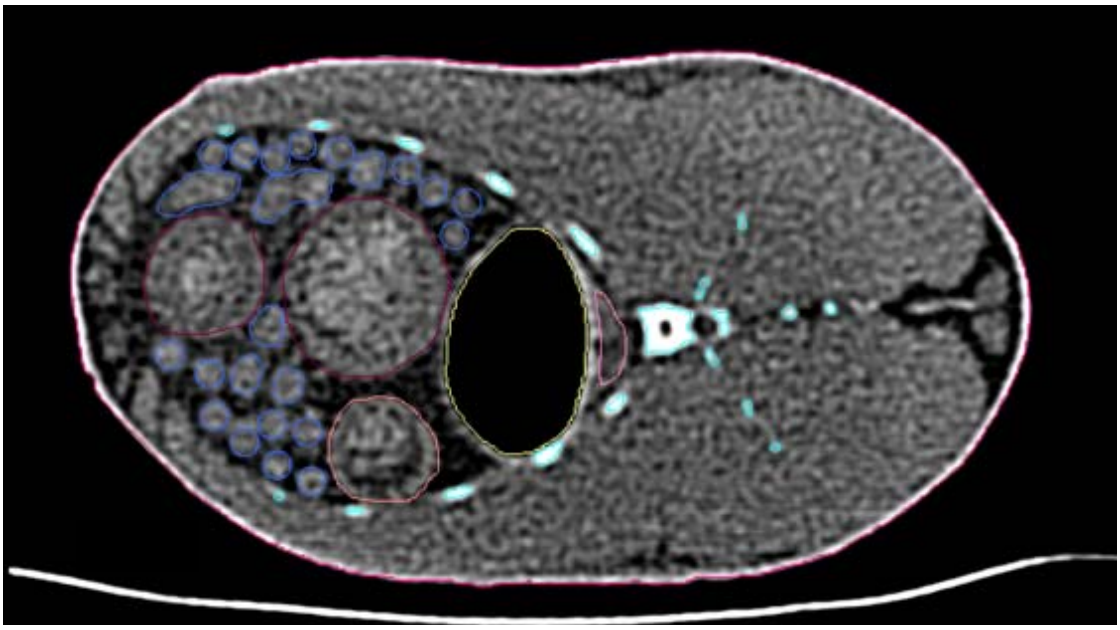

Figure 6: Coronal image slice of the trout showing the segmented boundaries of the organs.

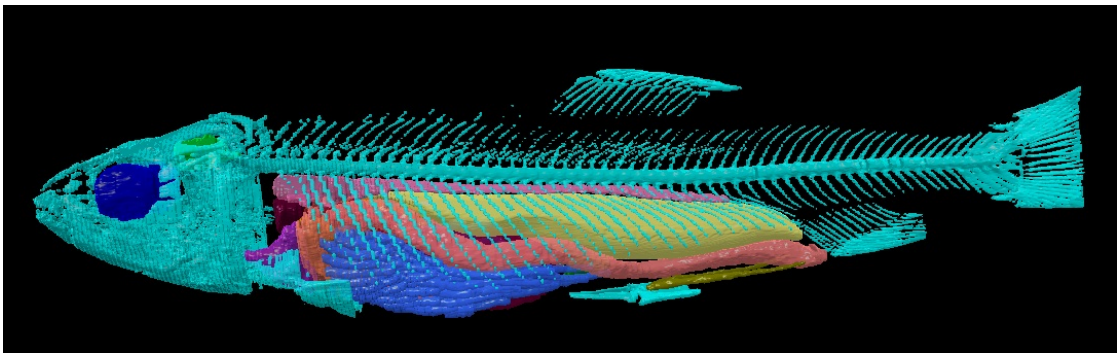

Figure 7: Complex surface rendering of the trout (side view) created in 3D-Doctor.

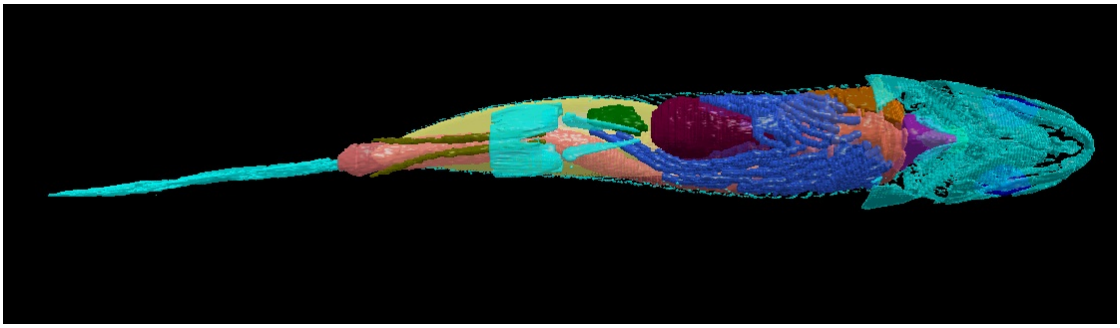

Figure 8: Complex surface rendering of the trout (plantar view) created in 3D-Doctor.

3D-Doctor is able to accurately calculate volume and surface area from these renderings. Volumes of each contoured object were calculated using this feature (Table 2). Using the densities of the equivalent human organ (where applicable), the mass of each organ was calculated (Table 2). Once the segmentation process was complete, a boundary file was created.

Table 2: Physical parameters used in the voxelized trout model.

Trout Organ or Tissue	Volume (cm^3)	Mass (g)	Density (g/cm^3)	Reference	Referenced Organ
Brain	0.566	0.58864	1.04	ICRU-44	Brain
Esophagus	13.751	14.369795	1.045	ICRP-89	Alimentary System
Eyes	1.936	2.07152	1.07	ICRU-44	Eye Lens
Heart	1.782	1.83546	1.03	ICRP-89	Hearat
Kidneys	4.02	4.221	1.05	ICRP-89	Kidney
Liver	7.145	7.5737	1.06	ICRP-89	Spleen
Muscle & Soft Tissue	554.325	582.04125	1.05	ICRU-44	Muscle, Skeletal
Pyloric Caeca	7.884	8.23878	1.045	ICRP-89	Alimentary System
Rectum	11.75	12.27875	1.045	ICRP-89	Alimentary System
Skeleton	12.502	24.00384	1.92	ICRU-44	Bone, Cortical
Spleen	0.512	0.54272	1.06	ICRP-89	Spleen
Swim Bladder	33.672	0.0404401	0.001201	Saunders	Lake Trout Swim Bladder (0-16.5 Feet)
Testes	0.372	0.38688	1.04	ICRU-44	Testis

3.5 Lattice Creation

The exportable boundary file from 3D-Doctor was imported into Voxelizer. For this project a compression factor of 4 was used. This decreases the array size by combining multiple voxels into one voxel. This will decrease the overall spatial resolution but is often necessary due to the computing power available and the limitations of MCNP (G. H. Kramer et al., 2010).

Along with the information from the uploaded boundary file, Voxelizer requires some information about the images to be input by the user in order to create the lattice: the number of columns, rows and planes, as well as the pixel width and slice thickness. This information can be found within 3D-Doctor. Voxelizer generates the geometry

portion, containing the lattice structure, of the MCNP input file. The user is left only with creating the source and materials.

3.6 Radiation Transport Simulations

Fourteen universes were created within the lattice geometry: muscle and miscellaneous soft tissues, swim bladder, skeleton, eyes, heart, liver, brain, esophagus/stomach, intestine/rectum, spleen, testes, pyloric caeca, kidney, and the surrounding water. The elemental composition (Table 3) of human organs and tissues were used as a substitute for trout tissue composition, consistent with previous models (E. A. Caffrey, 2012; E. Caffrey & Higley, 2013; Kinase, 2008; Stabin et al., 2006). According to the Food and Agriculture Organization of the United Nations, the chemical composition of trout is 70-79% water, 1.2-10.8% fat, and 18.8-19.1% protein (Murray & Burt, 2001). This is similar to human composition (Forbes, Cooper, & Mitchell, 1953) and thus thought to be an acceptable substitute. The gastrointestinal tract was modelled as a homogenous material; the contents of which were not taken into account. The swim bladder is unique in that there is not an analogous human organ. The gases that make up the swim bladder are hydrogen, oxygen, and nitrogen. The fractions of each can vary depending on the depth the fish is residing in water. In a study done by Saunders, the swim bladder gas contents of lake trout (*Salvelinus namaycush*) from Lake Huron were evaluated. The values obtained for fish residing at depths of 0-16.5 feet were used in this research (Saunders, 1953). While it is not necessary to calculate the energy deposited in the swim bladder, it is essential to have its density and elemental composition as it can affect the radiation transport when calculating energy absorption to the other organs.

Table 3: Referenced human organs used as substitutes for the elemental composition of the organs in the voxelized model of the trout.

Trout Organ or Tissue	Reference	Referenced Human organ
Brain	ICRU-44	Brain Gray/White Matter
Esophagus	ICRP-89	Esophagus
Eyes	ICRP-89	Eyes
Heart	ICRP-89	Heart
Kidney	ICRP-89	Kidneys
Liver	ICRP-89	Liver
Muscle & Soft Tissue	ICRP-89	Muscle
Pyloric Caeca	ICRP-89	Stomach
Rectum	ICRP-89	Large Intestine
Skeleton	ICRU-44	Cortical Bone
Spleen	ICRP-89	Spleen
Testes	ICRU-44	Testes

The composition of stream and lake water varies from one place to another, and can also vary both seasonally and along the stream's path. The major source of dissolved minerals in streams and lakes is the rocks the water moves over. Temperature influences the amount of dissolved gases (e.g., oxygen). Seasonal variations in stream-water composition may reflect differing precipitation amounts, as well as the portion of the stream's flow that is contributed by groundwater (Drever, 1982). The elemental composition of the water used in this study was the mean composition of river waters in North America as reported by Holland (Table 4).

Table 4: Mean Composition of River Waters in the World (Holland, 1978).

Mean Composition of River Waters of the World[a]

Continent	HCO_3^-	SO_4^{2+}	Cl^-	NO_3^-	Ca^{2+}	Mg^{2+}	Na^+	K^+	*Fe*	SiO_2	*Sum*
North America	68	20	8	1	21	5	9	1.4	0.16	9	142
South America	31	4.8	4.9	0.7	7.2	1.5	4	2	1.4	11.9	69
Europe	95	24	6.9	3.7	31.1	5.6	5.4	1.7	0.8	7.5	182
Asia	79	8.4	8.7	0.7	18.4	5.6	9.3		0.01	11.7	142
Africa	43	13.5	12.1	0.8	12.5	3.8	11		1.3	23.2	121
Australia	31.6	2.6	10	0.05	3.9	2.7	2.9	1.4	0.3	3.9	59
World	58.4	11.2	7.8	1	15	4.1	6.3	2.3	0.67	13.1	120
Anions[b]	0.958	0.233	0.220	0.017							1.428
Cations[b]					0.750	0.342	0.274	0.059			1.425

[a]Livingstone (1963); concentrations in ppm.
[b]Millequivalents of strongly ionized components.

The source of radiation was assumed to be homogenously distributed throughout each source organ. Due to the small size of some of the source organs, the source sampling efficiency had to be decreased from the default of 1% to 0.0001%. This has no effect on the results obtained. Absorbed energy in each segment was tabulated via the *f8 (energy deposition) tally. 2,000,000 histories were run for each electron energy and 5,000,000 histories were run for each photon energy. These history numbers were chosen to obtain results with an acceptable amount of error while attempting to keep the computer run time low.

In total, 210 radiation transport simulations were performed using MCNPX with each of the following segments as a source: skeleton, esophagus, kidney, liver, muscle and soft tissues, pyloric caeca, rectum, spleen, testes, and the water. Incident electron energies of 0.1, 0.2, 0.4, 0.5, 0.7, 1.0, 1.5, 2.0 and 4.0 MeV and photon energies of 0.01, 0.015, 0.02, 0.03, 0.05, 0.1, 0.2, 0.5, 1.0, 1.5, 2.0, and 4.0 MeV were used for

each source organ. A truncated version of one of the MCNP input files can be found in Appendix C.

4 Results and Discussion

Absorbed fractions (AFs) were calculated for each identified segment as both a source and a target; results for the surrounding water as an external source are also included. The complete tabulated data for photons can be found in Appendix A and electrons in Appendix B. This data presents all calculated AFs as a function of source, target, energy, and radiation type.

4.1 Photon Absorbed Fractions

4.1.1 Self-Absorbed Fraction Analysis

Figure 9 displays the self-AFs for self-irradiation (target organ is the source organ) of photon energy in the energy range of 0.01-4.0 MeV. The photon self-AF decreases with increasing energy, except in the 0.1-0.5 MeV range, where the values somewhat level off; consistent with the properties of photon interactions.

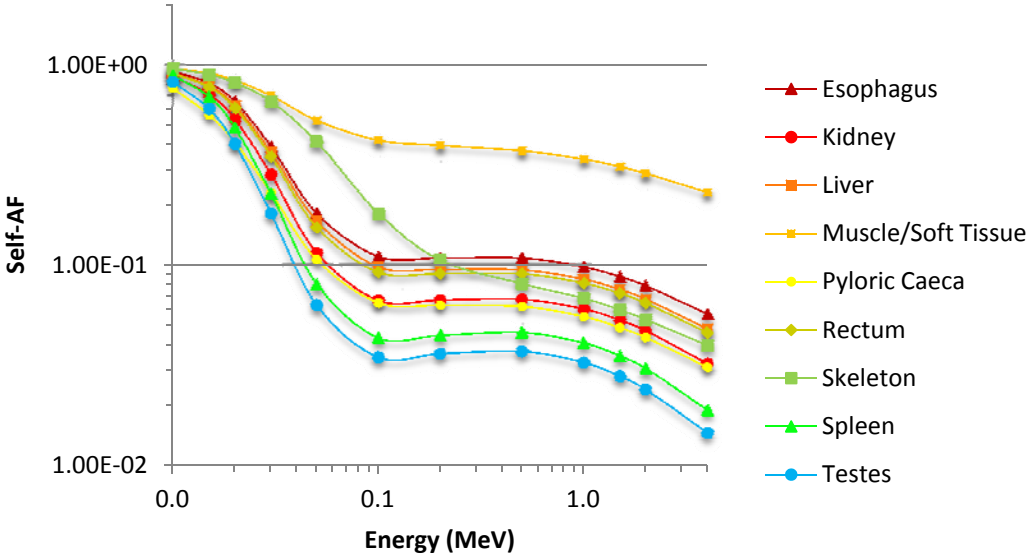

Figure 9: Self-AFs of photon energy in the trout model.

Figure 10 displays the self-AFs for the liver and the pyloric caeca. The physical properties of mass, volume and density for the two organs are very similar: 7.57 g and 8.24 g, 7.15 cm^3 and 7.89 cm^3, and 1.06 g/cm^3 and 1.045 g/cm^3 respectively. For both segments the self-AF decreases with increasing energy. However, the self-AF values for these segments display some significant differences, especially at energies below 0.1 MeV. The liver and pyloric caeca are rather different in shape, with the liver being a single solid mass and the pyloric caeca having many long thin tubes. This leads to the conclusion that photon self-AFs are dependent on photon energy and organ geometry rather than just the physical properties of mass, volume, or density.

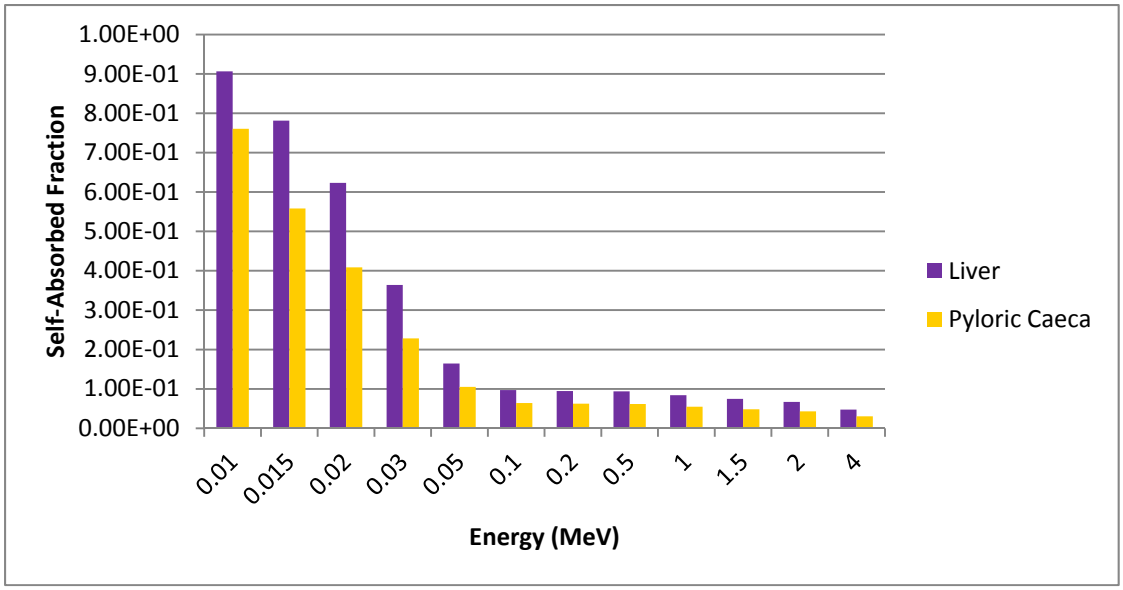

Figure 10: Self-absorbed fractions of photon energy for the liver and the pyloric caeca in the trout.

4.1.2 Cross-Irradiation Analysis

Figure 11 graphically presents the AFs as a function of energy for a photon source located in the kidney segment. The absorbed energy in the total body of the trout decreases from nearly 100% at 0.010 MeV to approximately 35% at 4.0 MeV.

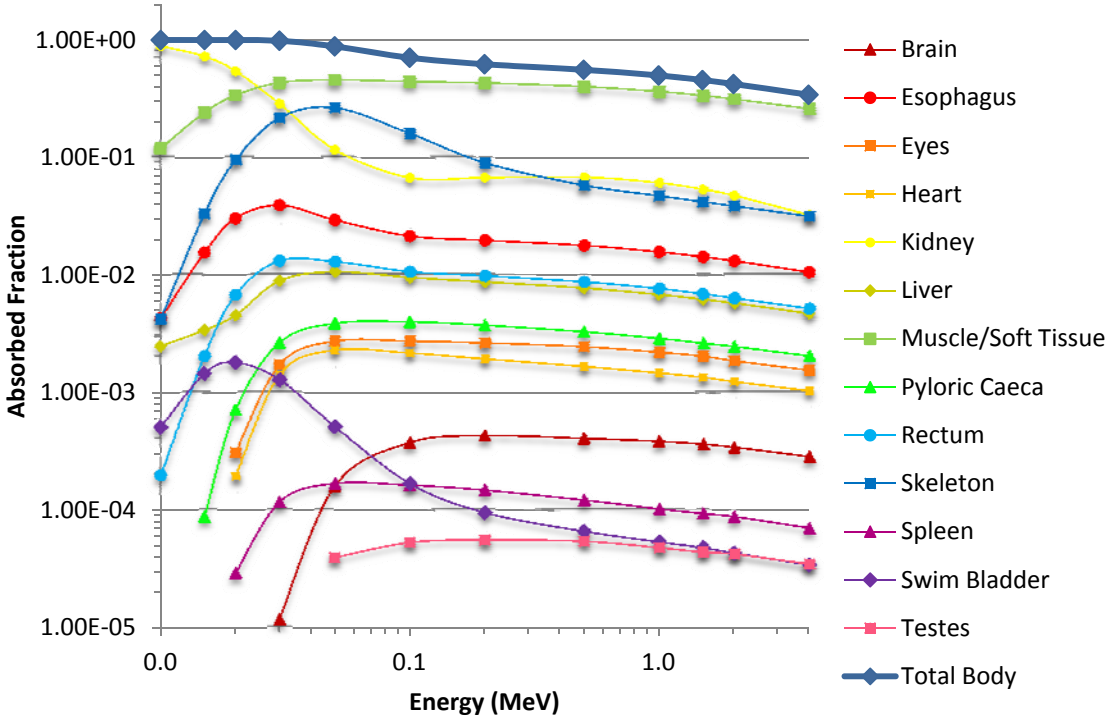

Figure 11: Photon AFs for a source located in the kidney segment. AFs whose relative error exceeded 10% have been omitted.

At the lowest energy (0.010 MeV), nearly 100% of the absorbed energy is in the source organ. Due to the penetrating nature of photons, at about 0.025 MeV, the majority of the deposited energy changes from the source segment to the muscle segment.

The AFs in most of the target organs increase sharply with increasing energy. This increase levels off around 0.1 MeV after which the AF in the target segments decrease minimally with increasing energy. At energies above 0.1 MeV, the photons can travel

greater distances compared to the size of the organs and the photons are able to escape the fish before depositing their full energy, if any.

The AF in the swim bladder segment behaves somewhat differently. The AF increases with increasing energy until approximately 0.02 MeV after which the AF decreases sharply with increasing energy. The AF does not appear to reach a threshold as the other target segments demonstrate. This is most likely due to the unique makeup of the swim bladder. The contents of the swim bladder are gaseous in nature and thus have a density far less than the other segments in the trout. This difference in density results in a reduced AF as photon interactions are less likely to occur in a gaseous medium.

Figure 12 displays the AFs for a source located in the skeleton. The AF results are consistent with the AF results obtained with the kidney as the source. The target AFs obtained with the skeleton source are generally closer in value to each other in comparison to the kidney as a source. This is due to the skeleton being distributed throughout the body of the fish allowing the incident photon energy to reach all target organs consistently.

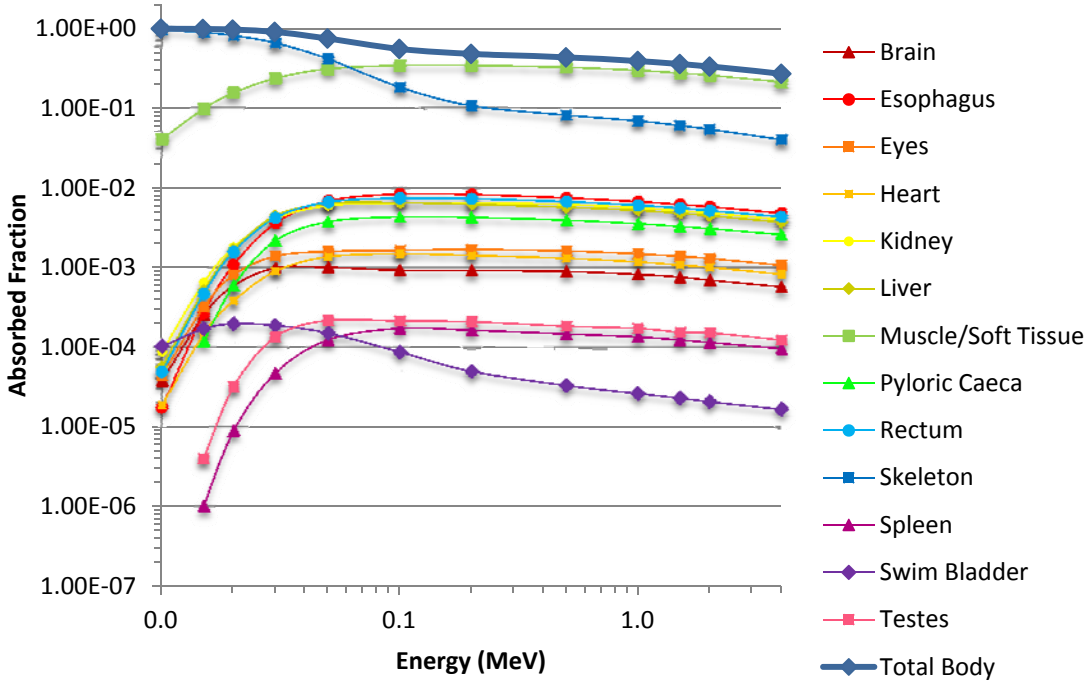

Figure 12: Photon AFs for a source located in the skeleton segment. AFs whose relative error exceeded 10% have been omitted.

4.1.3 External Source Analysis

Figure 13 graphically presents the AF in target organs for a photon source located externally in the surrounding water. The AF increases initially with increasing photon energy. The photoelectric effect is the dominant reaction at lower energies and indicates the full photon energy being absorbed. By about 0.1 MeV, all target segments are absorbing some of the incident radiation. At 0.1 MeV, the AF reaches a semi-threshold and does not increase with increasing energy. At these energies, Compton scattering begins to be the dominant reaction. Photons are more likely to

travel through the fish without interacting or without depositing their full energy. This is demonstrated by the threshold seen in the graph. This is true for all segments except the skeleton and the swim bladder segment. This is most likely due to their differing density and elemental composition in comparison with the other segments.

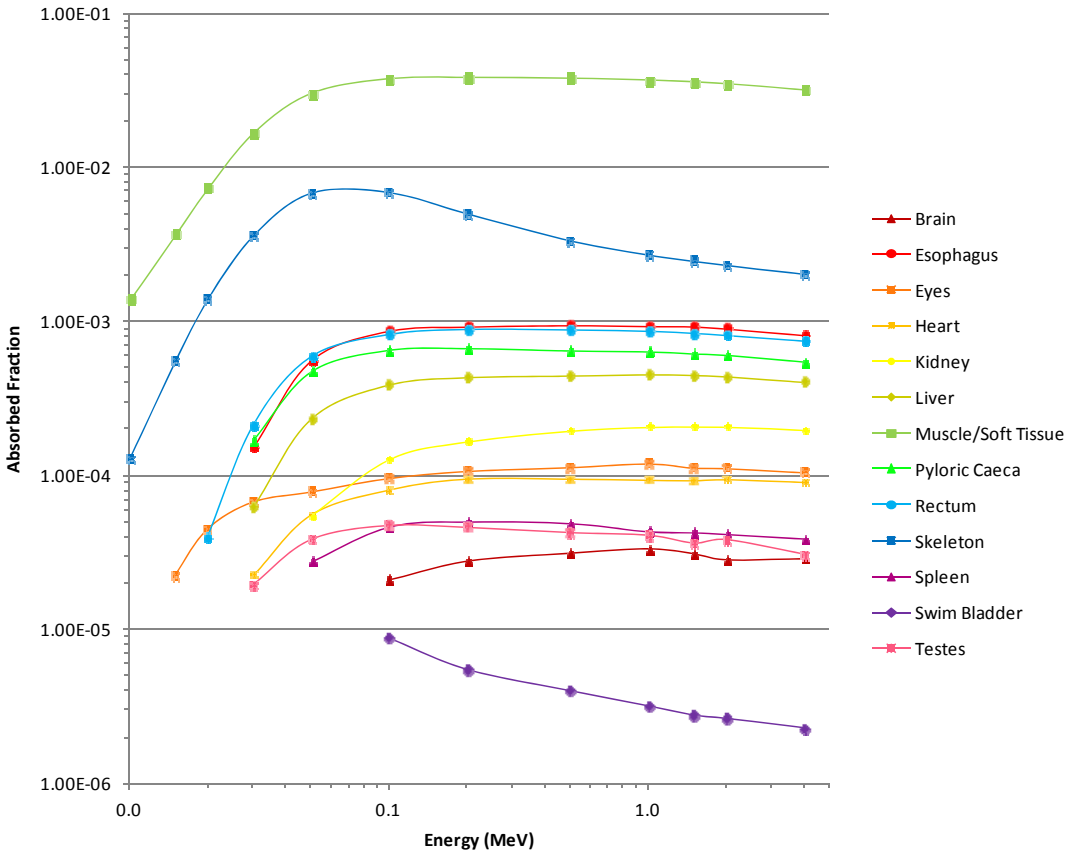

Figure 13: Photon AFs in the trout for an external source located in the surrounding water. AFs whose relative error exceeded 10% have been omitted.

4.2 Electron Absorbed Fractions

4.2.1 Self-Absorbed Fraction Analysis

Figure 14 displays the self-absorbed fractions for self-irradiation (target organ is the source organ) of electron energy in the energy range of 0.1-4.0 MeV. The AF in the source segments gradually decrease as the electron energy increases. This graph demonstrates that not all of the incident electron energy is deposited within the source organ; which differs from human dosimetry. This work validates that electrons should be treated as penetrating radiation in small organism dosimetry.

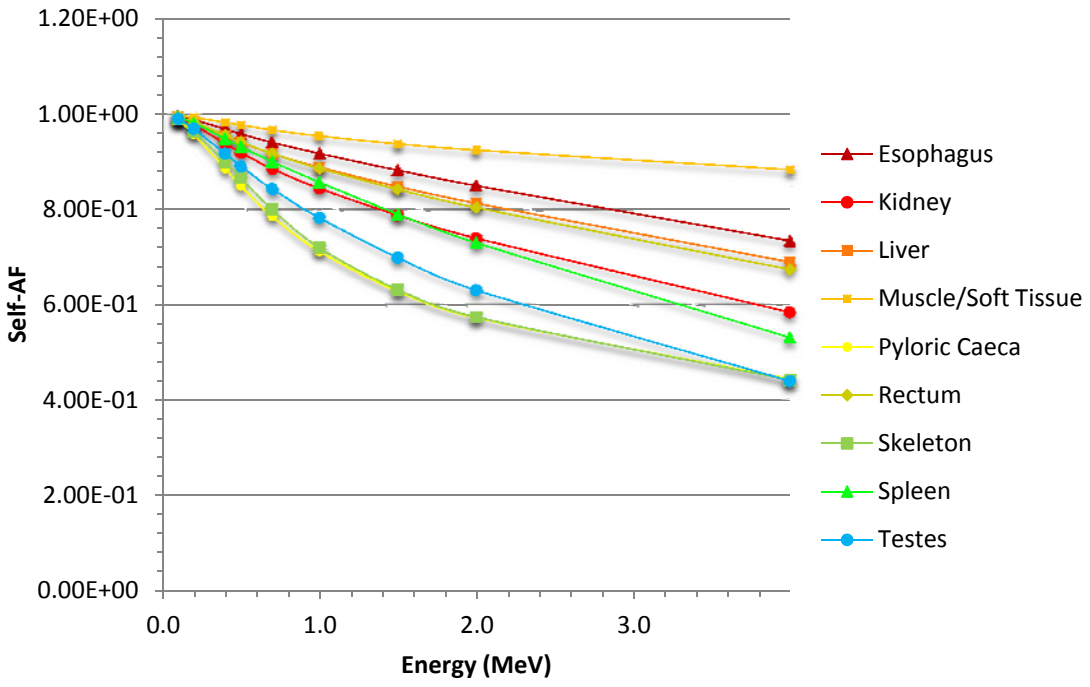

Figure 14: Self-AFs of electron energy in the trout.

Figure 15 presents the self-AFs of electron energy in the liver, pyloric caeca, rectum and esophagus of the trout. As mentioned previously, the liver and the pyloric caeca have similar mass, volumes, and density. As shown in the figure, the self-AFs can vary significantly, especially as the energy increases. On the other hand, the rectum and esophagus segments also have similar mass, volume, and density (Table 2). The AFs for these segments remain quite close, even as the energy increases. This demonstrates that the self-AF is not only dependent on the physical properties of mass and density. The liver and pyloric caeca are quite different in shape, while the rectum and esophagus are very similar. From this, it can be concluded that the shape of the organ plays a significant role in determining how much electron energy will be absorbed by the source organ.

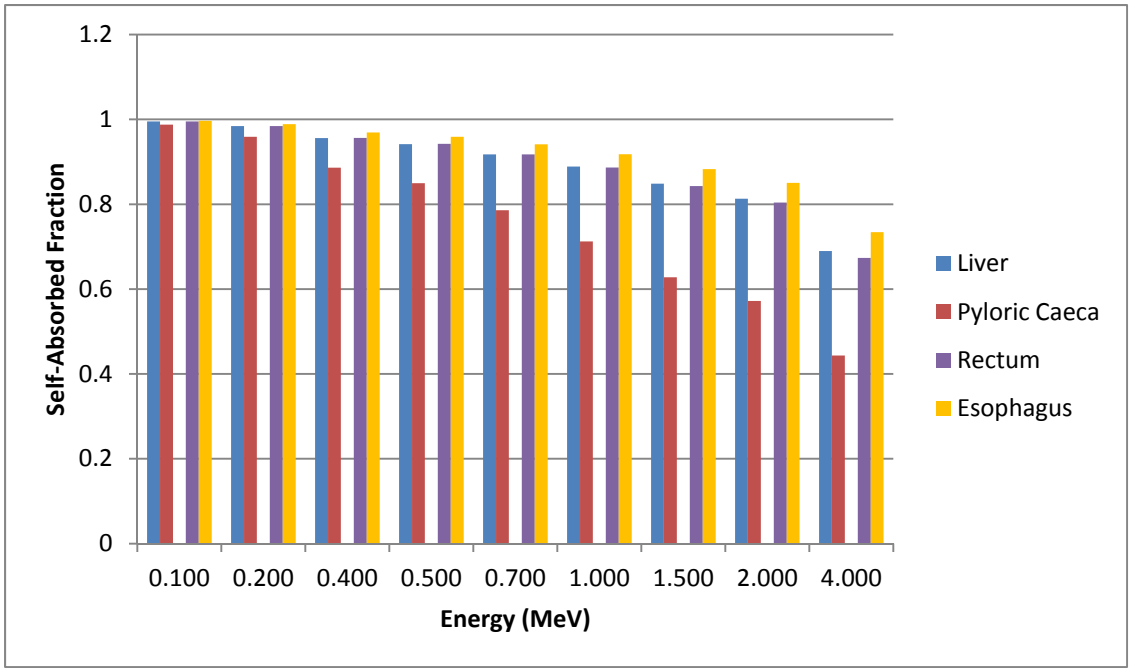

Figure 15: Self-AFs of electron energy in the liver, pyloric caeca, rectum and esophagus of the trout.

Figure 16 displays the self-AFs for incident electron energy of 2.0 MeV for all the source organs in order of increasing mass. There appears to be a trend of increasing self-AF with increasing mass, with the exception of the pyloric caeca and the skeleton. These two organs differ from the other organs mainly in their geometry. They are each made up of many small thin parts or tubes. This allows more electrons to escape as the electrons don't have to travel nearly as far to escape the organ. This demonstrates that mass and AF are correlated if the geometry of the organs isn't vastly different. This once again demonstrates that geometry plays an important role in determining the self-AF.

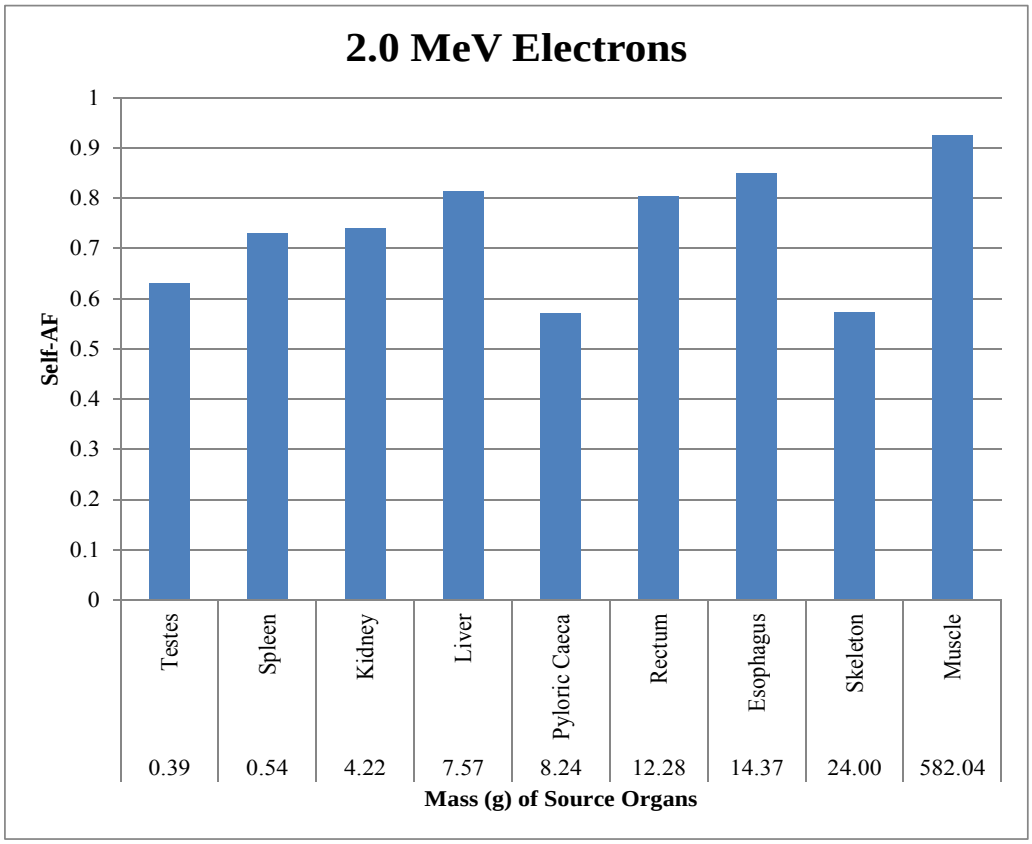

Figure 16: Self-AFs in source segments in order of increasing mass for incident electron energy of 2.0 MeV.

4.2.2 Cross-Irradiation Analysis

Figure 17 and Figure 18 graphically present the cross-irradiation that occurs with electrons in small organisms. AFs for a source located in the kidney and liver segment, respectively are shown. Nearly 100% of the radiation stays within the fish for electron sources at all energies, however, the graphs demonstrate that not all of the

incident electron energy is deposited within the source organ. The AF in the target segments gradually increases with increasing energy.

These graphs demonstrates that the location of the target segment in relation to the source segment is the primary indicator for what the AF will be in the target segments. Besides the source segment, those segments closest in location to the source will have the greatest AF.

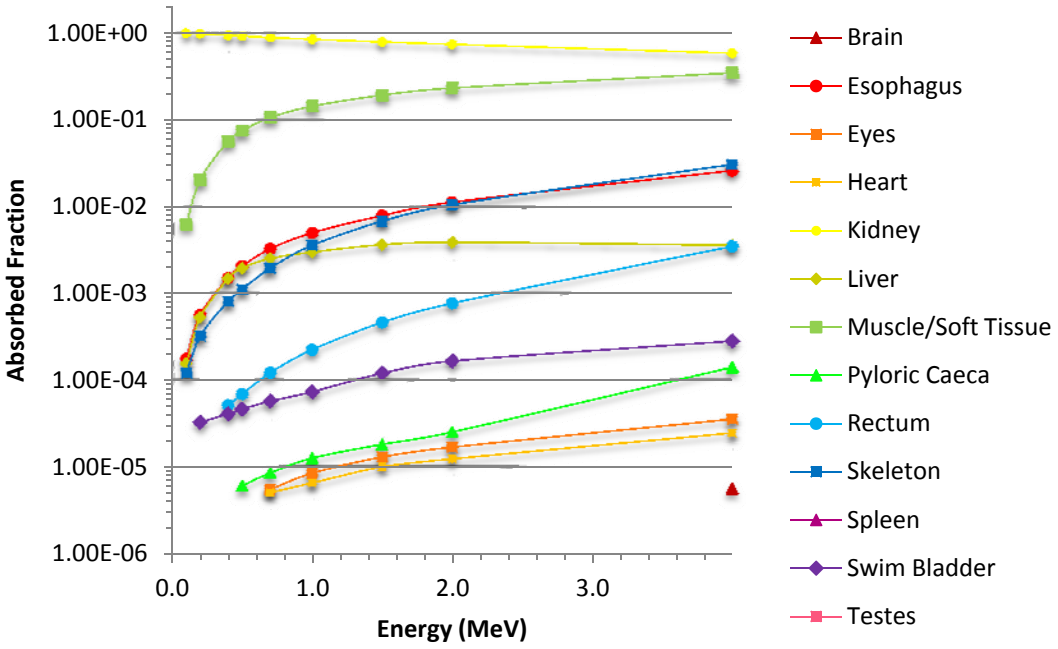

Figure 17: Electron AFs for a source located in the kidney segment of the trout. AFs whose relative error exceeded 10% have been omitted.

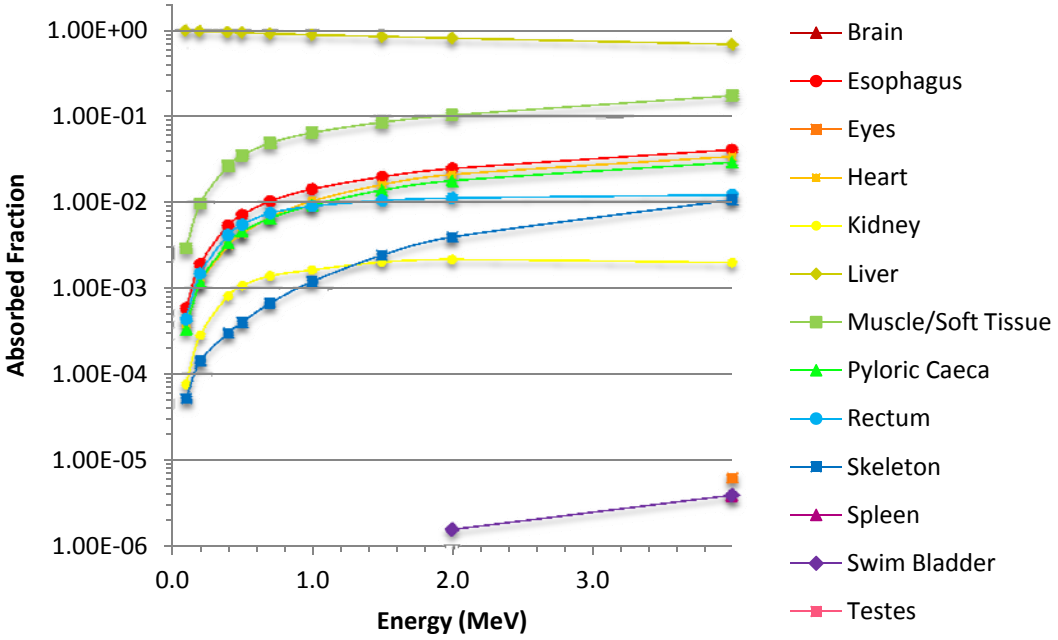

Figure 18: Electron AFs for a source located in the liver segment of the trout. AFs whose relative error exceeded 10% have been omitted.

4.2.3 External Source Analysis

Figure 19 graphically presents AFs for an external source located in the water surrounding the trout. As expected, due to the limited penetrability of electrons, most of the incident electron energy is deposited outside of the fish. With increasing energy, more energy is deposited in the trout, with the majority of that energy deposited in the muscle segment. This is primarily due to the location of the muscle in relationship to the water. The internal organs are generally surrounded by muscle and bone, providing them some protection from the incident electrons. As the incident

electron energy increases, however, more target segments begin to absorb some electron energy.

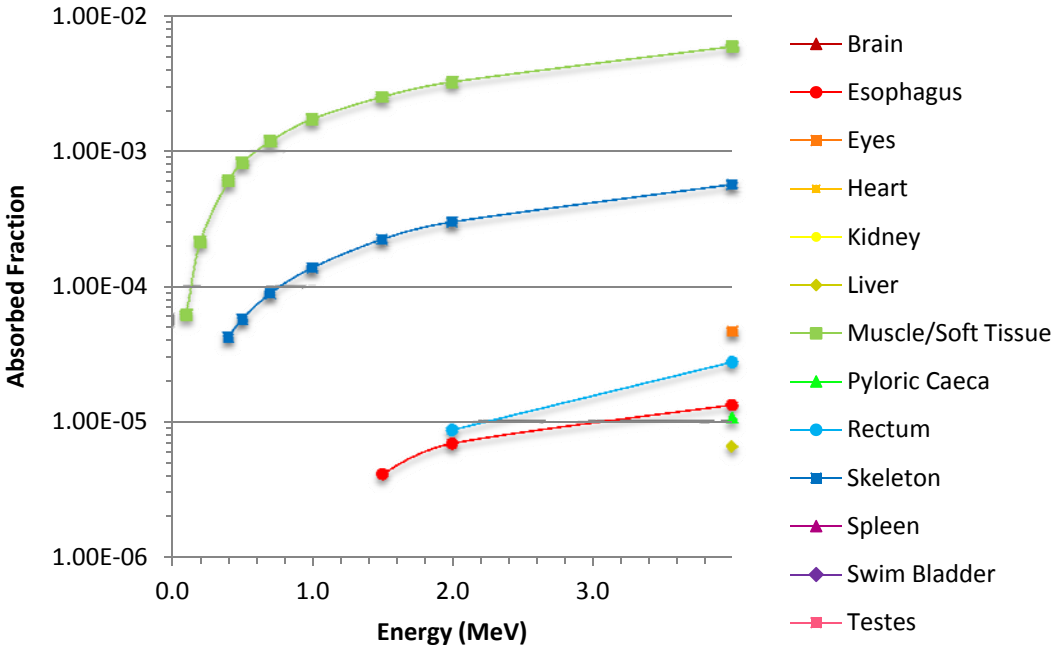

Figure 19: Electron AFs for an external source located in the surrounding water. AFs whose relative error exceeded 10% have been omitted.

4.3 Comparison with Other Models

4.3.1 Mouse and Rat Model

Figure 20 and Figure 21 are shown below and demonstrate the AFs of photon energy for a source located in the kidneys of a rat model (Stabin et al., 2006) and the trout model. The AFs for the rat model closely resemble those of the trout model, with the

small differences being attributable to differences in individual organ masses and geometries.

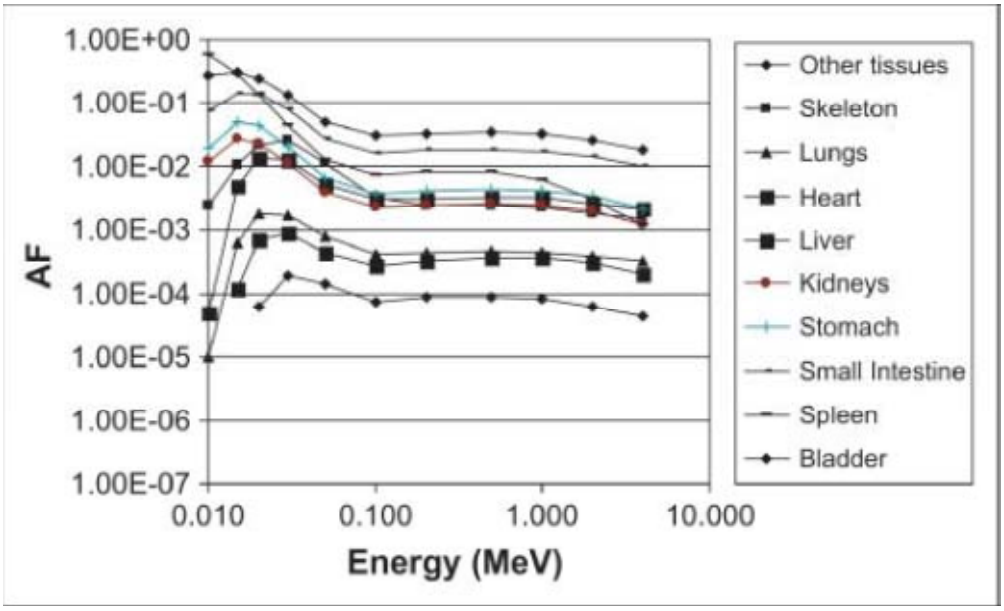

Figure 20: Plot of photon AFs for the spleen as a source in a rat model (Stabin et al., 2006).

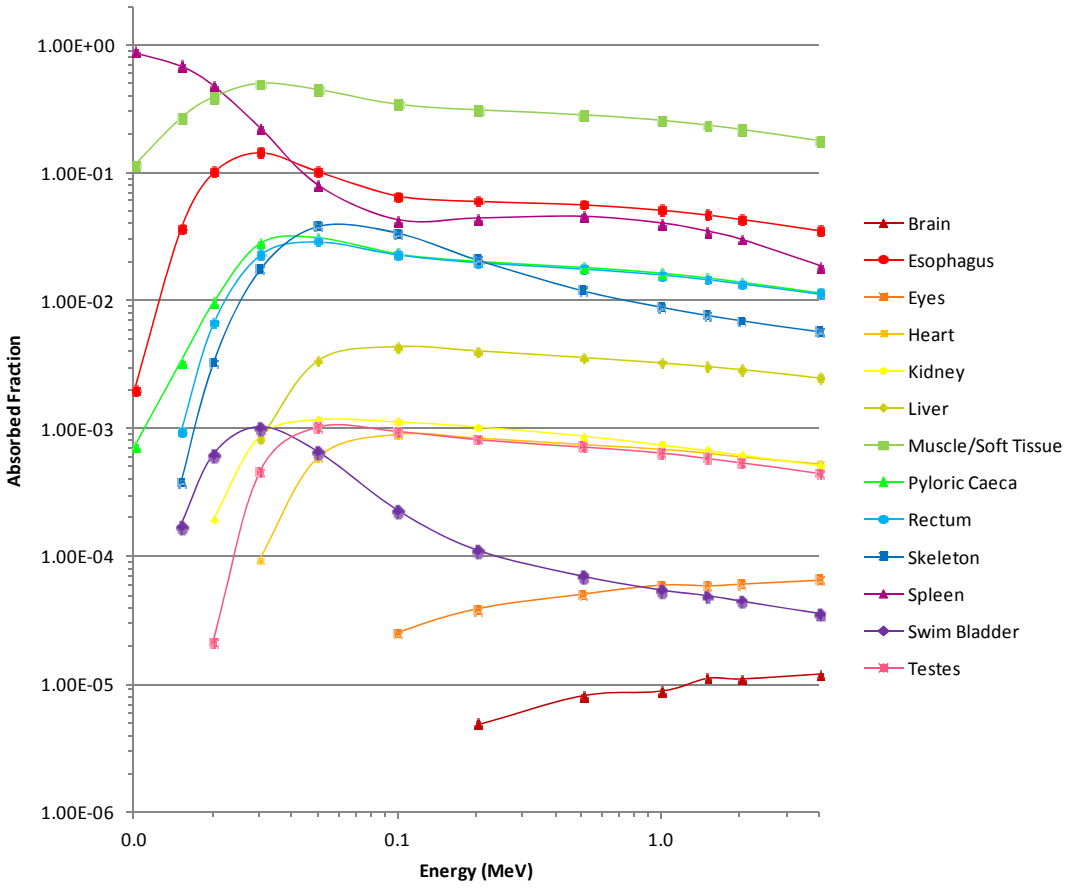

Figure 21: Photon AFs for the spleen as a source in the trout model.

Figure 22 and Figure 23 show the AFs of electron energy for a source located in the liver of a rat and mouse model, respectively (Stabin et al., 2006). Figure 24 presents the AFs of electron energy in the trout model with the liver as a source. Once again, the AF results in the trout model mirror those of the rat and mouse models, with the differences attributable to individual organ masses and geometries. These figures

demonstrate that there is significant cross-irradiation for high energy electrons. Thus, the assumption that all electron energy is absorbed in the source organ is inaccurate for small organs such as those in located in these animals.

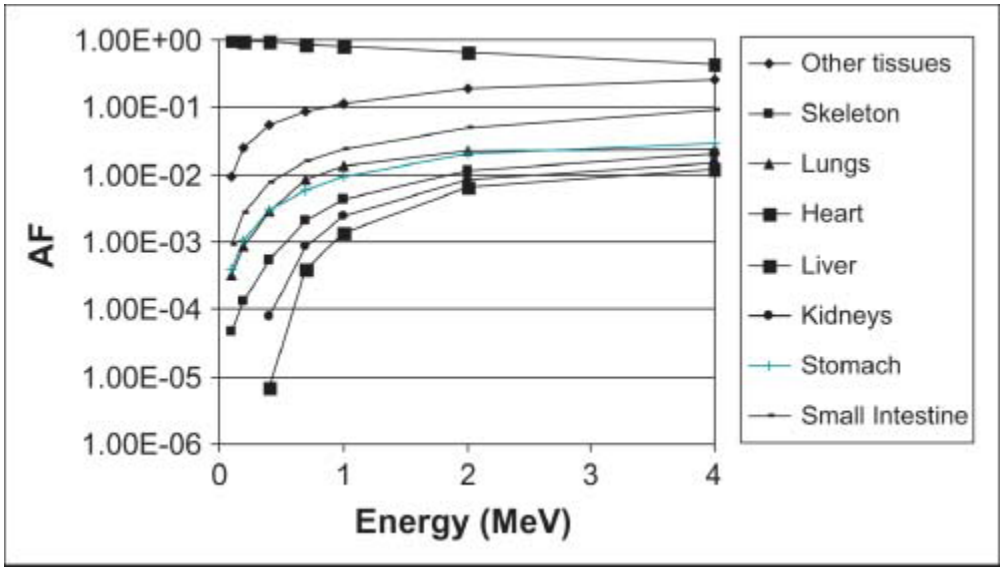

Figure 22: Plot of electron AFs for liver as a source in a rat model (Stabin et al., 2006).

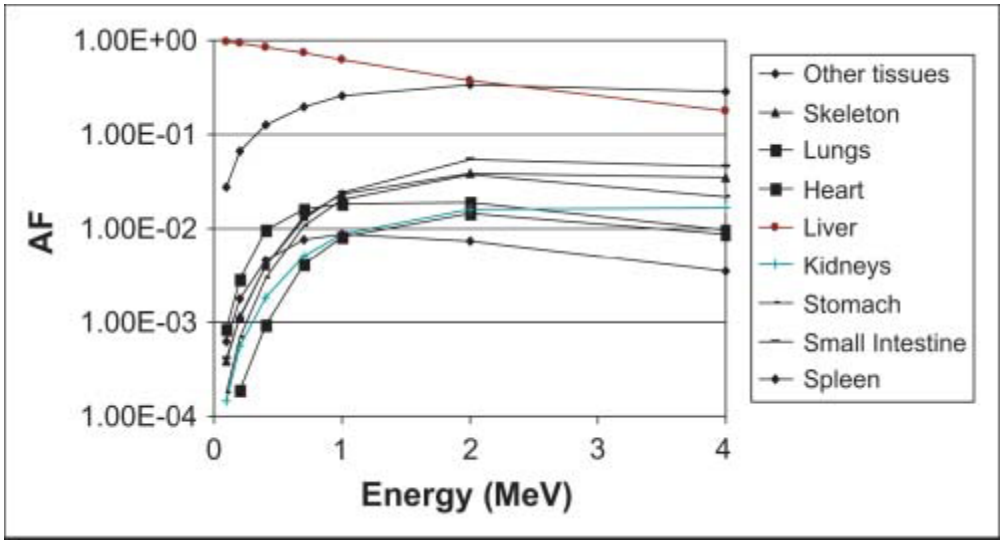

Figure 23: Plot of electron AFs for liver as a source in a mouse model (Stabin et al., 2006).

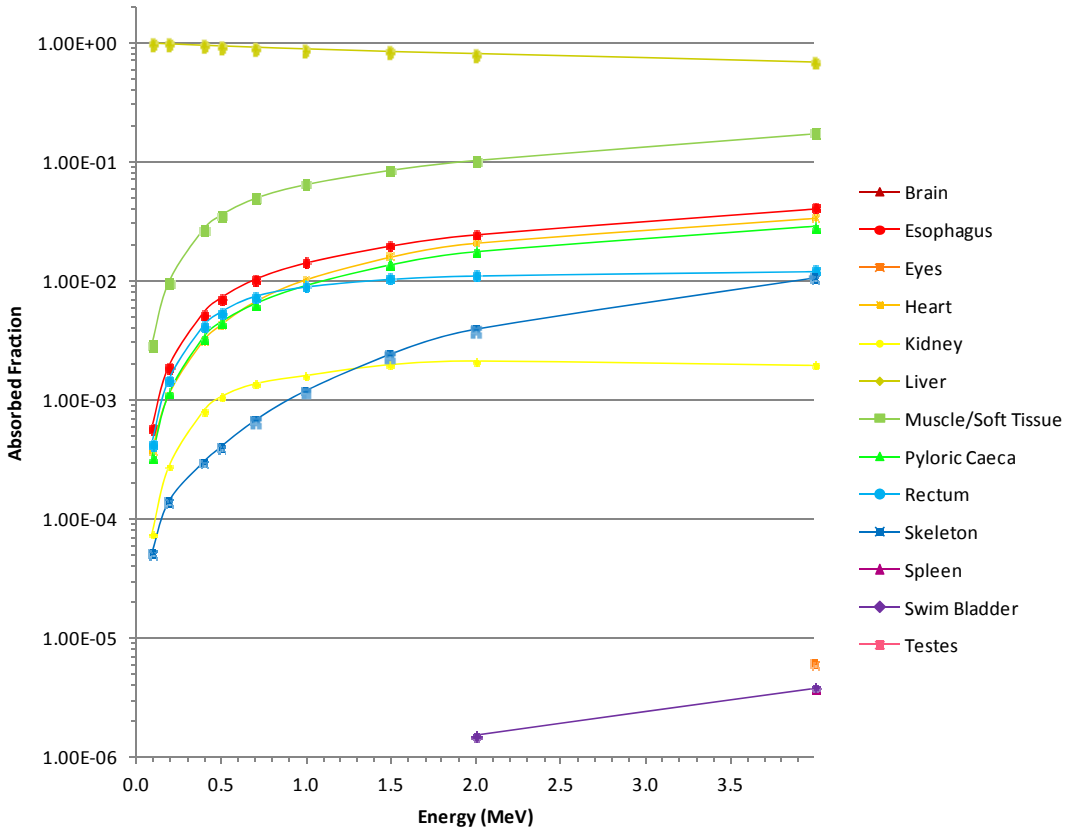

Figure 24: Plot of electron AFs in the trout model with the liver as the source. AFs whose relative error exceeded 10% have been omitted.

4.3.2 Frog Model

Figure 25 displays the self-absorbed fractions of electron energy for the liver, kidneys and spleen of a frog model, along with the kidneys of a mouse (Kinase, 2008). Figure 26 displays the self-AFs of electron energy for the liver, kidney and spleen of the trout model. While both graphs show that the self-absorbed fraction decreases with

increasing energy, the value of the self-AFs in the frog drop off much quicker at energies above 0.5 MeV, with almost all of the energy escaping the source organ at 4.0 MeV. In the trout model, the self-AF at 4.0 MeV ranged from 53-69% for the kidney, liver and spleen. These differences can be explained by the large differences in organ volume and mass. The respective trout organs are much larger in mass and volume than those of the frog resulting in a higher AF.

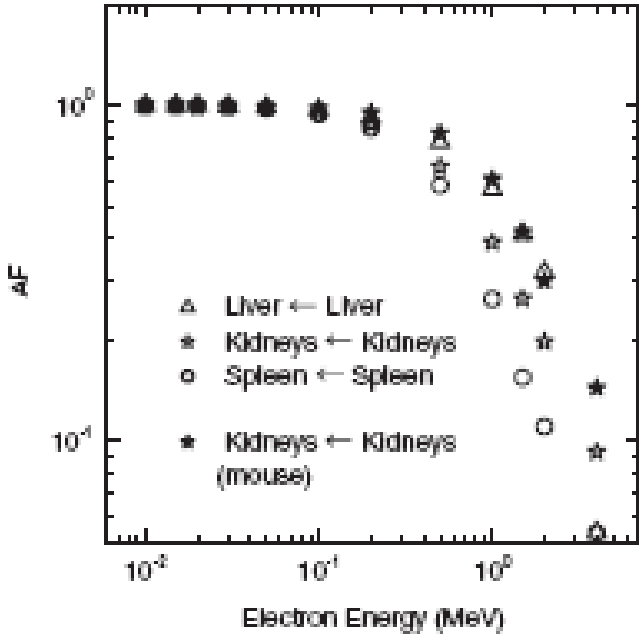

Figure 25: Self-AFs of electron energy in the spleen, kidneys, and liver of the voxel-based frog phantom. The self-AFs in the kidneys of a mouse phantom are also plotted (Kinase, 2008).

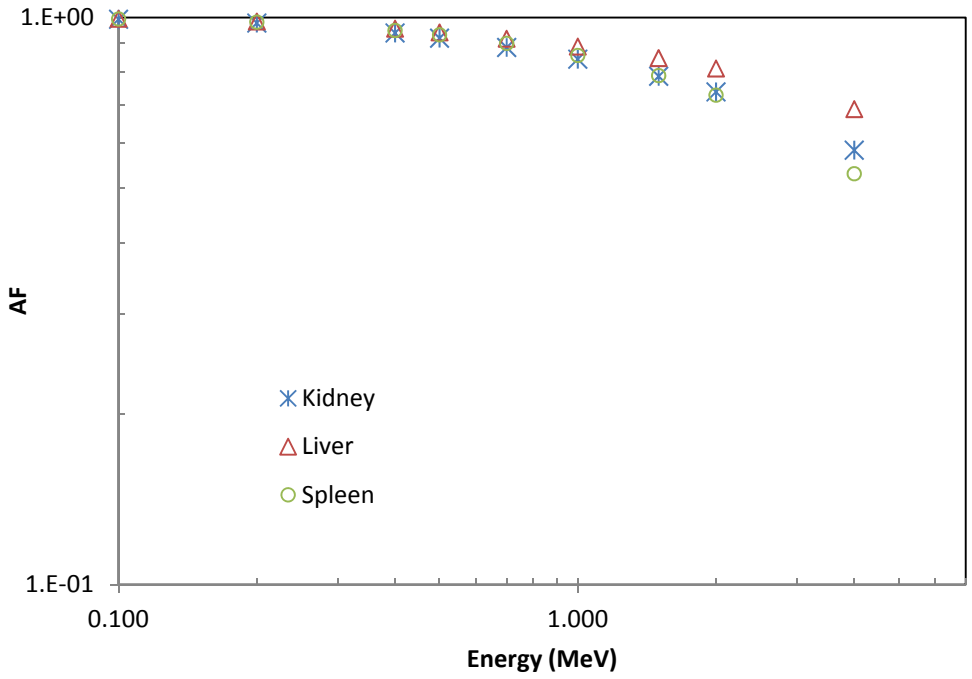

Figure 26: Electron Self-AFs for the kidney, liver and spleen in the trout model.

Figure 27 displays the self-AFs of photon energy for the liver, kidneys and spleen of a frog model, as well as the kidneys of a mouse model (Kinase, 2008). Figure 28 displays the self-AFs of photon energy for the kidney, liver and spleen of the trout model. Both graphs demonstrate a decrease in self-AF with increasing energy and both graphs show a levelling off of self-AF starting at 0.1 MeV. While the trends in the graphs are similar, the self-AF values in the trout model are much larger than those of the frog. This again can be explained by the larger sized trout organs in comparison with the frog organs.

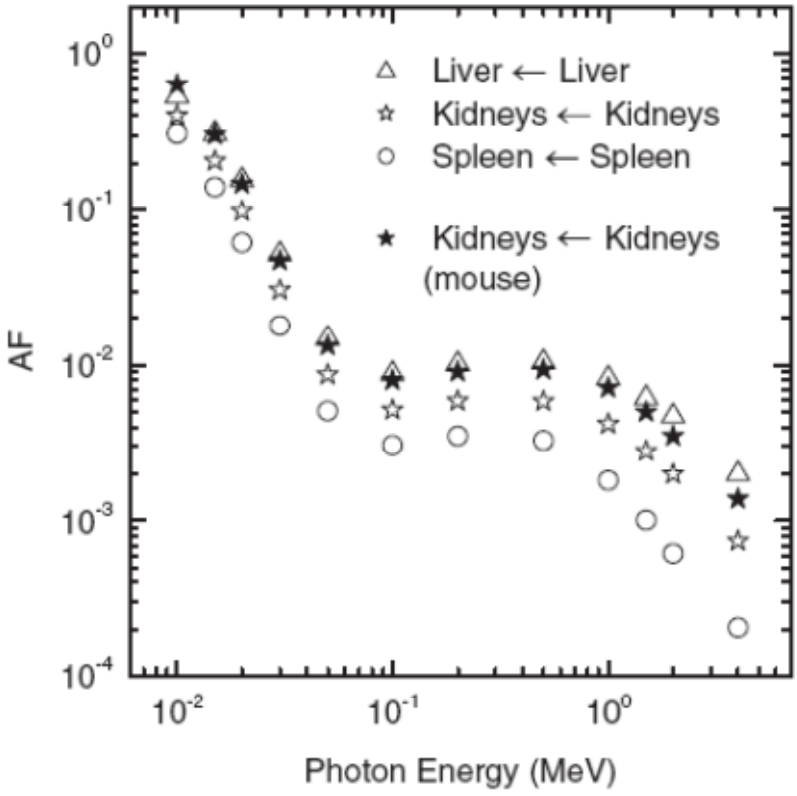

.

Figure 27: Self AFs of photon energy in the spleen, kidneys, and liver of the voxel-based frog phantom. The self AFs in the kidneys of the mouse are also plotted (Kinase, 2008).

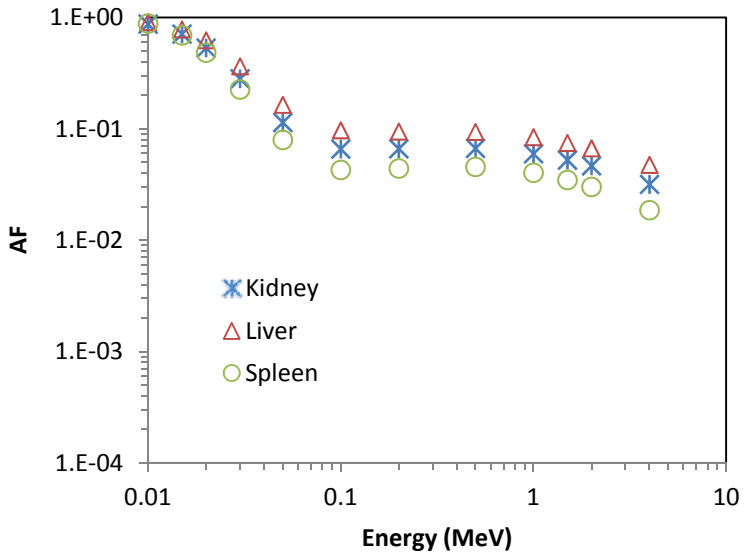

Figure 28: Photon self AFs for the kidney, liver and spleen of the trout model.

4.3.3 Flatfish Model

Figure 29 and Figure 30 display the AFs of electron energy for a source located in the gonads of a flatfish and a trout, respectively. The trout AFs closely resemble those of the flatfish. The differences can be attributed to small differences in organ size,

physical geometry and differing organs included in each modelled segment.

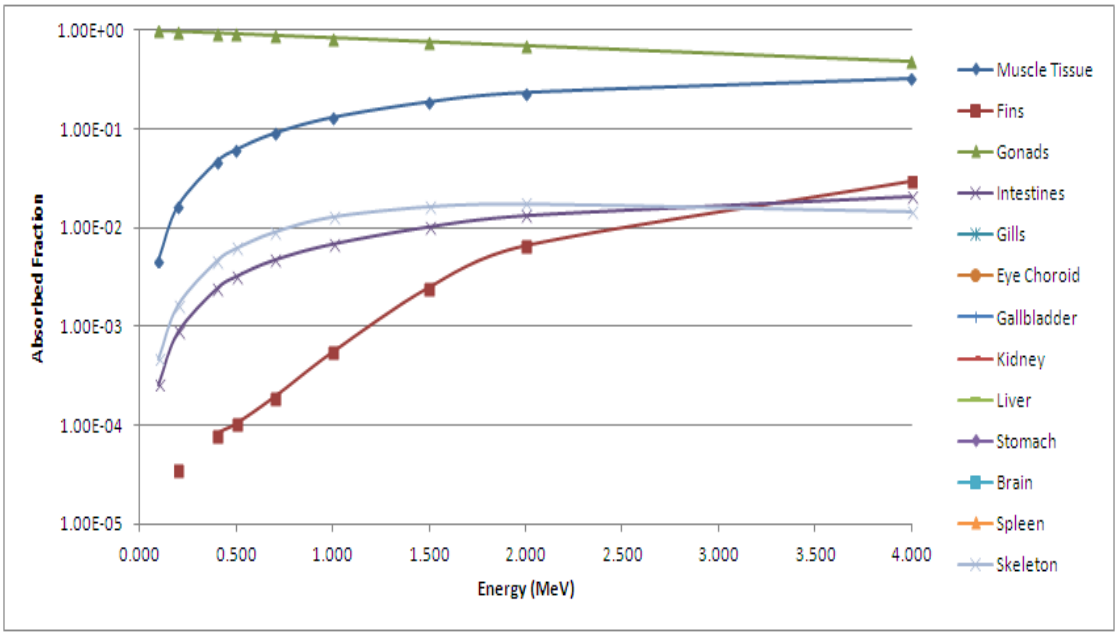

Figure 29: AFs of electron energy for a source located in the gonads of a voxelized flatfish model (E. A. Caffrey, 2012).

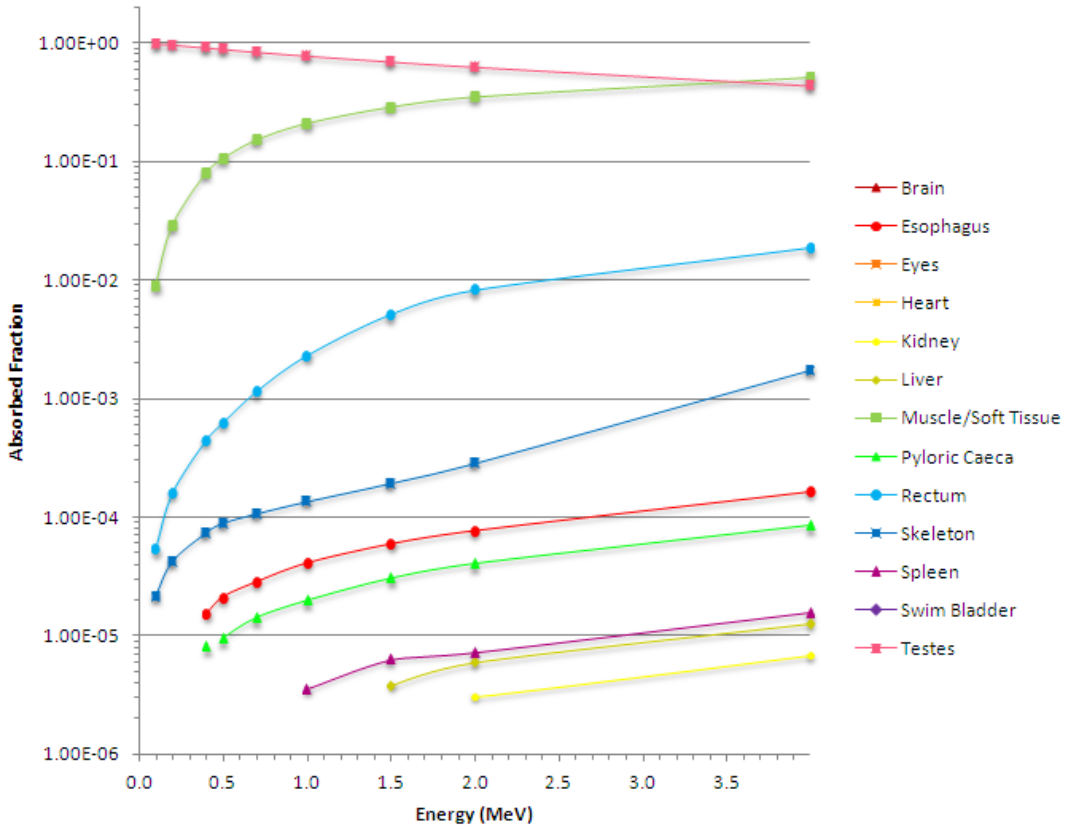

Figure 30: AFs of electron energy of a source located in the testes of the trout model.

Figure 31 and Figure 32 show the AFs of photon energy for a source located in the kidney of the flatfish and trout models. The AFs in the source organ decrease with increasing energy and the target organ AFs increase with increasing energy. These values somewhat level off at photon energies above 0.1 MeV in both models. Once again, the differences between the models can be attributed to differing organs and organ sizes, and the differing locations of each organ within the fish.

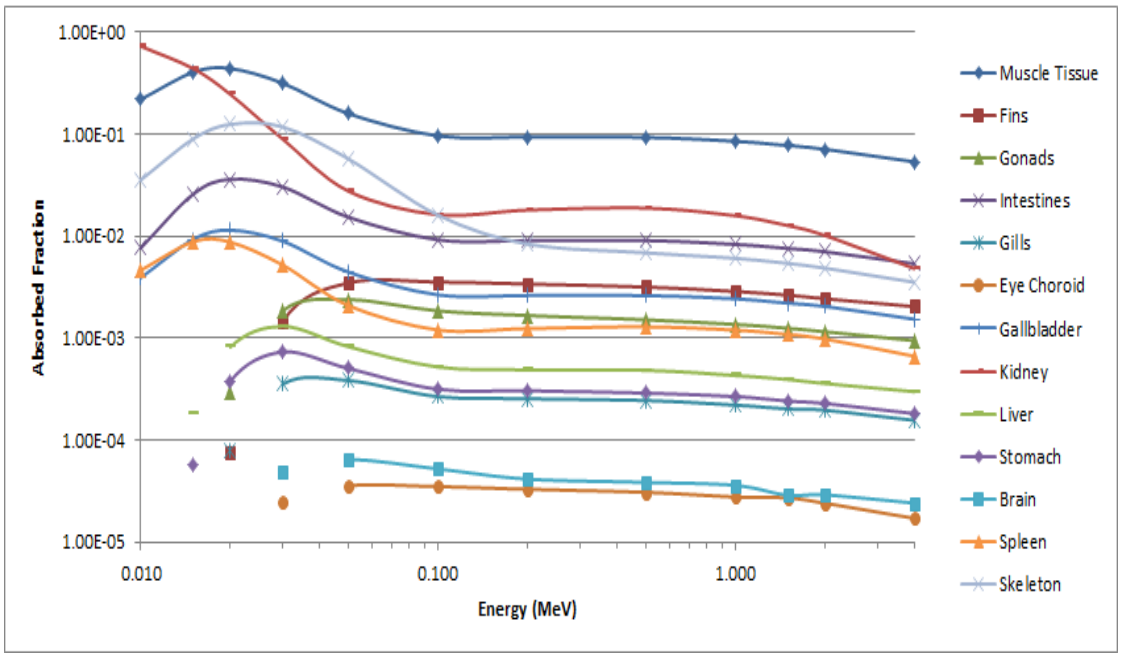

Figure 31: AFs of photon energy of a source located in the kidney of the flatfish model (E. A. Caffrey, 2012).

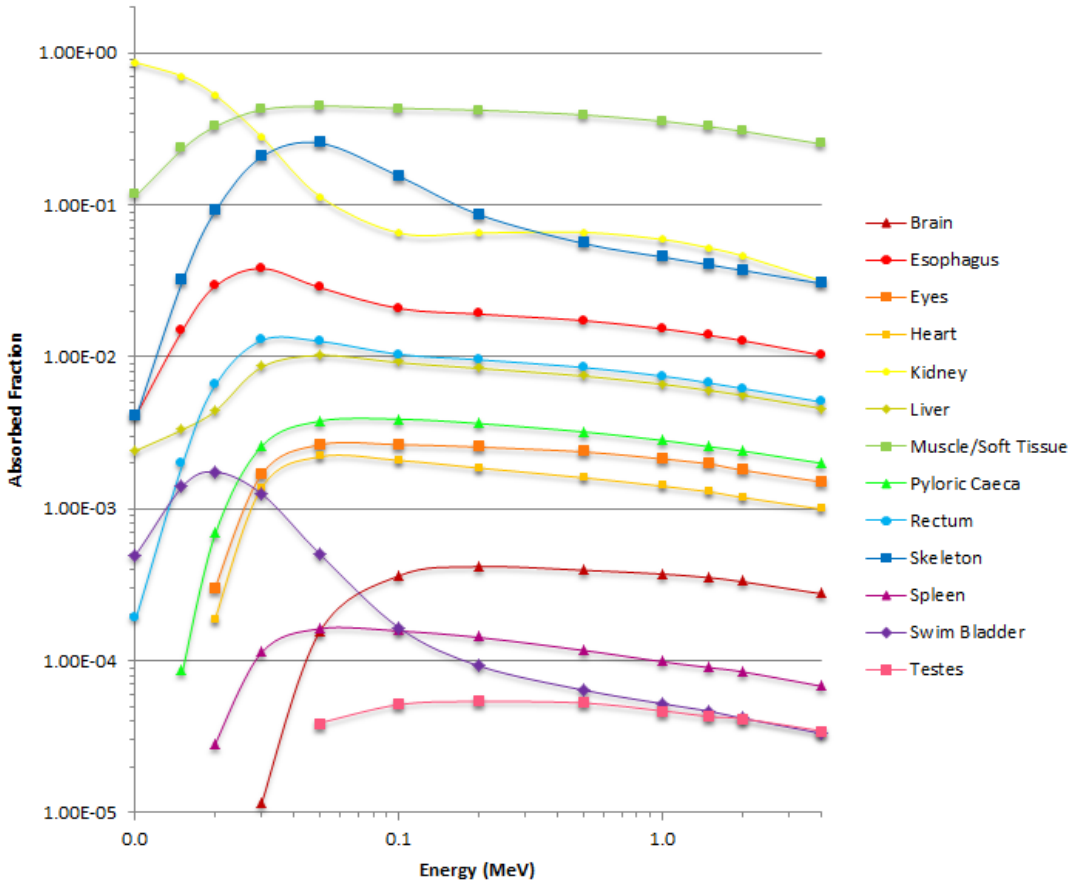

Figure 32: AFs of photon energy for a source located in the kidney of the trout model.

4.4 Summary of Analyses

For all plots, the self-AFs for photons are largely dependent on energy. The electron self-AFs for small organisms are nearly unity at energies below 0.1 MeV. Energies above this show a continual decrease in the self-AF, indicating that electrons with energies greater than 0.1 MeV should be treated as penetrating radiation for small

organism dosimetry. The data presented demonstrates that organ location, organ geometry, and incident photon or electron energy are the most important factors in determining the AF. It appears that that the geometry including the source size, target size and their distance significantly affect the AFs for cross-irradiation.

5 Conclusions and Future Work

The purpose of this research was to provide absorbed fraction data on a rainbow trout by creating a voxel model to be used in Monte Carlo simulations. In that sense, this research was successful. The voxel model presented in this thesis is a significant improvement upon existing dosimetric models for fish. While absorbed fraction data obtained with voxelized models are available for other species, this paper presents the first results for a rainbow trout. These results may be of considerable use to those engaged in environmental radioprotection. The data provided by this work can be used to derive dose conversion factors; factors that will be more accurate than those obtained with a simple homogenized model. These DCFs can then be used to determine what environmental protection, if any, is necessary for a given ecosystem.

There are three areas of additional work from which this study would benefit. The first is an improvement in the materials specification for the voxelized phantom. Elemental composition for NHB tissues is seldom available and utilizing fish specific tissue composition data, as opposed to human, would greatly improve the dosimetry calculations. Secondly, gaining a more complete understanding of radionuclide uptake, bioaccumulation and metabolism in trout would provide valuable information when estimating dose, as the method used to estimate activity concentrations in biota is one of the most important predictors of dose (Beresford et al., 2008; Higley et al., 2003). Lastly, it would be enlightening to use this voxelized fish model in a real world situation. Using real tissue concentration data from fish obtained at a contaminated site in a simple model as well as a voxel model would provide an interesting comparison on the costs or benefits of using a voxelized model.

6 Bibliography

Able Software Corporaton. (2008). *3D-DOCTOR User's Manual*. Lexington, MA.

Amiro, B. (1997). Radiological dose conversion factors for generic non-human biota used for screening potential ecological impacts. *Journal of Environmental Radioactivity*, *35*(1), 37–51. doi:10.1016/S0265-931X(96)00028-8

Beresford, N. A., Barnett, C. L., Brown, J. E., Cheng, J. J., Copplestone, D., Filistovic, V., … Yu, C. (2008). Inter-comparison of models to estimate radionuclide activity concentrations in non-human biota. *Radiation and Environmental Biophysics*, *47*(4), 491–514. doi:10.1007/s00411-008-0186-8

Beresford, N. A., Hosseini, A., Brown, J. E., Cailes, C., Beaugelin-Seiller, K., Barnett, C. L., & Copplestone, D. (2010). Assessment of risk to wildlife from ionising radiation: can initial screening tiers be used with a high level of confidence? *Journal of Radiological Protection*, *30*(2), 265–81. doi:10.1088/0952-4746/30/2/S04

Boroughs, H., Townsley, S. J., & Hiatt, R. W. (1956a). The Metabolism of Radionuclides by Marine Organisms. I. The Uptake, Accumulation, and Loss of Strontium by Fishes. *Biological Bulletin*, *111*(3), 336–351.

Boroughs, H., Townsley, S. J., & Hiatt, R. W. (1956b). The Metabolism of Radionuclides by Marine Organisms. II. The Uptake , Accumulation , and Loss of Yttrium by Marine Fish , and the Importance of Short-Lived Radionuclides in the Sea. *Biological Bulletin*, *111*(3), 352–357.

Bréchignac, F. (2003). Protection of the environment: how to position radioprotection in an ecological risk assessment perspective. *The Science of the Total Environment*, *307*(1-3), 35–54. doi:10.1016/S0048-9697(02)00545-4

Bréchignac, F. (2005). Impact of radioactivity on the environment: Problems, state of current knowledge and approaches for identification of radioprotection criteria. *Radioprotection*, *36*(4), 511–535. doi:10.1051/radiopro:2001106

Brèchignac, F., & Doi, M. (2009). Challenging the current strategy of radiological protection of the environment: arguments for an ecosystem approach. *Journal of Environmental Radioactivity*, *100*(12), 1125–1134. doi:10.1016/j.jenvrad.2009.06.022

Brown, J. E., Alfonso, B., Avila, R., Beresford, N. A., Copplestone, D., Pröhl, G., & Ulanovsky, A. (2008). The ERICA Tool. *Journal of Environmental Radioactivity*, *99*(9), 1371–83. doi:10.1016/j.jenvrad.2008.01.008

Brown, J., Gomez-Ros, J.-M., Jones, S., Prohl, G., Taranenko, V., Thorring, H., … Woodhead, D. (2003). *Dosimetric models and data for assessing radiation exposures to biota.* FASSET Deliverable 3. Report for the EC 5th Framework Programme Contract FIGE-CT-2000-00102.

Caffrey, E. A. (2012). *Improvements in the dosimetric models of selected benthic organisms*. Oregon State University.

Caffrey, E., & Higley, K. (2013). Creation of a voxel phantom of the ICRP reference crab. *Journal of Environmental Radioactivity*, *120*, 14–18. doi:10.1016/j.jenvrad.2013.01.006

Chambers, D. B., Osborne, R. V., & Garva, A. L. (2006). Choosing an alpha radiation weighting factor for doses to non-human biota. *Journal of Environmental Radioactivity*, *87*(1), 1–14. doi:10.1016/j.jenvrad.2005.10.009

Clulow, F., Dave, N., Lim, T., & Avadhanula, R. (1998). Radionuclides (lead-210, polonium-210, thorium-230, and -232) and thorium and uranium in water, sediments and fish from lakes near the city of Elliot Lake, Ontario, Canada. *Environmental Pollution*, *99*, 199–213.

Copplestone, D., Bielby, S., Jones, S., Patton, D., Daniel, P., & Gize, I. (2001). *Impact Assessment of Ionising Radiation on Wildlife*. Almondsbury, Bristol.

Copplestone, D., Hingston, J., & Real, A. (2008). The development and purpose of the FREDERICA radiation effects database. *Journal of Environmental Radioactivity*, *99*(9), 1456–63. doi:10.1016/j.jenvrad.2008.01.006

DOE. (2002). *A Graded Approach For Evaluating Radiation Doses to Aquatic and Terrestrial Biota. DOE-STD-1153-2002*. Washington, D.C.

Doi, M., & Kawaguchi, I. (2007). Ecological impacts of umbrella effects of radiation on the individual members. *Journal of Environmental Radioactivity*, *96*(1-3), 32–38. doi:10.1016/j.jenvrad.2007.01.031

Drever, J. I. (1982). *The Geochemistry of Natural Waters*. Englewood Cliffs, NJ: Prentice-Hall, Inc.

Edmundson Jr., E. H. (1976). Effects of Gamma Radiation and Temperature on the Growth of Juvenile Rainbow Trout (*Salmo gairdneri*). *Northwest Science*, *50*(3), 183–188.

Forbes, R. M., Cooper, A. R., & Mitchell, H. H. (1953). The Composition of the Adult Human Body as Determined by Chemical Analysis. *The Journal of Biological Chemistry*, *203*, 359–366.

Foster, R. F. (1949). *Some Effects on Embryo and Young Rainbow Trout (Salmo Gairdnerii richardson) From Exposing the Parent Fish to X-rays*. Oak Ridge, TN.

Frost, W. F., & Brown, M. E. (1967). *The Trout*. London: Collins.

Garnier, J., & Baudin, J. P. (1990). Retention of Ingested Ag-110m by a Freshwater Fish, *Salmo Trutta L*. *Water, Air and Soil Pollution*, *50*, 409–421.

Goldman, L. W. (2007). Principles of CT and CT Technology. *Journal of Nuclear Medicine Technology*, *35*(3), 115–128. doi:10.2967/jnmt.107.042978

Golikov, V., & Brown, J. (2003). *Internal and External Dose Models - A Deliverable Report for EPIC (Environmental Protection from Ionizing Contaminants in the Arctic)* Contract EU: ICA2-CT-2000-10032.

Gómez-Ros, J. M., Pröhl, G., Ulanovsky, A., & Lis, M. (2008). Uncertainties of internal dose assessment for animals and plants due to non-homogeneously

distributed radionuclides. *Journal of Environmental Radioactivity*, *99*(9), 1449–1455. doi:10.1016/j.jenvrad.2008.01.005

Hall, E. J., & Giaccia, A. J. (2006). *Radiobiology for the Radiologist* (Sixth.). Philadelphia, PA: Lippincott Williams & Wilkins.

Hendee, W. R., & Ritenour, E. R. (2002). *Medical Imaging Physics*. New York, USA: John Wiley & Sons, Inc. doi:10.1002/0471221155

Higley, K. A., Domotor, S. L., Antonio, E. J., & Kocher, D. C. (2003). Derivation of a screening methodology for evaluating radiation dose to aquatic and terrestrial biota. *Journal of Environmental Radioactivity*, *66*(1-2), 41–59. doi:10.1016/S0265-931X(02)00115-7

Hogstrand, C., Grosell, M., Wood, C. M., & Hansen, H. (2003). Internal Redistribution of Radiolabelled Silver Among Tissues of Rainbow Trout (*Oncorhynchus mykiss*) and European Eel (*Anguilla anguilla*): the influence of silver speciation. *Aquatic Toxicology (Amsterdam, Netherlands)*, *63*(2), 139–57.

Holland, H. D. (1978). *The Chemistry of the Atmosphere and Oceans* (p. 351). New York, USA: Wiley.

IAEA. (1992). Effects of Ionizing Radiation on Plants and Animals at Levels Implied by Current Radiation Protection Standards. In *Technical Report Series No. 332*. Vienna, Austria.

ICRP. (1959). 1954 Recommendations of the International Commission on Radiological Protection. *Annals of the ICRP*, *os-1*(iii). doi:10.1016/S0074-2740(28)80014-6

ICRP. (1975). Report on the Task Group on Reference Man. ICRP Publication 23. *Annals of the ICRP*, *4*(3-4).

ICRP. (1977). Recommendations of the International Commission on Radiological Protection. ICRP Publication 26. *Annals of the ICRP*, *1*(3).

ICRP. (1991). 1990 Recommendations of the International Commission on Radiological Protection. ICRP Publication 60. *Annals of the ICRP*, *21*(1-3).

ICRP. (1994). Human Respiratory Tract Model for Radiological Protection. ICRP Publication 66. *Annals of the ICRP*, *24*(1-3).

ICRP. (2002). Basic Anatomical and Physiological Data for Use in Radiological Protection Reference Values. ICRP Publication 89. *Annals of the ICRP*, *32*(3-4).

ICRP. (2003). A Framework for Assessing the Impact of Ionising Radiation on Non-human Species. ICRP Publication 91. *Annals of the ICRP*, *33*(3).

ICRP. (2006). Human Alimentary Tract Model for Radiological Protection. ICRP Publication 100. *Annals of the ICRP*, *36*(1-2).

ICRP. (2007). 2007 Recommendations of the International Commission on Radiological Protection. ICRP Publication 103. *Annals of the ICRP*, *37*(2-4).

ICRP. (2008). Environmental Protection - The Concept and Use of Reference Animals and Plants. ICRP Publication 108. *Annals of the ICRP*, *38*(4-6).

ICRP. (2009). Adult Reference Computational Phantoms. ICRP Publication 110. *Annals of the ICRP*, *39*(2).

ICRU. (1989). *Tissue Substitutes in Radiation Dosimetry and Measurement.* Bethesda, MD: Report 44 of the International Commission on Radiation Units and Measurements.

Kimura, Y., Honda, Y., & Nishiwaki, Y. (1978). Bioaccumulation and Retention of Some Radionuclides by Developing Eggs and Larvae of Rainbow Trout.

Kinase, S. (2008). Voxel-Based Frog Phantom for Internal Dose Evaluation. *Journal of Nuclear Science and Technology*, *45*(10), 1049–1052. doi:10.1080/18811248.2008.9711891

Knowles, J. F. (1992). The effect of chronic radiation on the humoral immune response of rainbow trout (Onchorhynchus mykiss Walbaum). *International Journal of Radiation Biology*, *62*(2), 239–248.

Kramer, G. H., Capello, K., Chiang, A., Cardenas-Mendez, E., & Sabourin, T. (2010). Tools for Creating and Manipulating Voxel Phantoms. *Health Physics*, *98*(3), 542–548.

Kramer, R., Vieira, J. W., Khoury, H. J., & Lima, F. D. A. (2004). MAX meets ADAM: a dosimetric comparison between a voxel-based and a mathematical model for external exposure to photons. *Physics in Medicine and Biology*, *49*(6), 887–910. doi:10.1088/0031-9155/49/6/002

Larsson, C.-M. (2004). The FASSET Framework for assessment of environmental impact of ionising radiation in European ecosystems—an overview. *Journal of Radiological Protection*, *24*(4A), A1–A12. doi:10.1088/0952-4746/24/4A/001

Larsson, C.-M. (2008). An overview of the ERICA Integrated Approach to the assessment and management of environmental risks from ionising contaminants. *Journal of Environmental Radioactivity*, *99*(9), 1364–70. doi:10.1016/j.jenvrad.2007.11.019

Loevinger, R., & Berman, M. (1976). *A revised schema for calculating the absorbed dose from biologically distributed radionuclides.* MIRD Pamphlet No. 1, Revised. New York: Society of Nuclear Medicine.

Loevinger, R., Budinger, T. F., & Watson, E. E. (1991). *MIRD Primer for Absobed Dose Calculations* (Revised Ed.). New York: Society of Nuclear Medicine.

McGregor, J. F., & Newcombe, H. B. (1972a). Decreased risk of embryo mortality following low doses of radiation to trout sperm. *Radiation Research*, *52*(3), 536–544.

McGregor, J. F., & Newcombe, H. B. (1972b). Dose-response relationships for yields of major eye malformations following low doses of radiation to trout sperm. *Radiation Research*, *49*(1), 155–169.

Mohammadi, A., & Kinase, S. (2011). Monte Carlo Simulations of Photon Specific Absorbed Fractions in a Mouse Voxel Phantom. *Progress in Nuclear Science and Technology*, *1*, 126–129.

Murray, J., & Burt, J. R. (2001). *The Composition of Fish*. Food and Agriculture Organization. Torry Research Station Advisory Note No. 38.

NCRP. (1991). *Effects of Ionizing Radiation on Aquatic Organisms.* NCRP Report No. 109. Bethesda, MD: National Council on Radiation Protection and Measurements.

Niiyama, H. (1957). Effects of X-Irradiation upon Rainbow Trouts (*Salmo-irideus*) II. Stimulative Effects of X-rays on Spermatogenesis in Fry. *Journal of the Faculty of Sceince Hokkaido University*, *13*, 281–288.

NOAA Fisheries: Office of Protected Resources. (2013). Steelhead Trout (*Oncorhynchus mykiss*). Retrieved from http://www.nmfs.noaa.gov/pr/species/fish/steelheadtrout.htm

Olson, K. R., Bergman, H. L., & Fromm, P. O. (1973). Uptake of Methyl Mercuric Chloride and Mercuric Chloride by Trout□: A Study of Uptake Pathways into the Whole Animal and Uptake by Erythrocytes in vitro. *Journal Fisheries Research Board of Canada*, *30*(9), 1293–1299.

Pentreath, R. J. (1998). Radiological protection criteria for the natural environment. *Radiation Protection Dosimetry*, *75*(1-4), 175–179.

Pentreath, R. J. (1999). A system for radiological protection of the environment: some initial thoughts and ideas. *Journal of Radiological Protection*, *19*(2), 117–28.

Pentreath, R. J. (2002). Radiation protection of people and the environment: developing a common approach. *Journal of Radiological Protection*, *22*, 45–56.

Pentreath, R. J. (2004). Ethics, genetics and dynamics: an emerging systematic approach to radiation protection of the environment. *Journal of Environmental Radioactivity*, *74*(1-3), 19–30. doi:10.1016/j.jenvrad.2004.01.024

Pentreath, R. J. (2009). Radioecology, radiobiology, and radiological protection: frameworks and fractures. *Journal of Environmental Radioactivity*, *100*(12), 1019–26. doi:10.1016/j.jenvrad.2009.06.004

Pentreath, R. J., & Woodhead, D. S. (2001). A system for protecting the environment from ionising radiation: selecting reference fauna and flora, and the possible dose models and environmental geometries that could be applied to them. *Science of The Total Environment*, *277*(1-3), 33–43. doi:10.1016/S0048-9697(01)00888-9

Ruedig, E. B. (2013). *Dose-effects Relationships in Non-Human Biota: Development of Field Sampling, Dosimetric and Analytic Techniques Through a Case Study of the Aquatic Snail Campeloma decisum at Chalk River Laboratories*. Oregon State University.

Saunders, R. L. (1953). The Swimbladder Gas Content of Some Freshwater Fish with Particular Reference to the Physostomes. *Canadian Journal of Zoology*, *31*(6), 547–560.

Sazykina, T., Kryshev, I., Katkova, M., & Kryshev, A. (2002). *Report on dose-effects relationships for reference (or related) Arctic biota.* EPIC database "radiation effects on biota". EPIC Project Deliverable 5.

Shultis, J. K., & Faw, R. E. (2004). *An MCNP Primer*. Manhattan, Kansas: Department of Mechanical and Nuclear Engineering, Kansas State University.

Snyder, W. S., Ford, M. R., & Warner, G. G. (1978). *Estimates of Specific Absorbed Fractions for Photon Sources Uniformly Distributed in Various Organs of a Heterogeneous Phantom.* MIRD Pamphlet No. 5. New York: Society of Nuclear Medicine.

Sparrow, A. H., Underbrink, A. G., & Sparrow, R. C. (1967). Chromosomes and Cellular Radiosensitivity: I. The Relationship of D_0 to Chromosome Volume and Complexity in Seventy-Nine Different Organisms. *Radiation Research*, *32*(4), 915–945.

Stabin, M. G., Peterson, T. E., Holburn, G. E., & Emmons, M. a. (2006). Voxel-based mouse and rat models for internal dose calculations. *Journal of Nuclear Medicine*, *47*(4), 655–9.

Strand, J. A., Fujihara, M. P., Burdett, R. D., & Poston, T. M. (1977). Suppression of the primary immune response in rainbow trout, (*Salmo gairdneri*), sublethally exposed to tritiated water during embryogenesis. *Journal of the Fisheries Research Board of Canada*, *34*, 1293–1304.

Strand, J. A., Fujihara, M. P., Poston, T. M., & Abernethy, C. S. (1982). Permanence of Suppression of the Primary Immune Response in Rainbow Trout, *Salmo gairdneri*, Sublethally Exposed to Tritiated Water during Embryogenesis. *Radiation Research*, *91*, 533–541.

Taranenko, V., Pröhl, G., & Gómez-Ros, J. M. (2004). Absorbed dose rate conversion coefficients for reference terrestrial biota for external photon and internal exposures. *Journal of Radiological Protection*, *24*(4A), A35–A62. doi:10.1088/0952-4746/24/4A/003

Ulanovsky, A., & Pröhl, G. (2006). A practical method for assessment of dose conversion coefficients for aquatic biota. *Radiation and Environmental Biophysics*, *45*(3), 203–14. doi:10.1007/s00411-006-0061-4

Ulanovsky, A., & Pröhl, G. (2012). Dosimetry for Reference Animals and Plants: current state and prospects. *Annals of the ICRP*, *41*(3-4), 218–32. doi:10.1016/j.icrp.2012.06.034

Vangenechten, J. H. D., Van Puymbroeck, S., & Vanderborght, O. L. J. (1989). Curium-244 and Americium-241 Uptake in Freshwater Fish. *Toxicological & Environmental Chemistry*, *19*(3-4), 147–152. doi:10.1080/02772248909357341

Vives i Battle, J., Jones, S., & Gómez-Ros, J. (2004). A method for calculation of dose per unit concentration values for aquatic biota. *Journal of Radiological Protection*, *24*(4A), A13–A34. doi:10.1088/0952-4746/24/4A/002

Welander, A. D., Wadley, G. W., & Dysart, D. K. (1971). Growth and Fecundity of Rainbow Trout (*Salmo gairdneti*) Exposed to Single Sublethal Doses of X-rays During the Eyed Embryo Stage. *Journal of the Fisheries Research Board of Canada*, *28*, 1181–1184.

Woodhead, D. S. (2003a). A model for exploring the impact of radiation on fish populations. In *Protection of the Environment from Ionising Radiation: The Development and Application of a System of Radiation Protection for the Environment* (pp. 32–42). Vienna, Austria: IAEA.

Woodhead, D. S. (2003b). A possible approach for the assessment of radiation effects on populations of wild organisms in radionuclide-contaminated environments. *Journal of Environmental Radioactivity*, *66*(1-2), 181–213. doi:10.1016/S0265-931X(02)00123-6

X-5 Monte Carlo Team. (2008). *MCNP A General Monte Carlo N-Particle Transport Code, Version 5*.

Zaidi, H., & Xu, X. G. (2007). Computational anthropomorphic models of the human anatomy: the path to realistic Monte Carlo modeling in radiological sciences. *Annual Review of Biomedical Engineering*, *9*, 471–500. doi:10.1146/annurev.bioeng.9.060906.151934

APPENDICES

A. Complete Photon Absorbed Fraction Data

In all tables, AFs whose relative error exceeded 10% appear as a dashed line (--); those AFs with a relative error between 5% and 10% are underlined. A zero entry indicates that no energy was deposited in that segment. In all figures, AFs whose relative error exceeded 10% have been omitted.

Table 5: Absorbed fraction of photon energy for a source located in the esophagus segment.

	Energy (MeV)											
	0.010	0.015	0.020	0.030	0.050	0.100	0.200	0.500	1.000	1.500	2.000	4.000
Target												
Brain	0.00E+00	0.00E+00	0.00E+00	--	--	3.25E-05	4.74E-05	4.87E-05	5.23E-05	5.09E-05	4.88E-05	4.57E-05
Esophagus	9.26E-01	8.07E-01	6.51E-01	3.87E-01	1.79E-01	1.09E-01	1.07E-01	1.07E-01	9.69E-02	8.65E-02	7.80E-02	5.63E-02
Eyes	0.00E+00	--	--	6.20E-05	2.15E-04	3.34E-04	3.62E-04	3.55E-04	3.45E-04	3.35E-04	3.25E-04	2.83E-04
Heart	1.91E-04	7.12E-04	3.34E-03	8.58E-03	8.12E-03	5.70E-03	5.06E-03	4.64E-03	4.19E-03	3.84E-03	3.57E-03	2.93E-03
Kidney	1.35E-03	4.95E-03	9.65E-03	1.25E-02	9.10E-03	6.30E-03	5.64E-03	5.06E-03	4.47E-03	4.06E-03	3.75E-03	3.03E-03
Liver	6.72E-03	1.62E-02	2.65E-02	3.46E-02	2.74E-02	1.94E-02	1.76E-02	1.64E-02	1.49E-02	1.37E-02	1.27E-02	1.03E-02
Muscle/Soft Tissue	5.96E-02	1.39E-01	2.28E-01	3.53E-01	3.80E-01	3.31E-01	3.04E-01	2.76E-01	2.48E-01	2.28E-01	2.13E-01	1.76E-01
Pyloric Caeca	5.21E-03	2.02E-02	3.92E-02	5.20E-02	3.98E-02	2.74E-02	2.47E-02	2.30E-02	2.08E-02	1.91E-02	1.78E-02	1.44E-02
Rectum	6.72E-04	4.27E-03	1.46E-02	3.39E-02	3.45E-02	2.58E-02	2.28E-02	2.07E-02	1.87E-02	1.71E-02	1.60E-02	1.31E-02
Skeleton	2.55E-04	4.37E-03	1.82E-02	6.01E-02	9.38E-02	6.71E-02	3.89E-02	2.27E-02	1.72E-02	1.50E-02	1.37E-02	1.12E-02
Spleen	8.66E-05	1.63E-03	4.50E-03	6.40E-03	4.38E-03	2.71E-03	2.39E-03	2.24E-03	2.01E-03	1.84E-03	1.70E-03	1.37E-03
Swim Bladder	4.08E-04	1.27E-03	1.92E-03	1.83E-03	9.06E-04	2.77E-04	1.35E-04	9.01E-05	7.16E-05	6.23E-05	5.82E-05	4.60E-05
Testes	0.00E+00	0.00E+00	--	1.90E-04	4.31E-04	4.24E-04	3.78E-04	3.30E-04	2.92E-04	2.69E-04	2.51E-04	2.11E-04

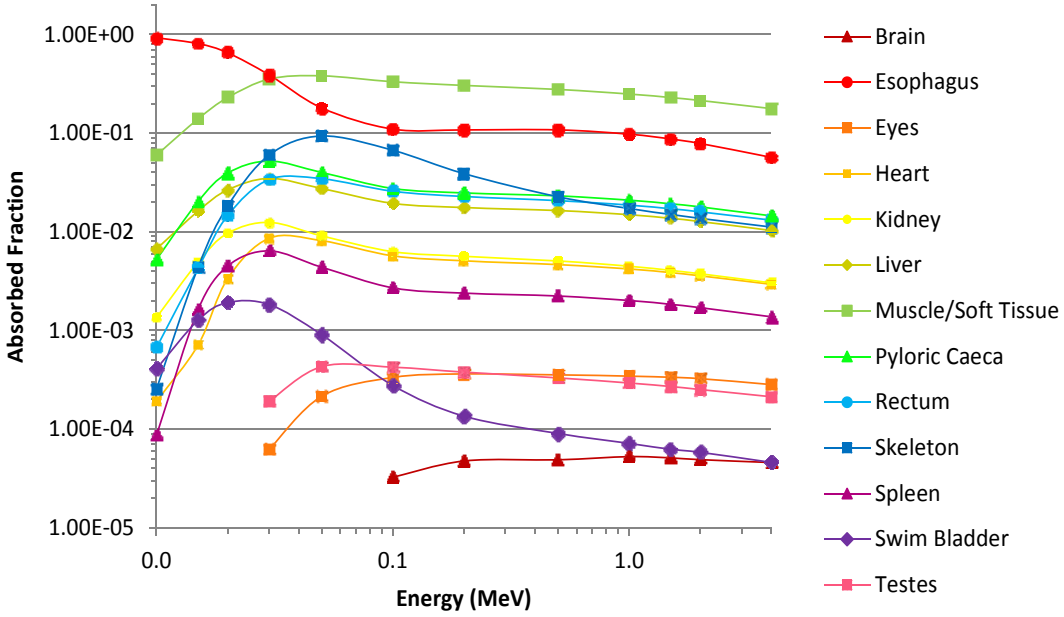

Figure 33: Photon AFs for a source located in the esophagus segment.

Table 6: Absorbed fractions of photon energy for source located in the kidney segment.

	Energy (MeV)											
	0.010	0.015	0.020	0.030	0.050	0.100	0.200	0.500	1.000	1.500	2.000	4.000
Target												
Brain	0.00E+00	0.00E+00	--	1.15E-05	1.57E-04	3.67E-04	4.20E-04	3.98E-04	3.76E-04	3.56E-04	3.35E-04	2.79E-04
Esophagus	4.18E-03	1.52E-02	2.97E-02	3.85E-02	2.87E-02	2.10E-02	1.93E-02	1.75E-02	1.54E-02	1.40E-02	1.29E-02	1.03E-02
Eyes	0.00E+00	--	3.01E-04	1.69E-03	2.68E-03	2.68E-03	2.58E-03	2.40E-03	2.15E-03	1.99E-03	1.82E-03	1.52E-03
Heart	0.00E+00	--	1.90E-04	1.39E-03	2.24E-03	2.12E-03	1.89E-03	1.63E-03	1.43E-03	1.32E-03	1.21E-03	1.01E-03
Kidney	8.72E-01	7.09E-01	5.31E-01	2.81E-01	1.14E-01	6.58E-02	6.61E-02	6.66E-02	5.96E-02	5.24E-02	4.65E-02	3.17E-02
Liver	2.42E-03	3.33E-03	4.46E-03	8.74E-03	1.04E-02	9.33E-03	8.55E-03	7.58E-03	6.67E-03	6.07E-03	5.63E-03	4.61E-03
Muscle/Soft Tissue	1.17E-01	2.37E-01	3.31E-01	4.25E-01	4.48E-01	4.34E-01	4.22E-01	3.93E-01	3.57E-01	3.29E-01	3.07E-01	2.54E-01
Pyloric Caeca	--	8.62E-05	6.95E-04	2.60E-03	3.80E-03	3.91E-03	3.66E-03	3.22E-03	2.82E-03	2.57E-03	2.41E-03	2.00E-03
Rectum	1.93E-04	2.00E-03	6.65E-03	1.30E-02	1.27E-02	1.04E-02	9.63E-03	8.55E-03	7.50E-03	6.76E-03	6.22E-03	5.07E-03
Skeleton	4.11E-03	3.25E-02	9.38E-02	2.13E-01	2.60E-01	1.57E-01	8.80E-02	5.67E-02	4.62E-02	4.11E-02	3.78E-02	3.09E-02
Spleen	0.00E+00	--	2.83E-05	1.15E-04	1.65E-04	1.59E-04	1.44E-04	1.19E-04	9.98E-05	9.14E-05	8.58E-05	6.89E-05
Swim Bladder	4.96E-04	1.42E-03	1.76E-03	1.26E-03	5.01E-04	1.64E-04	9.29E-05	6.43E-05	5.23E-05	4.67E-05	4.20E-05	3.33E-05
Testes	0.00E+00	0.00E+00	--	--	3.85E-05	5.18E-05	5.43E-05	5.31E-05	4.67E-05	4.28E-05	4.12E-05	3.40E-05

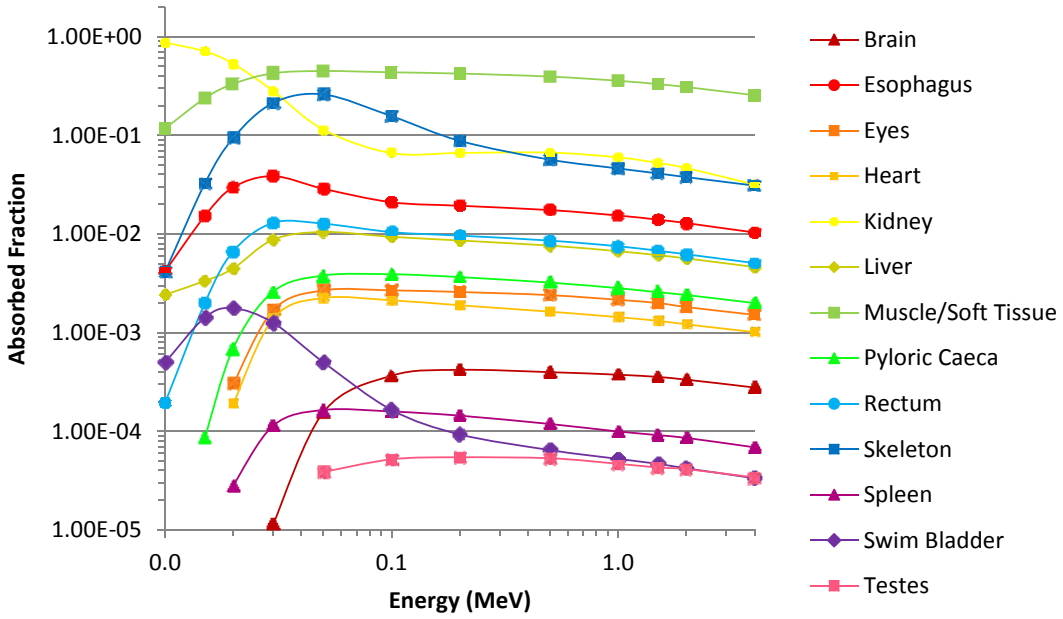

Figure 34: Photon AFs for a source located in the kidney segment.

Table 7: Absorbed fraction of photon energy for a source located in the liver segment.

	Energy (MeV)											
	0.010	0.015	0.020	0.030	0.050	0.100	0.200	0.500	1.000	1.500	2.000	4.000
Target												
Brain	0.00E+00	0.00E+00	0.00E+00	--	--	2.89E-05	4.77E-05	5.87E-05	6.17E-05	6.15E-05	6.13E-05	5.99E-05
Esophagus	1.19E-02	2.85E-02	4.67E-02	6.11E-02	4.91E-02	3.59E-02	3.32E-02	3.12E-02	2.83E-02	2.60E-02	2.41E-02	1.96E-02
Eyes	0.00E+00	0.00E+00	--	4.48E-05	2.45E-04	4.53E-04	5.14E-04	5.20E-04	4.89E-04	4.64E-04	4.42E-04	3.94E-04
Heart	9.08E-03	2.34E-02	3.18E-02	2.91E-02	1.75E-02	1.10E-02	1.02E-02	9.69E-03	8.77E-03	7.99E-03	7.39E-03	5.76E-03
Kidney	1.37E-03	1.90E-03	2.55E-03	4.94E-03	5.82E-03	5.13E-03	4.70E-03	4.17E-03	3.69E-03	3.37E-03	3.12E-03	2.58E-03
Liver	9.06E-01	7.81E-01	6.23E-01	3.64E-01	1.64E-01	9.69E-02	9.44E-02	9.37E-02	8.41E-02	7.46E-02	6.68E-02	4.74E-02
Muscle/Soft Tissue	5.43E-02	1.19E-01	2.01E-01	3.19E-01	3.56E-01	3.27E-01	3.09E-01	2.85E-01	2.59E-01	2.39E-01	2.24E-01	1.86E-01
Pyloric Caeca	8.10E-03	2.01E-02	3.02E-02	3.32E-02	2.39E-02	1.73E-02	1.60E-02	1.50E-02	1.36E-02	1.26E-02	1.16E-02	9.42E-03
Rectum	7.25E-03	1.05E-02	1.19E-02	1.27E-02	1.27E-02	1.14E-02	1.06E-02	9.59E-03	8.66E-03	7.98E-03	7.48E-03	6.16E-03
Skeleton	1.49E-03	1.47E-02	4.99E-02	1.33E-01	1.59E-01	9.37E-02	5.19E-02	3.13E-02	2.45E-02	2.15E-02	1.97E-02	1.60E-02
Spleen	0.00E+00	0.00E+00	--	7.10E-05	2.67E-04	3.36E-04	3.07E-04	2.70E-04	2.44E-04	2.28E-04	2.15E-04	1.80E-04
Swim Bladder	--	--	1.40E-04	4.86E-04	4.57E-04	1.97E-04	9.73E-05	5.58E-05	4.42E-05	3.82E-05	3.55E-05	2.86E-05
Testes	0.00E+00	0.00E+00	0.00E+00	--	2.15E-05	4.97E-05	5.69E-05	5.41E-05	4.91E-05	5.01E-05	5.02E-05	4.60E-05

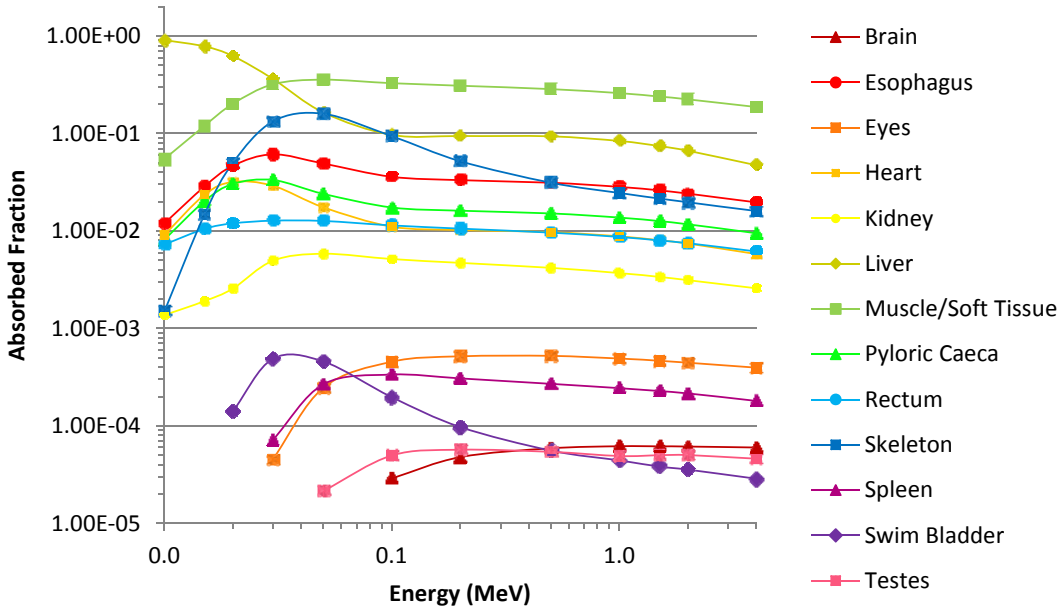

Figure 35: Photon AFs for a source located in the liver segment.

Table 8: Absorbed fraction of photon energy for a source located in the muscle segment.

	Energy (MeV)											
	0.010	0.015	0.020	0.030	0.050	0.100	0.200	0.500	1.000	1.500	2.000	4.000
Target												
Brain	1.64E-04	3.31E-04	4.39E-04	4.75E-04	4.61E-04	4.55E-04	4.47E-04	4.37E-04	3.91E-04	3.62E-04	3.37E-04	2.80E-04
Esophagus	1.65E-03	3.75E-03	6.24E-03	9.75E-03	1.08E-02	9.78E-03	9.20E-03	8.47E-03	7.65E-03	7.04E-03	6.56E-03	5.39E-03
Eyes	4.48E-04	9.80E-04	1.26E-03	1.34E-03	1.29E-03	1.25E-03	1.24E-03	1.17E-03	1.09E-03	1.01E-03	9.55E-04	7.75E-04
Heart	3.36E-04	7.61E-04	1.09E-03	1.31E-03	1.33E-03	1.23E-03	1.17E-03	1.07E-03	9.80E-04	9.07E-04	8.42E-04	7.03E-04
Kidney	1.03E-03	2.09E-03	2.93E-03	3.80E-03	3.94E-03	3.80E-03	3.72E-03	3.53E-03	3.21E-03	2.97E-03	2.75E-03	2.29E-03
Liver	8.41E-04	1.86E-03	3.15E-03	5.05E-03	5.70E-03	5.27E-03	4.98E-03	4.61E-03	4.20E-03	3.88E-03	3.61E-03	3.00E-03
Muscle/Soft Tissue	9.60E-01	9.03E-01	8.35E-01	6.98E-01	5.25E-01	4.17E-01	3.94E-01	3.70E-01	3.36E-01	3.07E-01	2.85E-01	2.29E-01
Pyloric Caeca	3.95E-03	6.62E-03	7.83E-03	8.48E-03	7.48E-03	6.32E-03	5.90E-03	5.49E-03	4.98E-03	4.58E-03	4.25E-03	3.48E-03
Rectum	1.99E-03	4.44E-03	6.93E-03	9.85E-03	1.01E-02	8.86E-03	8.24E-03	7.60E-03	6.90E-03	6.35E-03	5.91E-03	4.89E-03
Skeleton	1.69E-02	4.36E-02	7.14E-02	1.09E-01	1.18E-01	7.44E-02	4.37E-02	2.76E-02	2.21E-02	1.95E-02	1.79E-02	1.45E-02
Spleen	1.39E-04	3.20E-04	4.85E-04	5.99E-04	5.31E-04	4.14E-04	3.79E-04	3.36E-04	3.05E-04	2.83E-04	2.67E-04	2.16E-04
Swim Bladder	3.59E-04	3.70E-04	3.43E-04	3.02E-04	2.04E-04	9.49E-05	4.85E-05	3.11E-05	2.43E-05	2.12E-05	1.91E-05	1.62E-05
Testes	1.59E-04	3.46E-04	4.76E-04	4.80E-04	3.48E-04	2.58E-04	2.48E-04	2.27E-04	2.14E-04	1.95E-04	1.82E-04	1.47E-04

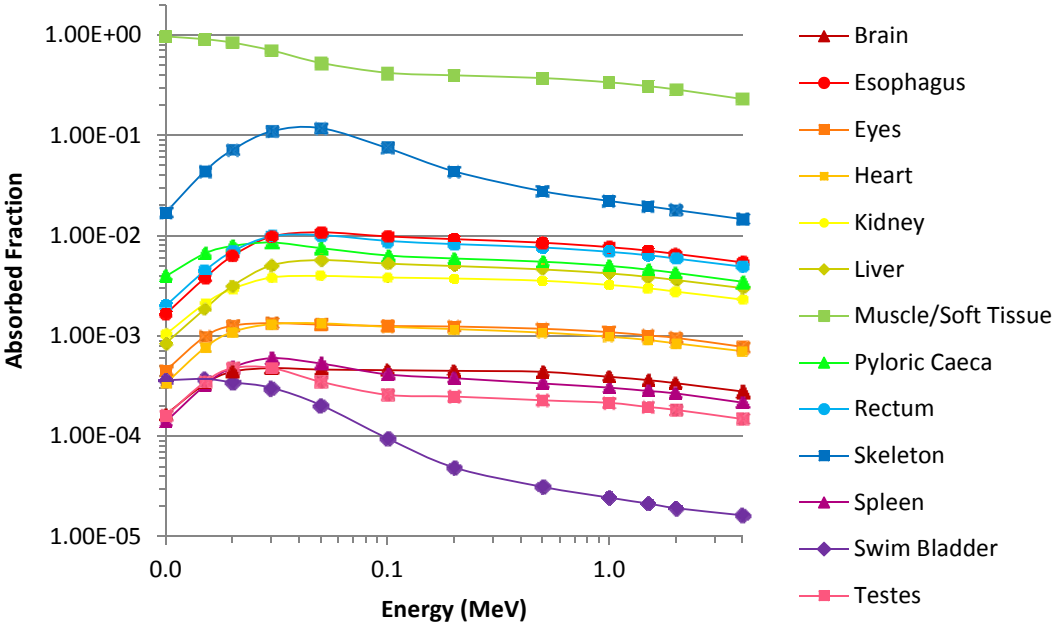

Figure 36: Photon AFs for a source located in the muscle segment.

Table 9: Absorbed fraction of photon energy for a source located in the pyloric caeca segment.

	Energy (MeV)											
	0.010	0.015	0.020	0.030	0.050	0.100	0.200	0.500	1.000	1.500	2.000	4.000
Target												
Brain	0.00E+00	0.00E+00	0.00E+00	--	--	--	1.09E-05	1.66E-05	2.03E-05	2.03E-05	2.19E-05	2.34E-05
Esophagus	7.63E-03	3.01E-02	5.83E-02	7.80E-02	6.06E-02	4.25E-02	3.87E-02	3.63E-02	3.29E-02	3.02E-02	2.80E-02	2.27E-02
Eyes	0.00E+00	0.00E+00	0.00E+00	--	2.23E-05	7.92E-05	1.09E-04	1.27E-04	1.37E-04	1.41E-04	1.35E-04	1.32E-04
Heart	--	7.30E-04	2.85E-03	5.32E-03	5.09E-03	3.89E-03	3.48E-03	3.20E-03	2.90E-03	2.67E-03	2.47E-03	2.02E-03
Kidney	--	3.59E-05	3.42E-04	1.27E-03	1.79E-03	1.81E-03	1.69E-03	1.49E-03	1.30E-03	1.19E-03	1.11E-03	9.41E-04
Liver	6.84E-03	1.70E-02	2.56E-02	2.82E-02	2.02E-02	1.45E-02	1.33E-02	1.25E-02	1.13E-02	1.04E-02	9.67E-03	7.83E-03
Muscle/Soft Tissue	2.12E-01	3.58E-01	4.27E-01	4.59E-01	4.04E-01	3.30E-01	3.06E-01	2.82E-01	2.56E-01	2.36E-01	2.20E-01	1.80E-01
Pyloric Caeca	7.61E-01	5.58E-01	4.09E-01	2.28E-01	1.05E-01	6.40E-02	6.23E-02	6.14E-02	5.46E-02	4.81E-02	4.29E-02	3.05E-02
Rectum	1.22E-02	3.18E-02	5.10E-02	6.15E-02	4.75E-02	3.36E-02	3.04E-02	2.82E-02	2.54E-02	2.32E-02	2.16E-02	1.74E-02
Skeleton	2.09E-04	2.85E-03	1.50E-02	5.48E-02	7.91E-02	5.42E-02	3.16E-02	1.87E-02	1.44E-02	1.25E-02	1.15E-02	9.42E-03
Spleen	4.94E-05	2.23E-04	6.48E-04	1.84E-03	2.05E-03	1.50E-03	1.28E-03	1.14E-03	1.01E-03	9.27E-04	8.67E-04	7.06E-04
Swim Bladder	--	3.73E-05	2.31E-04	5.82E-04	4.93E-04	2.00E-04	9.60E-05	5.64E-05	4.30E-05	3.83E-05	3.52E-05	2.89E-05
Testes	0.00E+00	0.00E+00	--	8.69E-05	2.90E-04	3.27E-04	3.03E-04	2.69E-04	2.41E-04	2.24E-04	2.18E-04	1.86E-04

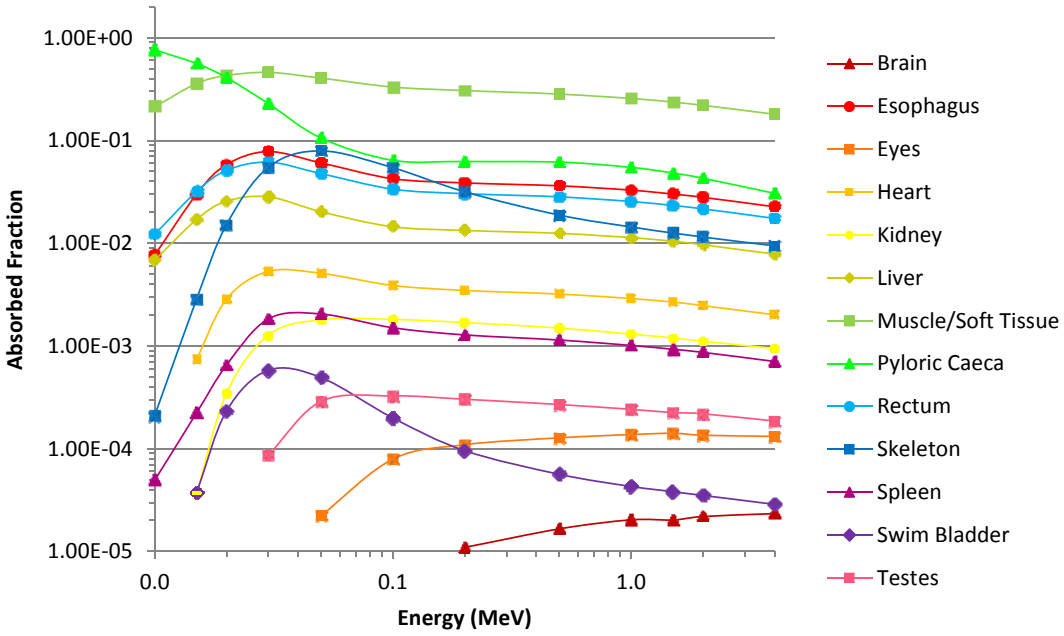

Figure 37: Photon AFs for a source located in the pyloric caeca segment.

Table 10: Absorbed fraction of photon energy for a source located in the rectum segment.

	Energy (MeV)											
	0.010	0.015	0.020	0.030	0.050	0.100	0.200	0.500	1.000	1.500	2.000	4.000
Target												
Brain	0.00E+00	0.00E+00	0.00E+00	0.00E+00	--	2.00E-05	2.80E-05	3.69E-05	4.05E-05	4.10E-05	4.00E-05	3.70E-05
Esophagus	7.25E-04	4.65E-03	1.60E-02	3.74E-02	3.86E-02	2.95E-02	2.63E-02	2.40E-02	2.17E-02	1.99E-02	1.85E-02	1.52E-02
Eyes	0.00E+00	0.00E+00	--	--	8.55E-05	2.05E-04	2.37E-04	2.48E-04	2.50E-04	2.41E-04	2.35E-04	2.18E-04
Heart	2.83E-03	7.61E-03	9.74E-03	8.82E-03	5.96E-03	4.25E-03	3.91E-03	3.66E-03	3.35E-03	3.05E-03	2.81E-03	2.23E-03
Kidney	7.27E-05	6.97E-04	2.36E-03	4.61E-03	4.47E-03	3.57E-03	3.27E-03	2.90E-03	2.53E-03	2.29E-03	2.11E-03	1.73E-03
Liver	4.52E-03	6.60E-03	7.47E-03	8.01E-03	7.89E-03	6.98E-03	6.46E-03	5.87E-03	5.31E-03	4.89E-03	4.52E-03	3.73E-03
Muscle/Soft Tissue	7.79E-02	1.76E-01	2.77E-01	3.94E-01	4.01E-01	3.41E-01	3.15E-01	2.89E-01	2.61E-01	2.40E-01	2.24E-01	1.85E-01
Pyloric Caeca	9.00E-03	2.35E-02	3.76E-02	4.54E-02	3.50E-02	2.48E-02	2.24E-02	2.08E-02	1.88E-02	1.72E-02	1.60E-02	1.29E-02
Rectum	9.03E-01	7.69E-01	6.05E-01	3.46E-01	1.53E-01	9.12E-02	8.97E-02	8.95E-02	8.03E-02	7.13E-02	6.39E-02	4.53E-02
Skeleton	7.91E-04	8.31E-03	2.92E-02	7.80E-02	1.02E-01	6.72E-02	3.85E-02	2.30E-02	1.77E-02	1.56E-02	1.42E-02	1.15E-02
Spleen	--	5.09E-05	3.25E-04	1.09E-03	1.40E-03	1.07E-03	9.31E-04	8.19E-04	7.33E-04	6.80E-04	6.30E-04	5.19E-04
Swim Bladder	4.53E-04	1.03E-03	1.36E-03	1.23E-03	6.55E-04	2.31E-04	1.21E-04	7.63E-05	6.01E-05	5.24E-05	4.84E-05	3.90E-05
Testes	8.14E-05	4.18E-04	1.00E-03	1.90E-03	1.69E-03	1.15E-03	1.00E-03	9.01E-04	8.31E-04	7.50E-04	7.10E-04	5.71E-04

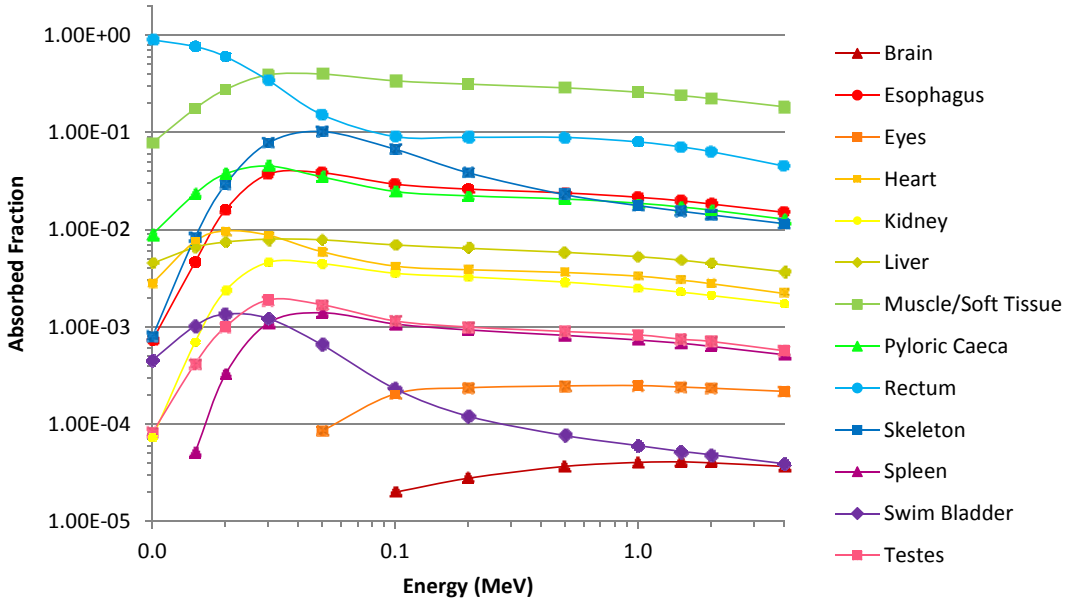

Figure 38: Photon AFs for a source located in the rectum segment.

Table 11: Absorbed fraction of photon energy for a source located in the skeleton segment.

	Energy (MeV)											
	0.010	0.015	0.020	0.030	0.050	0.100	0.200	0.500	1.000	1.500	2.000	4.000
Target												
Brain	3.80E-05	2.55E-04	5.94E-04	9.90E-04	1.01E-03	9.27E-04	9.23E-04	8.96E-04	8.23E-04	7.61E-04	6.96E-04	5.73E-04
Esophagus	1.75E-05	2.69E-04	1.08E-03	3.64E-03	6.94E-03	8.44E-03	8.31E-03	7.54E-03	6.77E-03	6.23E-03	5.82E-03	4.86E-03
Eyes	4.41E-05	3.21E-04	8.14E-04	1.40E-03	1.60E-03	1.65E-03	1.69E-03	1.62E-03	1.49E-03	1.39E-03	1.30E-03	1.07E-03
Heart	1.87E-05	1.50E-04	3.83E-04	9.03E-04	1.37E-03	1.49E-03	1.42E-03	1.31E-03	1.18E-03	1.08E-03	1.01E-03	8.27E-04
Kidney	8.80E-05	6.52E-04	1.81E-03	4.12E-03	6.02E-03	6.51E-03	6.54E-03	6.21E-03	5.65E-03	5.18E-03	4.87E-03	4.02E-03
Liver	5.65E-05	5.14E-04	1.68E-03	4.50E-03	6.41E-03	6.56E-03	6.26E-03	5.75E-03	5.26E-03	4.83E-03	4.51E-03	3.72E-03
Muscle/Soft Tissue	3.98E-02	9.66E-02	1.53E-01	2.34E-01	3.06E-01	3.39E-01	3.40E-01	3.21E-01	2.94E-01	2.72E-01	2.54E-01	2.09E-01
Pyloric Caeca	--	1.19E-04	5.98E-04	2.19E-03	3.78E-03	4.35E-03	4.28E-03	3.95E-03	3.57E-03	3.29E-03	3.09E-03	2.60E-03
Rectum	4.90E-05	4.68E-04	1.58E-03	4.23E-03	6.70E-03	7.46E-03	7.35E-03	6.77E-03	6.08E-03	5.61E-03	5.21E-03	4.37E-03
Skeleton	9.57E-01	8.89E-01	8.10E-01	6.52E-01	4.10E-01	1.79E-01	1.05E-01	7.99E-02	6.74E-02	5.89E-02	5.28E-02	3.91E-02
Spleen	--	9.99E-07	8.88E-06	4.73E-05	1.24E-04	1.73E-04	1.63E-04	1.47E-04	1.34E-04	1.23E-04	1.14E-04	9.60E-05
Swim Bladder	1.02E-04	1.70E-04	1.96E-04	1.88E-04	1.50E-04	8.68E-05	4.95E-05	3.28E-05	2.60E-05	2.29E-05	2.05E-05	1.65E-05
Testes	--	3.96E-06	3.18E-05	1.35E-04	2.17E-04	2.13E-04	2.08E-04	1.84E-04	1.72E-04	1.54E-04	1.51E-04	1.23E-04

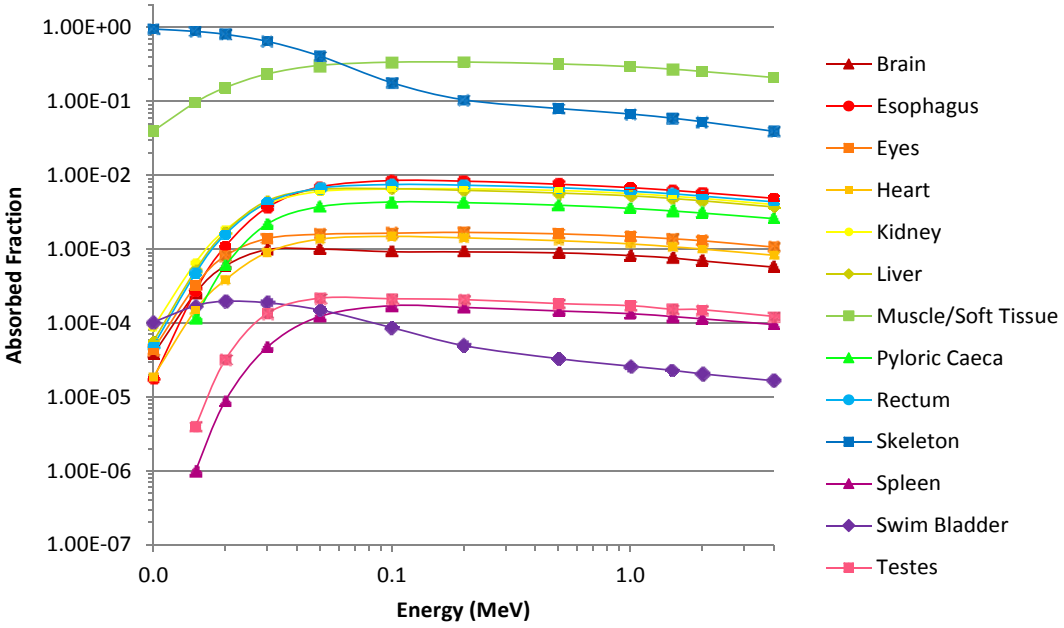

Figure 39: Photon AFs for a source located in the skeleton segment.

Table 12: Absorbed fraction of photon energy for a source located in the spleen segment.

	Energy (MeV)											
	0.010	0.015	0.020	0.030	0.050	0.100	0.200	0.500	1.000	1.500	2.000	4.000
Target												
Brain	0.00E+00	0.00E+00	0.00E+00	0.00E+00	--	--	4.94E-06	8.26E-06	8.96E-06	1.12E-05	1.11E-05	1.21E-05
Esophagus	2.03E-03	3.67E-02	1.02E-01	1.46E-01	1.03E-01	6.67E-02	6.06E-02	5.69E-02	5.15E-02	4.72E-02	4.38E-02	3.55E-02
Eyes	0.00E+00	0.00E+00	0.00E+00	--	--	2.56E-05	3.90E-05	5.11E-05	6.05E-05	5.96E-05	6.16E-05	6.62E-05
Heart	0.00E+00	0.00E+00	--	9.38E-05	5.89E-04	9.00E-04	8.43E-04	7.50E-04	6.89E-04	6.41E-04	6.01E-04	5.28E-04
Kidney	0.00E+00	--	1.96E-04	8.75E-04	1.19E-03	1.14E-03	1.05E-03	8.87E-04	7.59E-04	6.82E-04	6.29E-04	5.22E-04
Liver	0.00E+00	--	--	8.31E-04	3.39E-03	4.37E-03	4.06E-03	3.61E-03	3.28E-03	3.07E-03	2.92E-03	2.51E-03
Muscle/Soft Tissue	1.16E-01	2.69E-01	3.93E-01	5.03E-01	4.48E-01	3.44E-01	3.11E-01	2.86E-01	2.57E-01	2.36E-01	2.19E-01	1.78E-01
Pyloric Caeca	7.27E-04	3.36E-03	9.85E-03	2.85E-02	3.15E-02	2.35E-02	2.05E-02	1.85E-02	1.66E-02	1.52E-02	1.41E-02	1.16E-02
Rectum	--	9.51E-04	6.73E-03	2.29E-02	2.92E-02	2.32E-02	2.02E-02	1.80E-02	1.62E-02	1.48E-02	1.38E-02	1.14E-02
Skeleton	--	3.78E-04	3.36E-03	1.77E-02	3.87E-02	3.43E-02	2.12E-02	1.22E-02	9.05E-03	7.82E-03	7.10E-03	5.81E-03
Spleen	8.81E-01	6.90E-01	4.82E-01	2.25E-01	7.94E-02	4.27E-02	4.40E-02	4.54E-02	4.03E-02	3.47E-02	3.01E-02	1.86E-02
Swim Bladder	--	1.74E-04	6.36E-04	1.04E-03	6.58E-04	2.30E-04	1.12E-04	7.05E-05	5.48E-05	4.96E-05	4.49E-05	3.59E-05
Testes	0.00E+00	0.00E+00	2.17E-05	4.59E-04	1.04E-03	9.66E-04	8.34E-04	7.29E-04	6.55E-04	5.90E-04	5.49E-04	4.51E-04

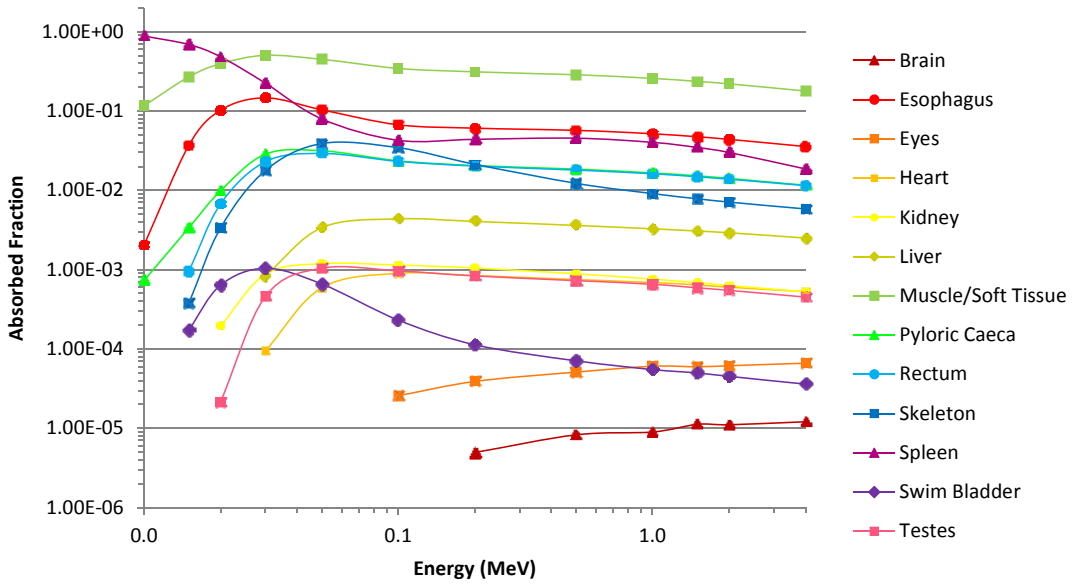

Figure 40: Photon AFs for a source located in the spleen segment.

Table 13: Absorbed fraction of photon energy for a source located in the testes segment.

	Energy (MeV)											
	0.010	0.015	0.020	0.030	0.050	0.100	0.200	0.500	1.000	1.500	2.000	4.000
Target												
Brain	0.00E+00	0.00E+00	0.00E+00	0.00E+00	--	--	--	7.31E-06	1.05E-05	1.24E-05	1.21E-05	1.27E-05
Esophagus	0.00E+00	--	3.03E-04	5.70E-03	1.35E-02	1.38E-02	1.24E-02	1.10E-02	9.85E-03	9.09E-03	8.49E-03	7.11E-03
Eyes	0.00E+00	0.00E+00	0.00E+00	--	--	1.19E-05	2.09E-05	2.72E-05	3.41E-05	4.05E-05	3.94E-05	4.26E-05
Heart	0.00E+00	0.00E+00	0.00E+00	--	8.78E-05	2.36E-04	2.66E-04	2.55E-04	2.43E-04	2.37E-04	2.31E-04	2.11E-04
Kidney	0.00E+00	0.00E+00	--	9.33E-05	3.46E-04	4.71E-04	4.98E-04	4.91E-04	4.57E-04	4.30E-04	3.97E-04	3.25E-04
Liver	0.00E+00	0.00E+00	0.00E+00	--	3.52E-04	8.69E-04	9.64E-04	9.32E-04	8.82E-04	8.62E-04	8.26E-04	7.68E-04
Muscle/Soft Tissue	1.78E-01	3.80E-01	5.14E-01	5.19E-01	3.79E-01	2.82E-01	2.62E-01	2.47E-01	2.26E-01	2.08E-01	1.94E-01	1.57E-01
Pyloric Caeca	0.00E+00	--	7.15E-05	1.75E-03	5.80E-03	6.94E-03	6.39E-03	5.67E-03	5.13E-03	4.75E-03	4.47E-03	3.78E-03
Rectum	2.37E-03	1.15E-02	2.75E-02	5.29E-02	4.69E-02	3.27E-02	2.91E-02	2.67E-02	2.39E-02	2.19E-02	2.03E-02	1.65E-02
Skeleton	--	1.94E-03	1.59E-02	6.66E-02	8.92E-02	4.98E-02	2.72E-02	1.74E-02	1.41E-02	1.24E-02	1.14E-02	9.42E-03
Spleen	0.00E+00	--	2.48E-05	5.89E-04	1.41E-03	1.28E-03	1.11E-03	9.51E-04	8.40E-04	7.69E-04	7.23E-04	6.06E-04
Swim Bladder	0.00E+00	--	--	7.03E-05	1.40E-04	8.84E-05	4.94E-05	2.73E-05	1.98E-05	1.72E-05	1.58E-05	1.37E-05
Testes	8.19E-01	5.99E-01	4.01E-01	1.80E-01	6.24E-02	3.42E-02	3.56E-02	3.66E-02	3.22E-02	2.74E-02	2.36E-02	1.43E-02

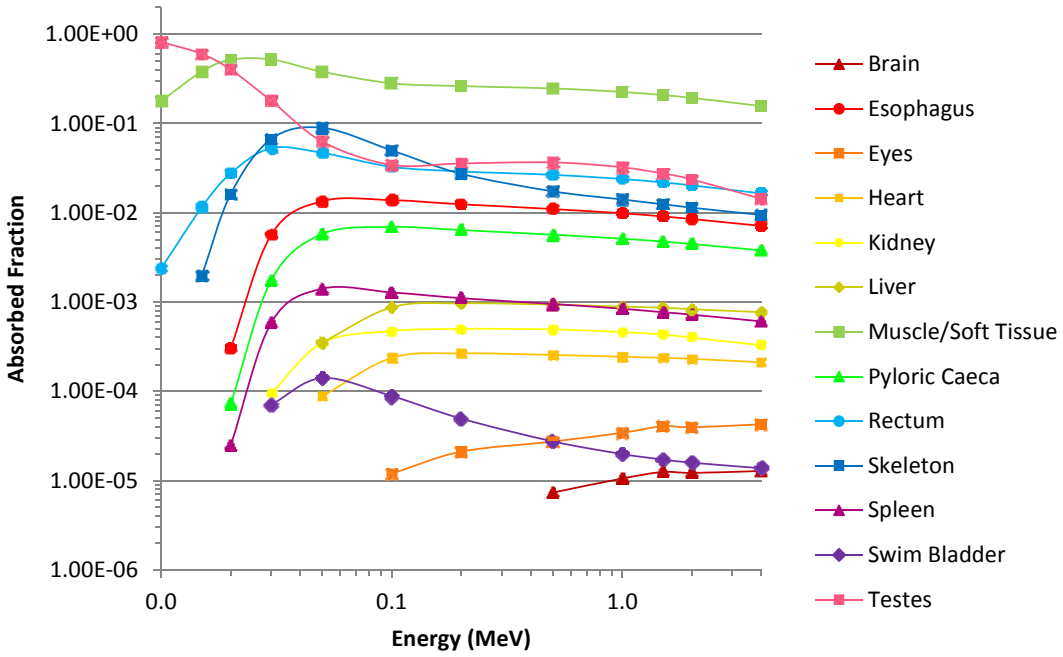

Figure 41: Photon AFs for a source located in the testes segment.

Table 14: Absorbed fraction of photon energy for an external source located in the surrounding water.

	Energy (MeV)											
	0.010	0.015	0.020	0.030	0.050	0.100	0.200	0.500	1.000	1.500	2.000	4.000
Target												
Brain	0.00E+00	0.00E+00	--	--	--	2.14E-05	2.82E-05	3.16E-05	3.36E-05	3.13E-05	2.87E-05	2.92E-05
Esophagus	0.00E+00	--	--	1.54E-04	5.63E-04	8.78E-04	9.35E-04	9.55E-04	9.44E-04	9.38E-04	9.08E-04	8.24E-04
Eyes	--	2.24E-05	4.49E-05	6.78E-05	7.88E-05	9.67E-05	1.08E-04	1.14E-04	1.21E-04	1.13E-04	1.12E-04	1.06E-04
Heart	0.00E+00	--	--	2.28E-05	5.60E-05	8.13E-05	9.58E-05	9.56E-05	9.41E-05	9.34E-05	9.49E-05	9.12E-05
Kidney	0.00E+00	0.00E+00	--	--	5.48E-05	1.28E-04	1.67E-04	1.97E-04	2.09E-04	2.10E-04	2.09E-04	2.00E-04
Liver	0.00E+00	--	--	6.29E-05	2.35E-04	3.92E-04	4.38E-04	4.48E-04	4.57E-04	4.52E-04	4.43E-04	4.08E-04
Muscle/Soft Tissue	1.39E-03	3.68E-03	7.34E-03	1.68E-02	3.03E-02	3.76E-02	3.84E-02	3.79E-02	3.69E-02	3.59E-02	3.50E-02	3.18E-02
Pyloric Caeca	--	--	--	1.70E-04	4.75E-04	6.60E-04	6.78E-04	6.54E-04	6.45E-04	6.24E-04	6.12E-04	5.53E-04
Rectum	--	--	4.00E-05	2.12E-04	5.93E-04	8.31E-04	8.97E-04	8.91E-04	8.73E-04	8.45E-04	8.19E-04	7.52E-04
Skeleton	1.30E-04	5.56E-04	1.40E-03	3.63E-03	6.83E-03	6.88E-03	5.01E-03	3.34E-03	2.70E-03	2.46E-03	2.31E-03	2.03E-03
Spleen	0.00E+00	0.00E+00	--	--	2.79E-05	4.67E-05	5.03E-05	4.91E-05	4.34E-05	4.28E-05	4.17E-05	3.90E-05
Swim Bladder	0.00E+00	--	--	--	--	8.96E-06	5.55E-06	4.02E-06	3.19E-06	2.77E-06	2.64E-06	2.29E-06
Testes	--	--	--	1.96E-05	3.86E-05	4.78E-05	4.64E-05	4.28E-05	4.12E-05	3.65E-05	3.85E-05	3.08E-05

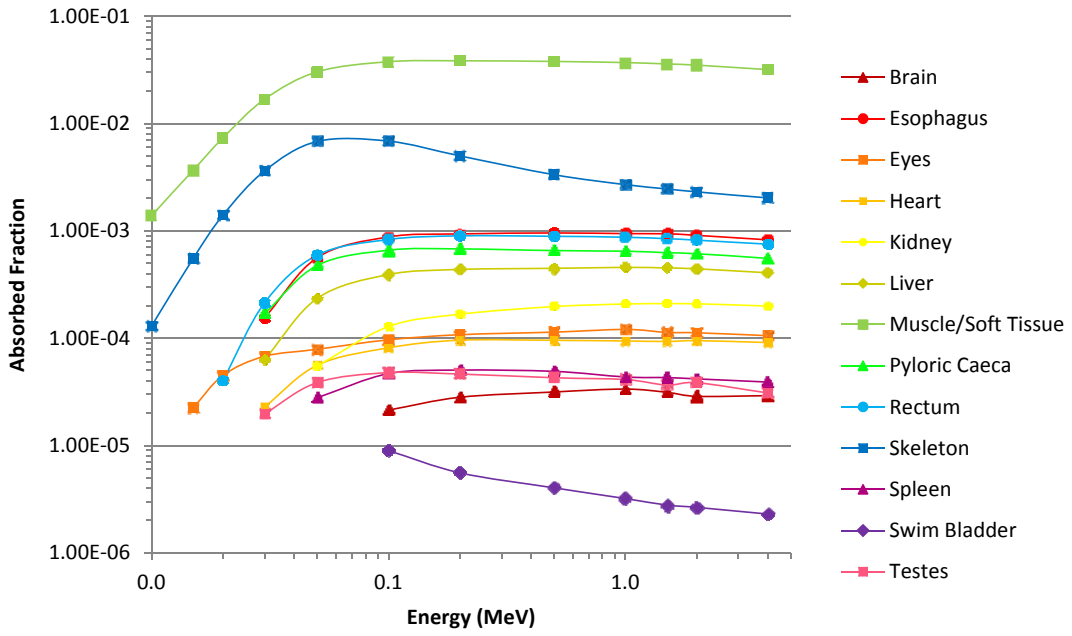

Figure 42: Photon AFs for an external source located in the surrounding water.

B. Complete Electron Absorbed Fraction Data

In all tables, AFs whose relative error exceeded 10% appear as a dashed line (--); those AFs with a relative error between 5% and 10% are underlined. A zero indicates that no energy was deposited in that segment. In all figures, AFs whose relative error exceeded 10% have been omitted.

Table 15: Absorbed fraction of electron energy for a source located in the esophagus segment.

	Energy (MeV)								
	0.100	0.200	0.400	0.500	0.700	1.000	1.500	2.000	4.000
Target									
Brain	0.00E+00	--	--	--	--	--	--	--	--
Esophagus	9.97E-01	9.89E-01	9.69E-01	9.59E-01	9.41E-01	9.18E-01	8.83E-01	8.50E-01	7.34E-01
Eyes	--	--	--	--	--	--	--	--	4.77E-06
Heart	--	--	8.81E-05	1.21E-04	1.85E-04	2.39E-04	3.04E-04	3.25E-04	8.24E-04
Kidney	4.43E-05	1.55E-04	4.39E-04	5.97E-04	9.27E-04	1.42E-03	2.27E-03	3.19E-03	7.47E-03
Liver	2.99E-04	9.88E-04	2.74E-03	3.68E-03	5.32E-03	7.40E-03	1.03E-02	1.29E-02	2.15E-02
Muscle/Soft Tissue	2.78E-03	9.10E-03	2.52E-02	3.33E-02	4.75E-02	6.54E-02	9.12E-02	1.13E-01	1.85E-01
Pyloric Caeca	1.81E-04	5.82E-04	1.61E-03	2.15E-03	3.33E-03	5.20E-03	8.86E-03	1.30E-02	3.08E-02
Rectum	3.35E-05	8.71E-05	2.36E-04	3.10E-04	4.40E-04	6.41E-04	1.24E-03	1.99E-03	6.15E-03
Skeleton	2.49E-05	5.48E-05	9.61E-05	1.22E-04	1.72E-04	3.31E-04	7.37E-04	1.26E-03	3.63E-03
Spleen	--	--	5.27E-06	6.33E-06	9.38E-06	2.87E-05	1.56E-04	4.48E-04	2.73E-03
Swim Bladder	--	--	1.67E-05	2.25E-05	3.37E-05	5.51E-05	8.70E-05	1.16E-04	2.07E-04
Testes	--	--	--	--	--	--	--	--	4.94E-06

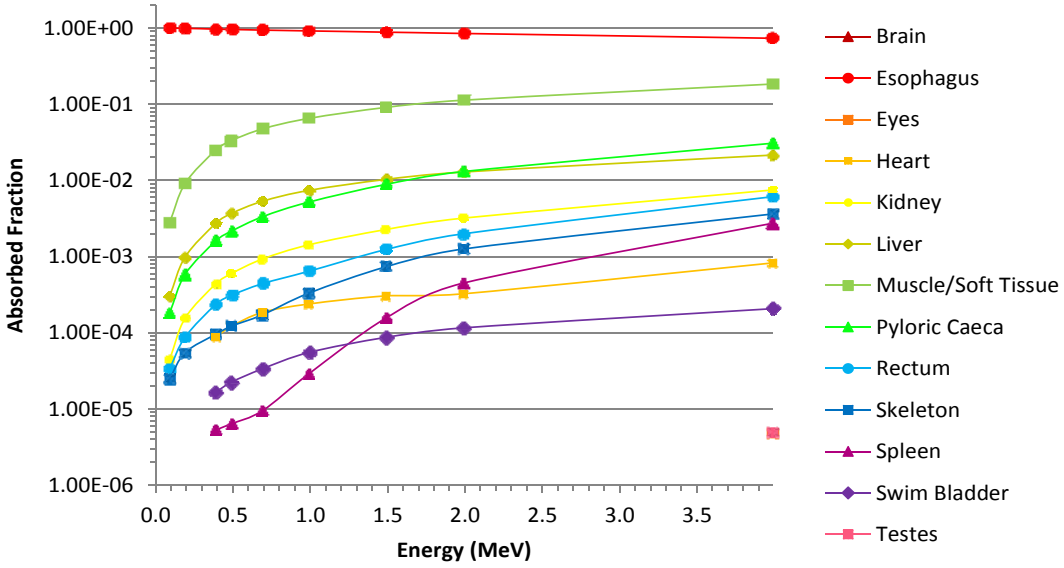

Figure 43: Electron AFs for a source located in the esophagus segment.

Table 16: Absorbed fraction of electron energy for a source located in the kidney segment.

	Energy (MeV)								
	0.100	0.200	0.400	0.500	0.700	1.000	1.500	2.000	4.000
Target									
Brain	--	--	--	--	--	--	--	--	5.51E-06
Esophagus	1.74E-04	5.56E-04	1.48E-03	2.04E-03	3.22E-03	4.93E-03	7.80E-03	1.11E-02	2.58E-02
Eyes	--	--	--	--	5.37E-06	8.32E-06	1.28E-05	1.66E-05	3.49E-05
Heart	--	--	--	--	4.95E-06	6.41E-06	9.86E-06	1.22E-05	2.41E-05
Kidney	9.93E-01	9.78E-01	9.39E-01	9.20E-01	8.86E-01	8.45E-01	7.88E-01	7.40E-01	5.84E-01
Liver	1.53E-04	5.22E-04	1.47E-03	1.94E-03	2.49E-03	2.95E-03	3.60E-03	3.85E-03	3.54E-03
Muscle/Soft Tissue	6.19E-03	2.03E-02	5.64E-02	7.45E-02	1.06E-01	1.43E-01	1.92E-01	2.31E-01	3.46E-01
Pyloric Caeca	--	--	--	5.94E-06	8.35E-06	1.24E-05	1.79E-05	2.48E-05	1.38E-04
Rectum	--	--	5.06E-05	6.82E-05	1.20E-04	2.21E-04	4.56E-04	7.59E-04	3.44E-03
Skeleton	1.19E-04	3.18E-04	7.98E-04	1.09E-03	1.93E-03	3.54E-03	6.71E-03	1.04E-02	3.03E-02
Spleen	--	--	--	--	--	--	--	--	--
Swim Bladder	--	3.22E-05	4.02E-05	4.55E-05	5.62E-05	7.22E-05	1.18E-04	1.63E-04	2.78E-04
Testes	--	--	--	--	--	--	--	--	--

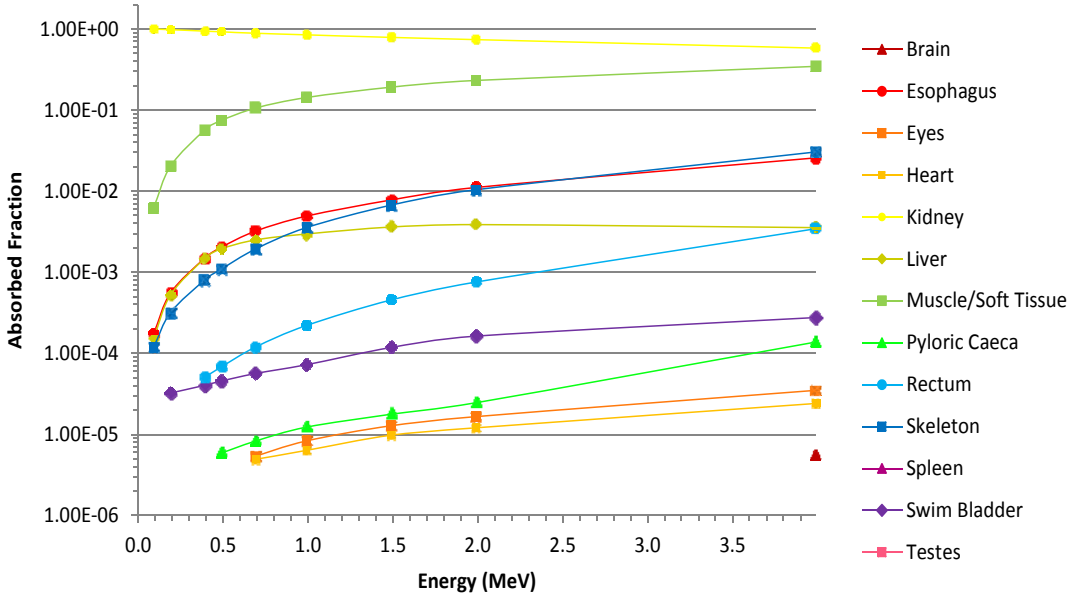

Figure 44: Electron AFs for a source located in the kidney segment.

Table 17: Absorbed fraction of electron energy for a source located in the liver segment.

	Energy (MeV)								
	0.100	0.200	0.400	0.500	0.700	1.000	1.500	2.000	4.000
Target									
Brain	0.00E+00	--	--	--	--	--	--	--	--
Esophagus	5.80E-04	1.90E-03	5.31E-03	7.09E-03	1.02E-02	1.41E-02	1.97E-02	2.46E-02	4.08E-02
Eyes	--	--	--	--	--	--	--	--	6.13E-06
Heart	3.73E-04	1.12E-03	3.13E-03	4.23E-03	6.65E-03	1.03E-02	1.59E-02	2.09E-02	3.40E-02
Kidney	7.50E-05	2.81E-04	8.06E-04	1.06E-03	1.38E-03	1.62E-03	2.00E-03	2.14E-03	1.97E-03
Liver	9.95E-01	9.84E-01	9.56E-01	9.42E-01	9.18E-01	8.89E-01	8.48E-01	8.13E-01	6.90E-01
Muscle/Soft Tissue	2.89E-03	9.62E-03	2.66E-02	3.50E-02	4.88E-02	6.43E-02	8.51E-02	1.03E-01	1.74E-01
Pyloric Caeca	3.29E-04	1.15E-03	3.38E-03	4.54E-03	6.46E-03	9.22E-03	1.37E-02	1.77E-02	2.90E-02
Rectum	4.30E-04	1.47E-03	4.13E-03	5.43E-03	7.41E-03	8.95E-03	1.04E-02	1.11E-02	1.21E-02
Skeleton	5.12E-05	1.40E-04	2.97E-04	3.95E-04	6.61E-04	1.18E-03	2.40E-03	3.91E-03	1.06E-02
Spleen	--	--	--	--	--	--	--	--	3.81E-06
Swim Bladder	--	--	--	--	--	--	--	1.53E-06	3.86E-06
Testes	--	--	--	--	--	--	--	--	--

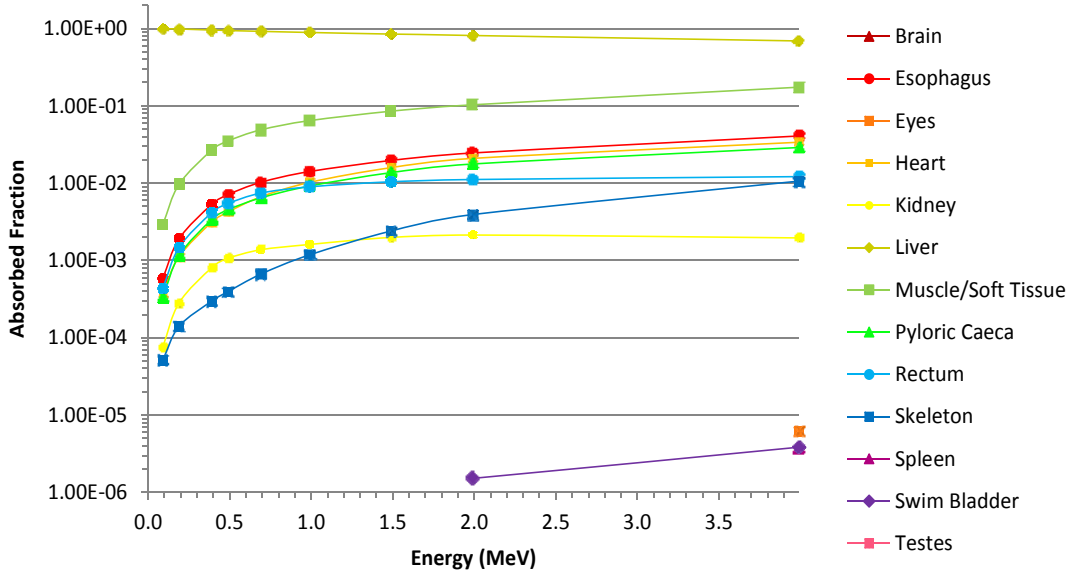

Figure 45: Electron AFs for a source located in the liver segment.

Table 18: Absorbed fraction of electron energy for a source located in the muscle segment.

	Energy (MeV)								
	0.100	0.200	0.400	0.500	0.700	1.000	1.500	2.000	4.000
Target									
Brain	--	2.53E-05	7.60E-05	9.85E-05	1.41E-04	1.96E-04	2.75E-04	3.36E-04	5.27E-04
Esophagus	8.77E-05	2.73E-04	8.02E-04	1.04E-03	1.48E-03	2.01E-03	2.80E-03	3.47E-03	5.63E-03
Eyes	--	6.55E-05	1.97E-04	2.54E-04	3.82E-04	5.46E-04	7.88E-04	1.01E-03	1.54E-03
Heart	--	5.29E-05	1.50E-04	1.90E-04	2.92E-04	4.08E-04	5.79E-04	7.21E-04	1.11E-03
Kidney	5.94E-05	1.80E-04	4.99E-04	6.69E-04	9.70E-04	1.28E-03	1.71E-03	2.03E-03	3.06E-03
Liver	4.73E-05	1.50E-04	4.18E-04	5.57E-04	8.07E-04	1.06E-03	1.38E-03	1.69E-03	2.83E-03
Muscle/Soft Tissue	9.98E-01	9.94E-01	9.83E-01	9.78E-01	9.68E-01	9.55E-01	9.38E-01	9.25E-01	8.84E-01
Pyloric Caeca	2.18E-04	7.32E-04	1.99E-03	2.65E-03	3.72E-03	4.94E-03	6.24E-03	6.95E-03	8.23E-03
Rectum	1.06E-04	3.45E-04	9.39E-04	1.25E-03	1.78E-03	2.43E-03	3.32E-03	4.07E-03	6.49E-03
Skeleton	6.99E-04	2.25E-03	6.16E-03	8.22E-03	1.22E-02	1.67E-02	2.15E-02	2.44E-02	2.97E-02
Spleen	--	1.95E-05	6.25E-05	7.84E-05	1.12E-04	1.66E-04	2.33E-04	2.99E-04	4.76E-04
Swim Bladder	4.44E-05	5.72E-05	5.74E-05	5.97E-05	6.17E-05	6.04E-05	5.82E-05	5.79E-05	5.63E-05
Testes	--	2.91E-05	8.12E-05	9.98E-05	1.42E-04	2.02E-04	2.75E-04	3.27E-04	4.97E-04

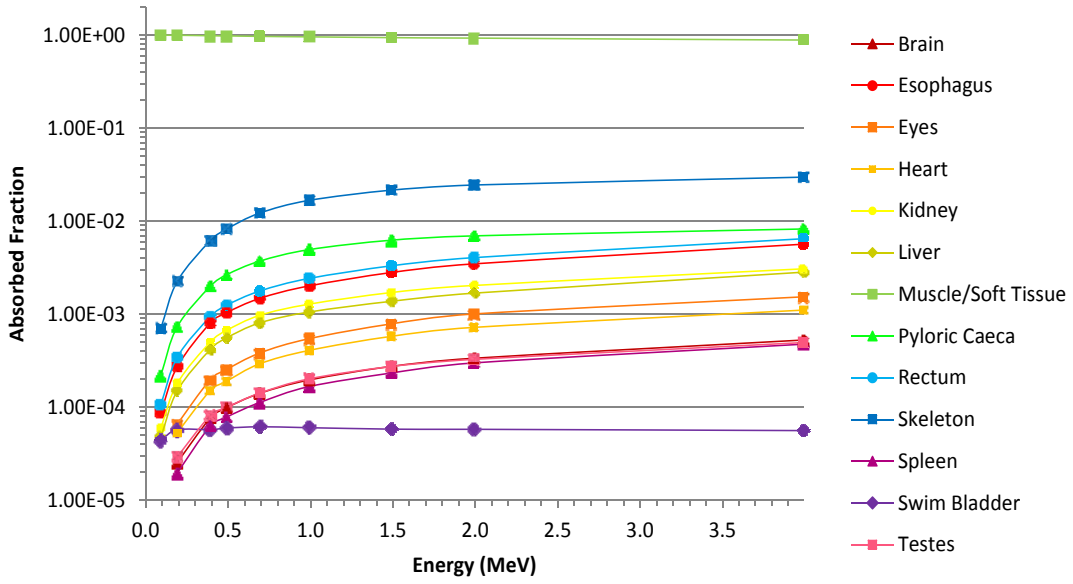

Figure 46: Electron AFs for a source located in the muscle segment.

Table 19: Absorbed fraction of electron energy for a source located in the pyloric caeca segment.

	Energy (MeV)								
	0.100	0.200	0.400	0.500	0.700	1.000	1.500	2.000	4.000
Target									
Brain	0.00E+00	0.00E+00	0.00E+00	--	--	--	--	--	--
Esophagus	2.45E-04	8.45E-04	2.43E-03	3.34E-03	5.17E-03	8.09E-03	1.39E-02	2.06E-02	4.86E-02
Eyes	0.00E+00	--	--	--	--	--	--	--	--
Heart	--	--	5.77E-06	6.71E-06	9.35E-06	1.32E-05	2.00E-05	2.93E-05	1.24E-03
Kidney	--	--	--	--	3.88E-06	5.69E-06	8.09E-06	1.16E-05	6.02E-05
Liver	3.08E-04	1.01E-03	2.83E-03	3.74E-03	5.37E-03	7.67E-03	1.13E-02	1.46E-02	2.40E-02
Muscle/Soft Tissue	1.12E-02	3.70E-02	1.03E-01	1.35E-01	1.92E-01	2.56E-01	3.23E-01	3.62E-01	4.24E-01
Pyloric Caeca	9.88E-01	9.59E-01	8.86E-01	8.50E-01	7.86E-01	7.12E-01	6.28E-01	5.72E-01	4.43E-01
Rectum	5.63E-04	1.81E-03	5.08E-03	6.77E-03	9.97E-03	1.40E-02	2.02E-02	2.62E-02	4.68E-02
Skeleton	--	5.01E-05	1.07E-04	1.36E-04	1.82E-04	2.68E-04	4.80E-04	7.13E-04	2.18E-03
Spleen	--	--	--	--	--	4.69E-05	1.07E-04	1.70E-04	3.74E-04
Swim Bladder	--	--	--	--	--	--	--	1.29E-06	7.19E-06
Testes	--	--	--	--	--	--	--	--	--

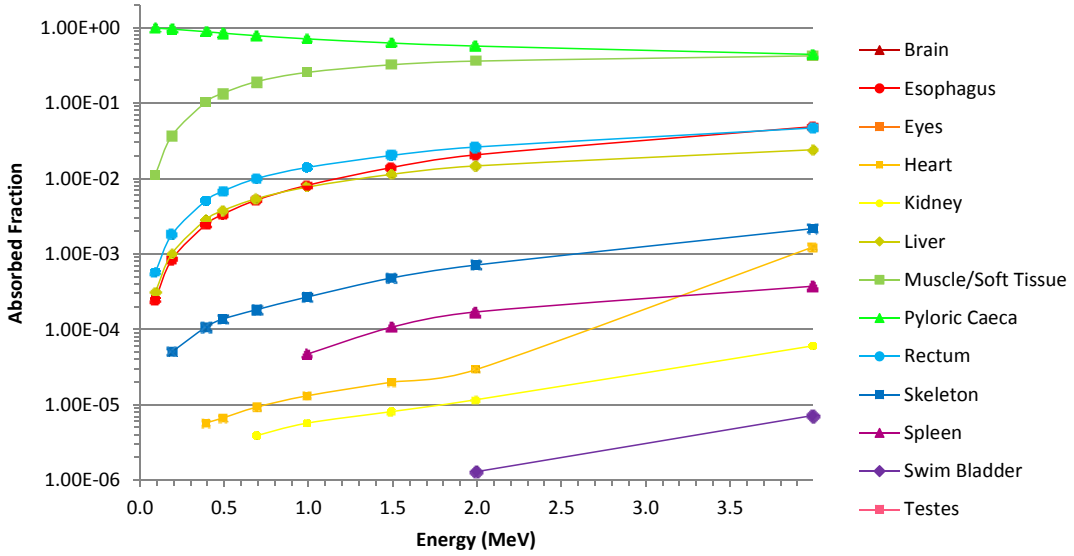

Figure 47: Electron AFs for a source located in the pyloric caeca segment.

Table 20: Absorbed fraction of electron energy for a source located in the rectum segment.

	Energy (MeV)								
	0.100	0.200	0.400	0.500	0.700	1.000	1.500	2.000	4.000
Target									
Brain	0.00E+00	--	--	--	--	--	--	--	--
Esophagus	3.26E-05	9.51E-05	2.57E-04	3.55E-04	5.18E-04	7.80E-04	1.44E-03	2.30E-03	7.13E-03
Eyes	--	--	--	--	--	--	--	--	--
Heart	1.08E-04	3.20E-04	8.88E-04	1.21E-03	1.87E-03	3.04E-03	5.27E-03	7.27E-03	1.10E-02
Kidney	--	--	--	--	3.66E-05	7.63E-05	1.51E-04	2.51E-04	1.18E-03
Liver	2.95E-04	9.21E-04	2.55E-03	3.37E-03	4.55E-03	5.49E-03	6.41E-03	6.87E-03	7.45E-03
Muscle/Soft Tissue	3.95E-03	1.27E-02	3.53E-02	4.66E-02	6.65E-02	9.12E-02	1.25E-01	1.53E-01	2.45E-01
Pyloric Caeca	3.78E-04	1.30E-03	3.68E-03	4.99E-03	7.35E-03	1.04E-02	1.49E-02	1.92E-02	3.45E-02
Rectum	9.95E-01	9.84E-01	9.56E-01	9.42E-01	9.18E-01	8.87E-01	8.43E-01	8.04E-01	6.74E-01
Skeleton	3.41E-05	9.91E-05	2.19E-04	2.90E-04	4.51E-04	7.44E-04	1.48E-03	2.40E-03	7.05E-03
Spleen	--	--	--	--	--	3.03E-06	5.45E-06	7.03E-06	4.70E-05
Swim Bladder	--	3.70E-05	4.34E-05	4.71E-05	5.88E-05	7.17E-05	9.67E-05	1.20E-04	1.81E-04
Testes	--	--	--	--	2.75E-05	8.02E-05	1.98E-04	2.95E-04	6.78E-04

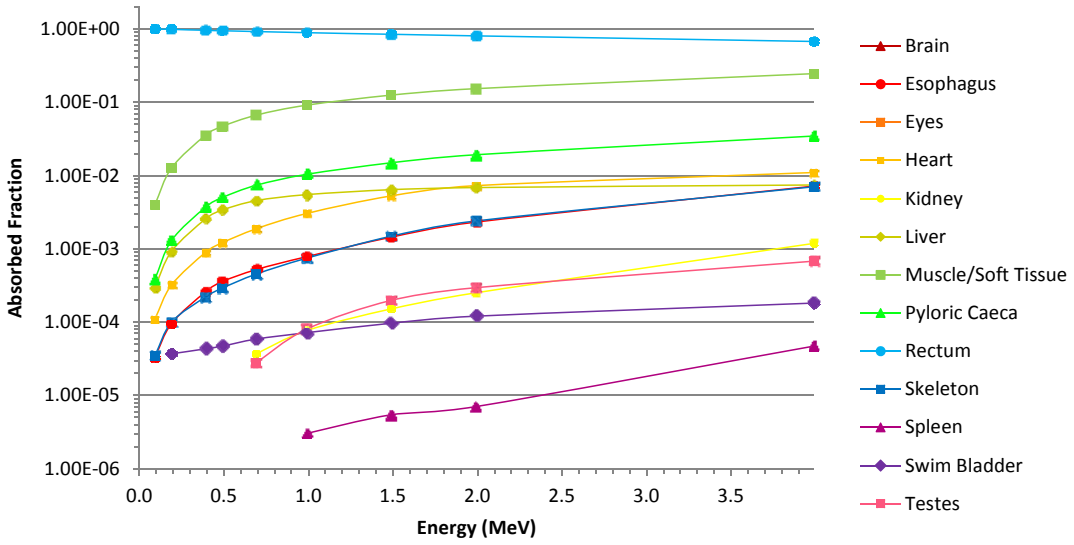

Figure 48: Electron AFs for a source located in the rectum segment.

Table 21: Absorbed fraction of electron energy for a source located in the skeleton segment.

	Energy (MeV)								
	0.100	0.200	0.400	0.500	0.700	1.000	1.500	2.000	4.000
Target									
Brain	--	--	--	3.75E-05	8.50E-05	2.01E-04	4.57E-04	7.44E-04	1.77E-03
Esophagus	--	--	2.13E-05	3.09E-05	5.94E-05	1.17E-04	3.06E-04	5.57E-04	1.63E-03
Eyes	--	--	3.91E-05	5.78E-05	1.17E-04	2.38E-04	4.71E-04	7.71E-04	1.95E-03
Heart	--	--	--	--	2.46E-05	8.50E-05	2.59E-04	4.61E-04	8.49E-04
Kidney	--	3.19E-05	9.62E-05	1.31E-04	2.51E-04	4.92E-04	9.25E-04	1.44E-03	4.16E-03
Liver	--	--	6.29E-05	8.03E-05	1.52E-04	2.76E-04	5.80E-04	9.42E-04	2.60E-03
Muscle/Soft Tissue	9.54E-03	3.31E-02	9.32E-02	1.26E-01	1.88E-01	2.60E-01	3.34E-01	3.78E-01	4.59E-01
Pyloric Caeca	--	--	1.35E-05	1.87E-05	2.96E-05	5.78E-05	1.09E-04	1.77E-04	6.30E-04
Rectum	--	--	7.55E-05	9.44E-05	1.63E-04	2.95E-04	5.78E-04	9.62E-04	2.81E-03
Skeleton	9.90E-01	9.65E-01	9.01E-01	8.66E-01	8.00E-01	7.20E-01	6.31E-01	5.74E-01	4.41E-01
Spleen	--	--	--	--	--	--	--	--	--
Swim Bladder	3.32E-05	5.61E-05	6.32E-05	6.84E-05	8.02E-05	9.03E-05	9.69E-05	9.23E-05	7.85E-05
Testes	--	--	--	--	--	--	--	--	2.64E-05

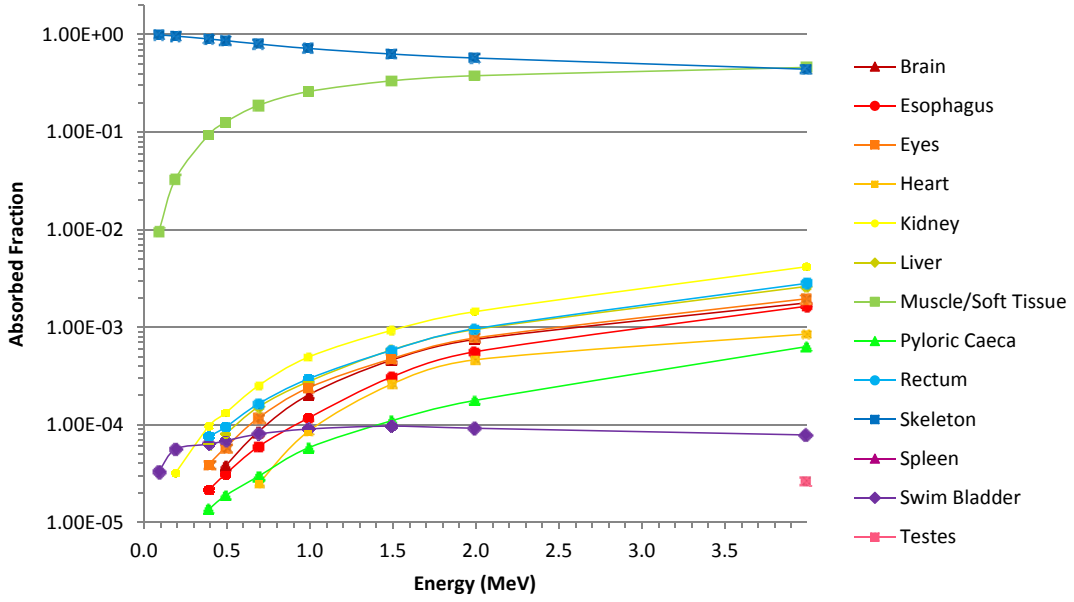

Figure 49: Electron AFs for a source located in the skeleton segment.

Table 22: Absorbed fraction of electron energy for a source located in the spleen segment.

	Energy (MeV)								
	0.100	0.200	0.400	0.500	0.700	1.000	1.500	2.000	4.000
Target									
Brain	0.00E+00	0.00E+00	0.00E+00	--	0.00E+00	--	--	--	--
Esophagus	4.09E-05	7.73E-05	1.31E-04	1.56E-04	2.25E-04	8.01E-04	4.26E-03	1.16E-02	6.93E-02
Eyes	0.00E+00	0.00E+00	--	--	--	--	--	--	--
Heart	--	--	--	--	--	--	4.09E-06	5.11E-06	1.06E-05
Kidney	--	--	--	--	--	3.35E-06	5.81E-06	7.57E-06	2.19E-05
Liver	--	--	--	6.61E-06	7.98E-06	1.31E-05	1.87E-05	2.65E-05	5.26E-05
Muscle/Soft Tissue	5.50E-03	1.79E-02	5.00E-02	6.65E-02	9.76E-02	1.39E-01	2.01E-01	2.52E-01	3.84E-01
Pyloric Caeca	--	7.67E-05	1.89E-04	2.53E-04	4.26E-04	7.43E-04	1.64E-03	2.67E-03	6.07E-03
Rectum	--	1.67E-05	3.18E-05	4.16E-05	5.38E-05	7.27E-05	1.08E-04	1.45E-04	1.10E-03
Skeleton	--	2.23E-05	3.80E-05	4.83E-05	6.28E-05	8.32E-05	1.10E-04	1.35E-04	4.33E-04
Spleen	9.94E-01	9.82E-01	9.49E-01	9.32E-01	9.01E-01	8.58E-01	7.90E-01	7.30E-01	5.30E-01
Swim Bladder	--	--	--	--	--	--	1.31E-06	1.92E-06	3.77E-05
Testes	--	--	--	--	--	--	--	5.95E-06	1.16E-05

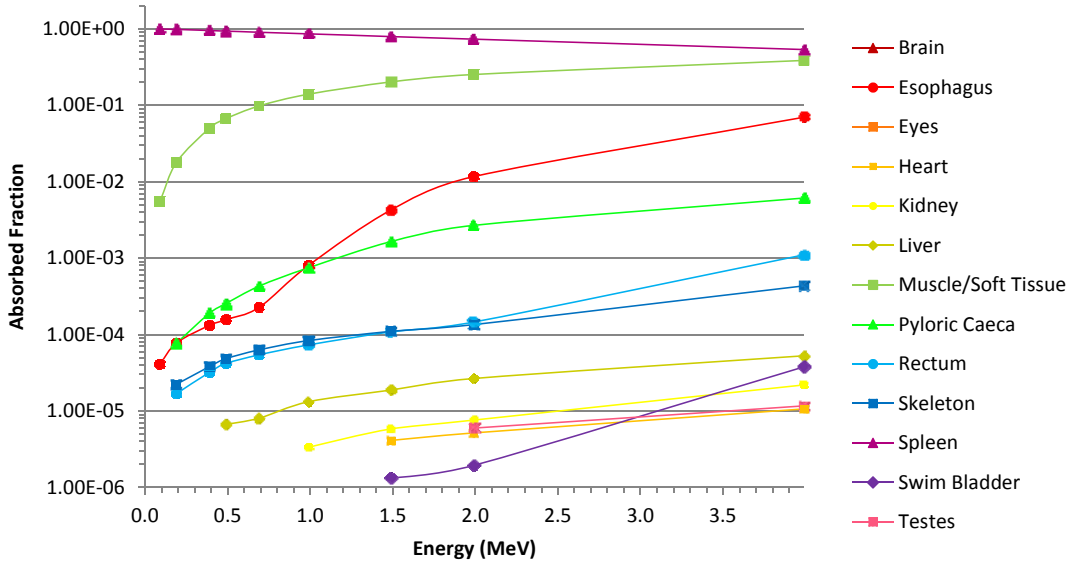

Figure 50: Electron AFs for a source located in the spleen segment.

Table 23: Absorbed fraction of electron energy for a source located in the testes segment.

	Energy (MeV)								
	0.100	0.200	0.400	0.500	0.700	1.000	1.500	2.000	4.000
Target									
Brain	0.00E+00	0.00E+00	--	--	0.00E+00	0.00E+00	--	--	--
Esophagus	--	--	1.53E-05	2.13E-05	2.86E-05	4.14E-05	6.03E-05	7.81E-05	1.68E-04
Eyes	0.00E+00	0.00E+00	0.00E+00	--	--	--	--	--	--
Heart	--	0.00E+00	--	--	--	--	--	--	--
Kidney	--	--	--	--	--	--	--	3.11E-06	6.86E-06
Liver	--	--	--	--	--	--	3.88E-06	6.01E-06	1.28E-05
Muscle/Soft Tissue	9.03E-03	2.93E-02	8.10E-02	1.07E-01	1.54E-01	2.13E-01	2.93E-01	3.56E-01	5.21E-01
Pyloric Caeca	--	--	8.20E-06	9.58E-06	1.42E-05	1.98E-05	3.06E-05	4.07E-05	8.58E-05
Rectum	5.33E-05	1.61E-04	4.47E-04	6.28E-04	1.15E-03	2.31E-03	5.13E-03	8.23E-03	1.87E-02
Skeleton	2.17E-05	4.32E-05	7.51E-05	9.07E-05	1.09E-04	1.38E-04	1.97E-04	2.90E-04	1.77E-03
Spleen	--	--	--	--	--	3.60E-06	6.38E-06	7.33E-06	1.57E-05
Swim Bladder	--	--	--	--	--	--	--	--	5.82E-07
Testes	9.91E-01	9.70E-01	9.18E-01	8.91E-01	8.43E-01	7.83E-01	6.99E-01	6.30E-01	4.39E-01

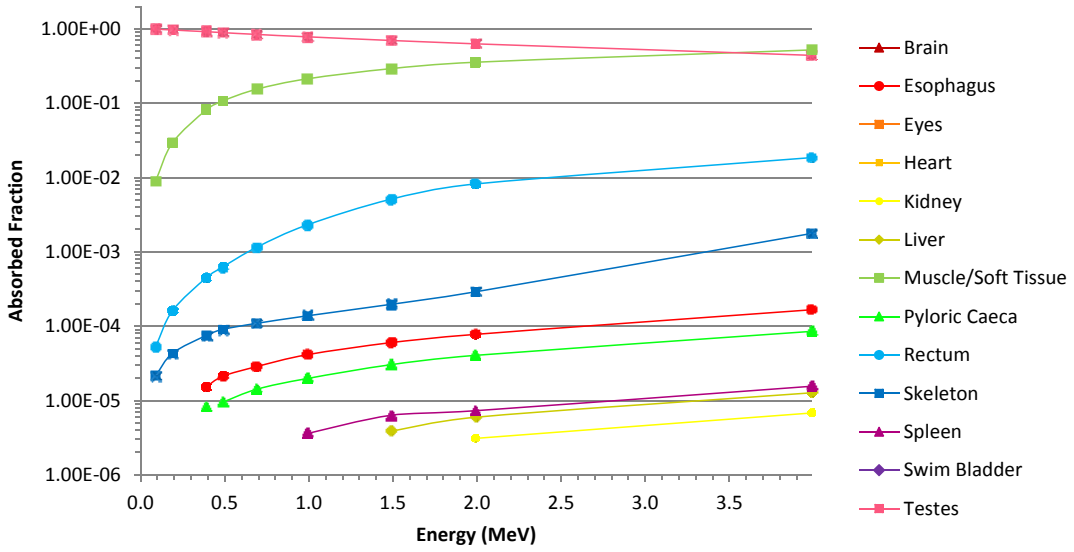

Figure 51: Electron AFs for a source located in the testes segment.

Table 24: Absorbed fraction of electron energy for an external source located in the surrounding water.

	Energy (MeV)								
	0.100	0.200	0.400	0.500	0.700	1.000	1.500	2.000	4.000
Target									
Brain	0.00E+00	--	--	--	--	--	--	--	--
Esophagus	--	--	--	--	--	--	4.04E-06	6.81E-06	1.32E-05
Eyes	0.00E+00	--	--	--	--	--	--	--	4.63E-05
Heart	0.00E+00	--	--	--	--	--	--	--	--
Kidney	0.00E+00	--	--	--	--	--	--	--	--
Liver	--	--	--	--	--	--	--	--	6.50E-06
Muscle/Soft Tissue	6.10E-05	2.13E-04	5.99E-04	8.17E-04	1.18E-03	1.72E-03	2.51E-03	3.24E-03	5.94E-03
Pyloric Caeca	--	--	--	--	--	--	--	--	1.06E-05
Rectum	--	--	--	--	--	--	--	8.59E-06	2.73E-05
Skeleton	--	--	4.19E-05	5.67E-05	8.81E-05	1.36E-04	2.22E-04	2.98E-04	5.65E-04
Spleen	--	--	--	--	--	--	--	--	--
Swim Bladder	--	--	--	--	0.00E+00	--	--	--	--
Testes	0.00E+00	--	--	--	--	--	--	--	--

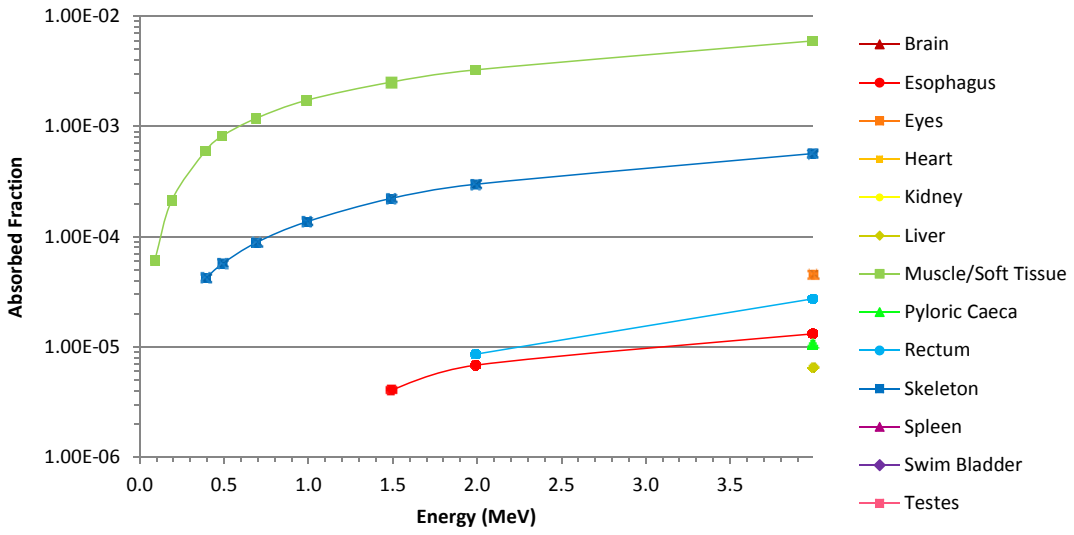

Figure 52: Electron AFs for an external source located in the surrounding water.

C. Sample MCNP Input Deck

The MCNP input file presented here has been modified from the original version. Approximately 6,400 lines detailing the lattice structure have been removed. Several lines of the lattice structure are left to demonstrate the format required.

```
Reference Trout
c  This input file was created by the HML Boundary File Voxelizer
c  created by Human Monitoring Laboratory, Health Canada
c  Erick Cardenas-Mendez, & Kevin Capello
c
c  Input file originally created on:
c  Saturday, August 18, 2012 9:36:31 PM
c
c  compression factor: 4
c
c
c
c ++++++++++++++++++++++++++++++++++++++++++++++++++++++++++++
c
c    Cells
c
c ++++++++++++++++++++++++++++++++++++++++++++++++++++++++++++
c
 999  0         999         imp:p 0 imp:e 0   $ outside everything void
 998  14 -1.00  -999  1111    imp:p 1 imp:e 1   $ river water
c
c Filling Universes
1     1  -1.05       -4444  u = 1   imp:p 1 imp:e 1   $ muscle soft tissue
100   0             4444  u = 1   imp:p 0 imp:e 0
2     2  -0.001201   -4444  u = 2   imp:p 1 imp:e 1   $ Air Bladder
200   0             4444  u = 2   imp:p 0 imp:e 0
3     3  -1.92       -4444  u = 3   imp:p 1 imp:e 1   $ Bone Complete
300   0             4444  u = 3   imp:p 0 imp:e 0
4     4  -1.07       -4444  u = 4   imp:p 1 imp:e 1   $ Eyes
400   0             4444  u = 4   imp:p 0 imp:e 0
5     5  -1.03       -4444  u = 5   imp:p 1 imp:e 1   $ Heart
500   0             4444  u = 5   imp:p 0 imp:e 0
6     6  -1.06       -4444  u = 6   imp:p 1 imp:e 1   $ Liver
600   0             4444  u = 6   imp:p 0 imp:e 0
7     7  -1.04       -4444  u = 7   imp:p 1 imp:e 1   $ Brain
```

```
700   0            4444  u = 7   imp:p 0 imp:e 0
8     8  -1.045     -4444  u = 8   imp:p 1 imp:e 1   $ esophagus
800   0            4444  u = 8   imp:p 0 imp:e 0
9     9  -1.045     -4444  u = 9   imp:p 1 imp:e 1   $ Rectum
900   0            4444  u = 9   imp:p 0 imp:e 0
10    10 -1.06      -4444  u = 10  imp:p 1 imp:e 1   $ spleen
1000  0            4444  u = 10  imp:p 0 imp:e 0
11    11 -1.04      -4444  u = 11  imp:p 1 imp:e 1   $ testes
1100  0            4444  u = 11  imp:p 0 imp:e 0
12    12  -1.045     -4444  u = 12  imp:p 1 imp:e 1   $ pyloric caeca
1200  0            4444  u = 12  imp:p 0 imp:e 0
13    13  -1.05     -4444  u = 13  imp:p 1 imp:e 1   $ kidneys
1300  0            4444  u = 13  imp:p 0 imp:e 0
14    14  -1.00     -4444  u = 14  imp:p 1 imp:e 1   $ Surrounding water
1400  0            4444  u = 14  imp:p 0 imp:e 0
c
c Lattice Unit Cell
c
   996    0   -3333    lat = 1 u = 996  imp:p 1 imp:e 1
              fill = 0:127  0:127 0:361
      14 10262R 1 8R 14 115R 1 2R 14 9R 1 3R 14 33R 1 5R 14 129R 1
      3R 14 5804R
      14 10262R 1 7R 14 116R 1 2R 14 9R 1 2R 14 34R 1 6R 14 127R 1
      4R 14 5804R
      14 10263R 1 6R 14 117R 1 2R 14 7R 1 4R 14 32R 1 6R 14 128R 1
      3R 14 5805R
      14 10263R 1 6R 14 35R 1 14 80R 1 3R 14 5R 1 4R 14 34R 1 5R 14
      88R 1 4R 14 34R 1 3R 14 91R 1 14 34R 1 14 5676R
      14 10264R 1 4R 14 34R 1 1R 14 81R 1 3R 14 4R 1 4R 14 22R 1
      14 11R 1 4R 14 72R 1 14 13R 1 4R 14 2R 1 14 10R 1 14 19R 1
      4R 14 5805R
      14 10265R 1 3R 14 34R 1 1R 14 82R 1 12R 14 22R 1 2R 14 8R 1
      5R 14 72R 1 14 12R 1 4R 14 4R 1 14 8R 1 1R 14 19R 1 3R 14
      87R 1 14 12R 1 14 24R 1 14 5677R
      14 10303R 1 3R 14 81R 1 11R 14 24R 1 3R 14 5R 1 4R 14 74R 1
      1R 14 10R 1 3R 14 4R 1 2R 14 9R 1 1R 14 15R 1 6R 14 85R 1
      3R 14 3R 1 14 3R 1 2R 14 5704R
      14 10305R 1 1R 14 81R 1 11R 14 24R 1 4R 14 3R 1 5R 14 74R 1
      2R 14 8R 1 4R 14 4R 1 2R 14 9R 1 1R 14 15R 1 5R 14 84R 1 5R 14
      7R 1 3R 14 24R 1 1R 14 5677R
      14 10305R 1 14 82R 1 10R 14 26R 1 2R 14 4R 1 4R 14 75R 1 3R 14
      7R 1 3R 14 5R 1 3R 14 8R 1 1R 14 14R 1 5R 14 85R 1 5R 14 4R 1
      14 1 4R 14 23R 1 2R 14 5677R
      14 10305R 1 14 83R 1 9R 14 26R 1 2R 14 2R 1 6R 14 75R 1 4R 14
```

```
6R 1 4R 14 4R 1 3R 14 8R 1 2R 14 12R 1 6R 14 85R 1 5R 14 7R 1
3R 14 22R 1 2R 14 5678R
14 10303R 1 14 87R 1 7R 14 25R 1 13R 14 75R 1 5R 14 2R 1 6R 14
5R 1 4R 14 6R 1 4R 14 11R 1 4R 14 87R 1 4R 14 6R 1 6R 14 19R 1
4R 14 5678R
```

NOTE: The lattice structure continues in a similar manner for approximately another 6,400 lines.

```
c
c Cell Containing Lattice
c
   997    0     -1111   fill = 996 imp:p 1 imp:e 1
c

c ++++++++++++++++++++++++++++++++++++++++++++++++++++++++++
c
c    Surfaces
c
c ++++++++++++++++++++++++++++++++++++++++++++++++++++++++++
c
  999 so  500     $ 500 cm universe sphere
c
c Box for Filling Universes
c
1111  rpp       0.000   112.128     0.000   112.128     0.000    36.2
3333  rpp       0.000     0.876     0.000     0.876     0.000     0.1
4444  rpp      -0.010     0.880    -0.010     0.880    -0.010     0.12
c

c ++++++++++++++++++++++++++++++++++++++++++++++++++++++++++
c
c    Materials
c
c ++++++++++++++++++++++++++++++++++++++++++++++++++++++++++
c
c ------------------------------------------
c Muscle, Skin & non-segmented tissue
c Muscle (ICRP-89)
m1
           1000       -0.102000
           6000       -0.143000
           7000       -0.034000
```

```
          8000      -0.710000
          11000     -0.001000
          15000     -0.002000
          16000     -0.003000
          17000     -0.001000
          19000     -0.004000
c ---------------------------------------------
c Air Bladder
m2
          14000    -0.990321
          6000     -0.001708
          8000     -0.007971
c ---------------------------------------------
c Bone
c Cortical Bone (ICRU-44)  1.92 g/cm^3
m3
          1000      -0.034000
          6000      -0.155000
          7000      -0.042000
          8000      -0.435000
          11000     -0.001000
          12000     -0.002000
          15000     -0.103000
          16000     -0.003000
          20000     -0.225000
c ---------------------------------------------
c Eyes
c Eyes(ICRP-89) 1.026 g/cm^3
m4
          1000      -0.096000
          6000      -0.195000
          7000      -0.057000
          8000      -0.646000
          11000     -0.001000
          15000     -0.001000
          16000     -0.003000
          17000     -0.001000
c ---------------------------------------------
c Heart
c Heart (ICRP-89) 1.03 g/cm^3
m5
          1000      -0.104
          6000      -0.139
          7000      -0.029
```

```
        8000    -0.718
        11000    -0.001
        15000    -0.002
        16000    -0.002
        17000    -0.002
        19000    -0.003
c -------------------------------------------------
c Liver
c Liver (ICRP-89)
m6
        1000    -0.103
        6000    -0.186
        7000    -0.028
        8000    -0.671
        11000    -0.002
        15000    -0.002
        16000    -0.003
        17000    -0.002
        19000    -0.003
c -------------------------------------------------
c Brain
c Brain, grey/white matter (ICRU-44) 1.04 g/cm^3
m7
        1000    -0.107
        6000    -0.145
        7000    -0.022
        8000    -0.712
        11000    -0.002
        15000    -0.004
        16000    -0.002
        17000    -0.003
        19000    -0.003
c ----------------------------------------
c oesophagus
c oesophagus (ICRP-89) 1.045 g/cm^3
m8
        1000    -0.105
        6000    -0.256
        7000    -0.027
        8000    -0.602
        11000    -0.001
        15000    -0.002
        16000    -0.003
        17000    -0.002
```

```
          19000     -0.002
c ----------------------------------------
c Rectum
c Large Intestine (ICRP-89) 1.045 g/cm^3
m9
          1000      -0.106
          6000      -0.115
          7000      -0.022
          8000      -0.751
          11000     -0.001
          15000     -0.001
          16000     -0.001
          17000     -0.002
          19000     -0.001
c ---------------------------------------
c spleen
c Spleen (ICRP-89) 1.06 g/cm^3
m10
          1000      -0.103
          6000      -0.113
          7000      -0.032
          8000      -0.741
          11000     -0.001
          15000     -0.003
          16000     -0.002
          17000     -0.002
          19000     -0.003
c -------------------------------------------
c testes
c Testis (ICRU-44) 1.04 g/cm^3
m11
          1000      -0.106
          6000      -0.099
          7000      -0.020
          8000      -0.766
          11000     -0.002
          15000     -0.001
          16000     -0.002
          17000     -0.002
          19000     -0.002
c -------------------------------------------
c pyloric caeca
c stomach (ICRP-89) 1.045 g/cm^3
m12
```

```
             1000        -0.106
             6000        -0.115
             7000        -0.022
             8000        -0.751
             11000        -0.001
             15000        -0.001
             16000        -0.001
             17000        -0.002
             19000        -0.001
c -------------------------------------------------
c kidneys
c Kidneys (ICRP-89) 1.05 g/cm^3
m13
             1000         -0.103
             6000         -0.132
             7000         -0.030
             8000         -0.724
             11000         -0.002
             15000         -0.002
             16000         -0.002
             17000         -0.002
             19000         -0.002
             20000         -0.001
c -------------------------------------------------
c Surrounding Water
c River Water (Murray, Univ. of Washington)
m14
             1000         -0.109992406
             6000         -0.000013377
             7000         -0.000000226
             8000         -0.889938564
             11000         -0.000009000
             12000         -0.000005000
             14000         -0.000004200
             16000         -0.000006667
             17000         -0.000008000
             19000         -0.000001400
             20000         -0.000021000
             26000         -0.000000160
c -------------------------------------------------
c
c +++++++++++++++++++++++++++++++++++++++++++++++++++++++++++++
c
c
```

```
c Source
c
c
c ++++++++++++++++++++++++++++++++++++++++++++++++++++++++++
c
mode p e
sdef  erg=1.5  par=2  eff=0.000001  X=d1 Y=d2 Z=d3 cel=d4
si1 0.001 0.876
sp1 0 1
si2 0.001 0.876
sp2 0 1
si3 0.001 0.1
sp3 0 1
si4 L u=(1<996<997)
sp4 1
*f8:e u=(1)  $ muscle
*f18:e u=(2) $ swim bladder
*f28:e u=(3) $ bone
*f38:e u=(4) $ eyes
*f48:e u=(5) $ heart
*f58:e u=(6) $ liver
*f68:e u=(7) $ brain
*f78:e u=(8) $ oesophagus
*f88:e u=(9) $ rectum
*f98:e u=(10) $ spleen
*f108:e u=(11) $ testes
*f118:e u=(12) $ pyloric caeca
*f128:e u=(13) $ kidneys
*f138:e u=(14) $ water
e8 0 0.000001 6.0
e18 0 0.000001 6.0
e28 0 0.000001 6.0
e38 0 0.000001 6.0
e48 0 0.000001 6.0
e58 0 0.000001 6.0
e68 0 0.000001 6.0
e78 0 0.000001 6.0
e88 0 0.000001 6.0
e98 0 0.000001 6.0
e108 0 0.000001 6.0
e118 0 0.000001 6.0
e128 0 0.000001 6.0
e138 0 0.000001 6.0
nps 500000
```